



2011

Annual Report Jahresbericht

Remote Sensing Technology Institute

Department
Atmospheric Processors



Published by **German Aerospace Center (DLR)**
A member of the Helmholtz Association

Remote Sensing Technology Institute
Institut für Methodik der Fernerkundung (IMF)

Department
Atmospheric Processors (IMF-AP)

Department Head Prof. Dr. Thomas Trautmann

Editorial Team Prof. Dr. Thomas Trautmann
Dr. Manfred Gottwald
Brigitte Rüba

Layout Dr. Manfred Gottwald

Cover Demonstration of the 22° halo in the framework of the DLR_School_Lab
Neustrelitz (see chapter 4.4).

Contents

1.	Foreword	3
2.	Atmospheric Remote Sensing – Instrument Operation, Calibration and Measurement Techniques	5
2.1	SCIAMACHY Level 0-2 Processing.....	5
2.2	The Satellite Collocation Tool and Validation of the SCIAMACHY Ozone Profiles.....	9
2.3	SCIAMACHY Operations Support	11
2.4	Hard Drive Encryption	13
3.	Atmospheric Remote Sensing – Retrieval Methods	15
3.1	SCIAMACHY Methane Retrievals	15
3.2	Assessment of Independent Macrophysical Cloud Properties in the Oxygen A-Band.....	17
3.3	Multi-Dimensional Radiative Transfer	19
3.4	Current Status and Recent Results of TELIS Retrievals.....	21
3.5	Intercomparison of the GARLIC and PIRATES IR Radiative Transfer Codes	23
3.6	A Case Study on the Reciprocity in Light Scattering Computations	24
3.7	Dust/Urban Aerosol Radiative Forcing Based on Surface Aerosol Measurements	26
3.8	Light Scattering of 3D Chebyshev Particles.....	28
3.9	New Database Interfaces for the WDC-RSAT.....	30
4.	Atmospheric Remote Sensing – Applications	33
4.1	DLR Science Award 2011: Global Long-term Environmental Satellite Data for Climate Monitoring.....	33
4.2	Tropospheric Trace Gas Products from GOME-2.....	38
4.3	Spaceborne Measurements of Air Quality During the World Expo 2010 in Shanghai.....	41
4.4	The Light Scattering Laboratory within the DLR_School_Lab Neustrelitz	45
4.5	Spectroscopic Characterization of the Atmospheres of Potentially Habitable Planets: GL 581 d as a Model Case Study	47
4.6	High Resolution Infrared Emission Spectra of Earth-like Planets Influenced by Clouds.....	49
4.7	Textbook SCIAMACHY – Exploring the Changing Earth’s Atmosphere.....	51
5.	Documentation	53
5.1	Books and Book Contributions.....	53
5.2	Journal Papers.....	54
5.3	Conference Proceeding Papers and Presentations	56
5.4	Attended Conferences and Professional Leaves.....	59
5.5	Diploma and Doctoral Theses.....	60
5.6	Seminar Talks.....	61
	Abbreviations and Acronyms	63

1. Foreword

With the current report we enter the second decade of the 21st century. This will be a period with exciting new undertakings in the field of space-borne atmospheric remote sensing. The ESA sentinels, including the Sentinel 5 Precursor mission, ADM-Aeolus, MERLIN as a bi-lateral project between Germany and France or CarbonSat as a potential new Explorer mission are either already on track for an anticipated launch in the second half of the decade or are studied in detail for achieving implementation. Together with our partners we intend to contribute to the success of these missions by participating in associated ground segment preparation activities.

Placing new space-borne instruments into orbit is always a challenge. However, sometimes the opposite has to occur, namely de-orbiting spacecraft which have reached the end of their in-orbit lifetime. This was the case for one of our workhorses, the Global Ozone Monitoring Experiment (GOME) on ESA's ERS-2 platform. On July 4th 2011, after more than 16 years of continuous operations, ESA terminated this highly successful Earth Observation mission. However, the GOME heritage sensors SCIAMACHY on ENVISAT and GOME-2 on the MetOp series are still providing us with a wealth of atmospheric data. Particularly the envisaged mission extension 2014+ of ENVISAT will be crucial for maintaining the data record from SCIAMACHY with its unrivalled observation capabilities.

One of the key requirements for remotely sensed atmospheric data is maintaining very accurately calibrated radiances and irradiances over long instrument in-orbit lifetimes and to achieve as good as possible inter-comparisons between different sensors on different platforms. Our long-standing involvement in the algorithm and processor development for GOME, SCIAMACHY and GOME-2 has enabled our department to combine their ozone related results into a unique data set. It was the basis for an outstanding work on *Global long-term environmental satellite data for climate monitoring* which received the Science Award, the most prestigious science price of DLR (see chapter 4.1). Besides being a highly reputable acknowledgement of the achievements of our colleagues having elaborated this subject we also consider it as a stimulus for the entire department to continue exploring ingenious methods in atmospheric remote sensing.

We thank all our staff for their efforts and achievements in 2011 and their contributions to this annual report.

Prof. Dr. Thomas Trautmann
Dr. Manfred Gottwald

2. Atmospheric Remote Sensing – Instrument Operation, Calibration and Measurement Techniques

2.1 SCIAMACHY Level 0-2 Processing

G. Lichtenberg, B. Aberle, A. Doicu, S. Gimeno García (TUM), M. Meringer, F. Schreier, S. Slijkhuis, D. Sherbakov

In 2011 releasing new versions of the operational processing chain required thorough preparations. Additionally support was given to the re-processing of all data with the latest processor version. The operational processing chain consists of three elements:

- Level 0-1b Processor: It takes level 0 as input, i.e. time ordered raw data from the instrument, and produces level 1b data. Level 1b data contain all data needed to produce calibrated Earthshine radiances.
- SciCal: The SciCal tool collects all calibration measurements, calibrates them using the level 0-1b prototype processor and saves them to auxiliary files that are later picked up by the level 0-1b processor and used in the calibration of Earthshine data.
- Level 1b-2 Processor: It provides geophysical products like trace gas columns, trace gas profiles and cloud parameters by taking level 1b as input and generating level 2 products.

All data are processed at the D-PAC hosted by DLR's Earth Observation Center (EOC) at Oberpfaffenhofen. ESA provides the user with level 1b data and level 2 data. Additionally a tool - *Scial1c* - is available for extracting and calibrating data from the level 1b products.

Re-processing Campaign

In the first check of level 2 and level 1 data from the recent re-processing campaign some deficiencies of the products were discovered. The CO and SO₂ trace gas columns were not as expected and the calibration data (Sun Mean References and Dead and Bad Pixel Mask) were not regularly updated. The missing updates for the calibration data could be traced back to the design of the ground segment and the need for parallel processing. Calibration files, usually termed ADF (Auxiliary Data File), contain more than one calibration parameter, e.g. the Sun calibration data file contains Sun Mean References (SMRs) from different diffuser measurements. However these parameters are derived from measurements executed at different times, such that at any given time, not all calibration parameters can be calculated. The ground segment requires complete ADFs, i.e. all calibration parameters must have valid values. Therefore, calibration parameters that could not be generated for a given time are copied from the previous ADF. During the re-processing the generation of the different Sun Mean References was not always finished at the same time, i.e. outdated data were copied to the ADFs (Fig. 2-1). The problem was solved by re-generating all affected ADFs. At the same time a monitoring tool was written and all calibration parameters for the complete mission were checked for proper updates. The analysis showed that the new ADF data base did no longer contain outdated parameters. For the next version of the processor the SciCal tool will be re-designed preventing the usage of outdated data in the processing (see below).

During the validation of the level 2 data it was discovered that the CO total columns were partly unphysical. Further investigation showed the effect to be caused by an unexpected wavelength shift of the instrument since the launch. In order to correct for this effect, a fit of a linear wavelength shift was added to the retrieval. This led to physical CO values (Fig. 2-2). In addition, for SO₂ the background database was corrected. Since a new version of the operational processor was required to deliver corrected level 2 products to the user, the opportunity was taken to additionally add small improvements to the OCIO retrieval and to port the processor to 64 bit architecture and to the newest compiler and library versions. The new processor was delivered in May 2011 and the re-processing of the level 2 data started in November after all level 1 data had been generated.

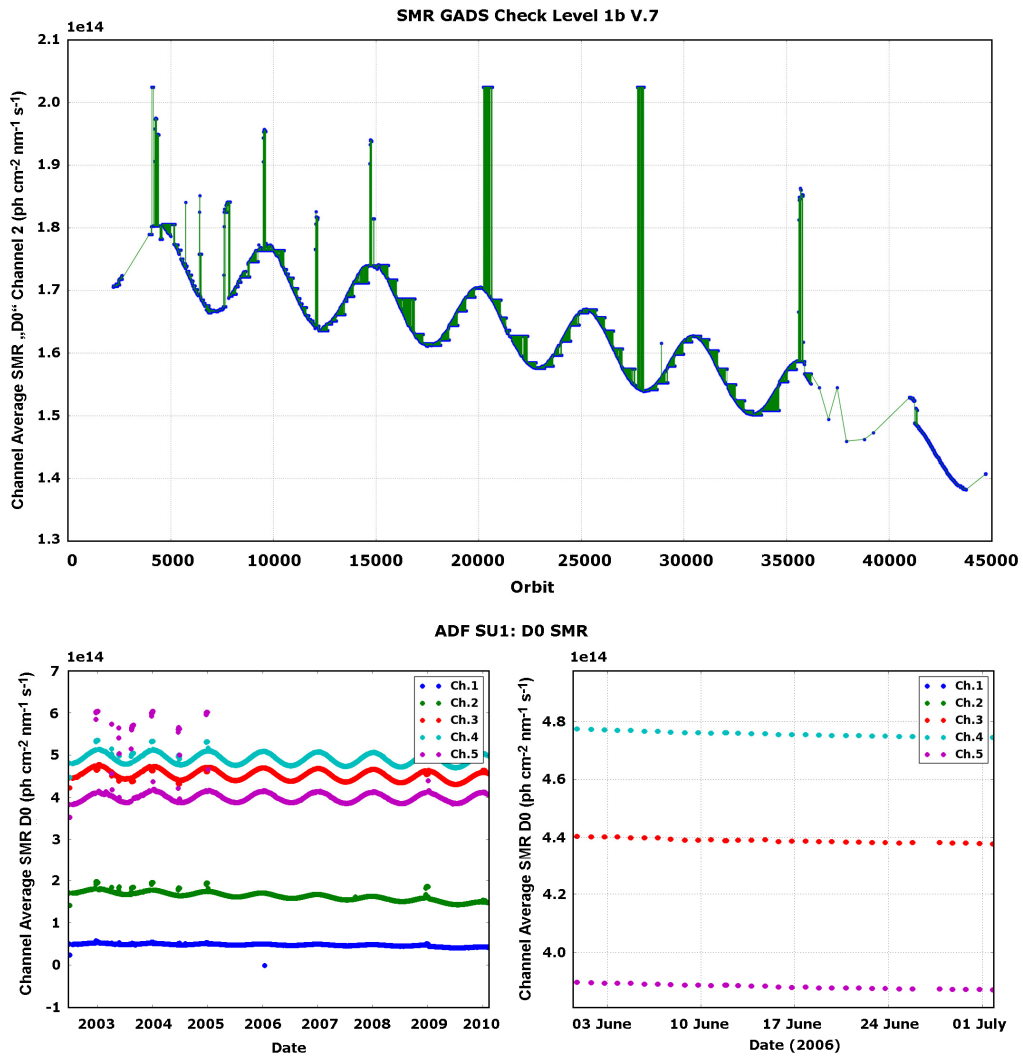


Fig. 2-1: Top: Average for SMR data in channel 2. It is obvious that for longer periods the average is constant, i.e. outdated data are used. Bottom: Re-generated SMR. Shown is the average value for the UV/VIS channels over the whole mission and a zoom to check for daily updates. The SMR data are now correctly updated.

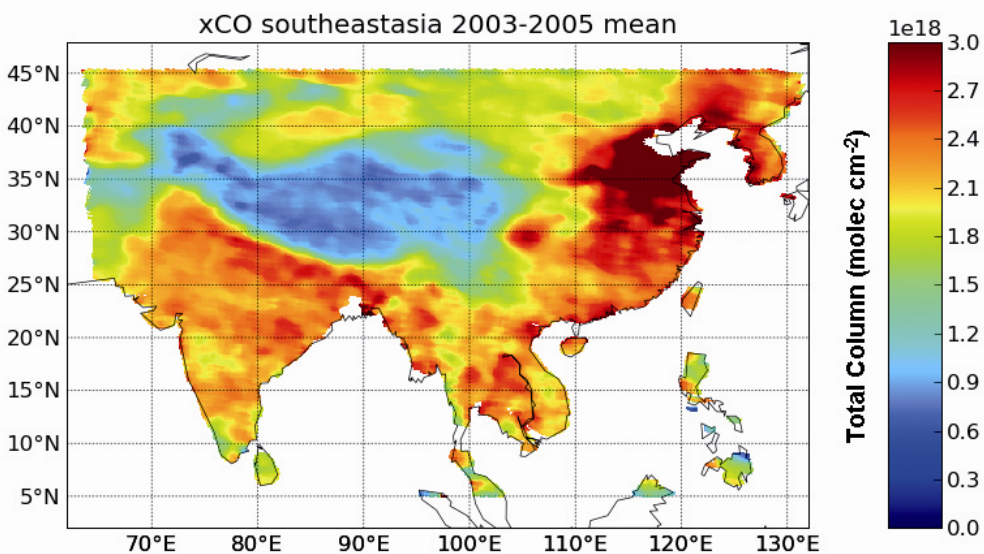


Fig. 2-2: Long term mean of CO total column (molec/cm²) over South-East Asia using the corrected algorithm (for details see text).

New operational level 0-1b processing chain

The main improvements for the level 0-1 chain included the implementation of a new scan mirror model and new calibration key data. The scan mirror model was developed by SRON and captures the scan angle dependent degradation of the mirrors. It was implemented and checked rather recently in November. Current tests investigate the impact of the change to the level 2 products. Additionally new key data were calculated from scratch by SRON to achieve a consistent set of calibration parameters. These were also implemented into the level 0-1 processor.

A new design for the SciCal tool for generating the calibration parameters was developed by us after it was discovered that outdated data can be fed into the operational chain (see above). Instead of calibrating the data and just write them to a file on hard disk, a proper database holding the calibration data will be implemented. The processing of the data will then be changed as follows:

- For re-processing:
 - Calculate all calibration parameters and put them into a database together with timing information (can be done in parallel).
 - Determine when a new ADF is needed. This depends on the measurement frequency of the measurements used for the calibration parameters which are combined into one ADF.
 - Fill the ADFs with proper entries from the database.
 - Set the validation start and stop from the calibration parameters written into a given ADF. The method needs to be defined such that the ground segment selection rules lead to a proper selection for the level 0-1b processing. The validation start and stop from the ADF will be fed back to the database in order to keep the association between measurements and ADFs.
 - The database will be kept on site for quality checking and problem tracking.
- For forward processing:
 - Calculate calibration parameters as measurement data arrive needed for the parameters and put them into a 'rolling' database, i.e. keeping only recent measurements. The retention time of old entries in the database depends on the update frequency.
 - Keep a log for recording the association of all measurements to validity start and stop of the generated ADF for problem tracking.

By introducing a database which stores all calibration data before writing them to the ADFs, the availability of the files on the file system is decoupled from the time needed for the processing of the calibration parameters. Thus one can choose always the optimal file for the ADF and for the ADF correction, e.g. for dark signals. The database also facilitates quality checking and ensures traceability of the ADF content.

New operational Level 1b-2 processing chain

During the last years, new products were added continuously to the operational processing. Table 2-1 below shows the products available now (Version 5). In addition it lists the products of the new version 6 which is planned for 2012. All products are developed by the Quality Working Group member institutes BIRA, DLR-IMF and IUP Bremen. The operational implementation occurs at DLR-IMF.

Apart from new trace gas columns for CH₄, CHOCHO and HCHO, tropospheric columns for NO₂ will be implemented. The latter will be the first operational product which makes use of the unique limb/nadir matching of SCIAMACHY: The observations are planned and executed such that the same air volumes are observed in limb and nadir geometry. Thus, in principle tropospheric columns can be derived by combining the information from limb stratospheric columns and nadir total columns. The limb/nadir matching algorithm will be implemented in a generic way to facilitate easy addition of other tropospheric columns at a later stage.

	Version 5	Version 6 (planned for 2012)
Nadir Products		
O₃	VCD	VCD
NO₂	VCD	VCD tropospheric from limb/nadir matching
SO₂	VCD (volcanic & anthropogen.)	VCD
OCIO	SCD	SCD
BrO	VCD	VCD
H₂O	VCD	VCD
CO	VCD	VCD
CH₄	-	VCD
CHOCHO	-	VCD
HCHO	-	VCD
Aerosol	Index	Index
Clouds	cover/top height/optical thickness	add snow/ice separation
Limb Products		
O₃	profile	add altitudes 40-65 km
NO₂	profile	profile
BrO	profile	profile
Clouds	water clouds/PSC detection	add NLC detection

Table 2-1: Nadir and limb products of the V5 and the planned V6 processing chain.

2.2 The Satellite Collocation Tool and Validation of the SCIAMACHY Ozone Profiles

D. Zlatkov (TUM), S. Hrechanyy, A. Doicu, G. Lichtenberg, T. Trautmann

Validation of trace gas constituents retrieved from SCIAMACHY measurements, both total columns or profiles, requires – among others – comparison with results from other satellite sensors. Owing to the large data sets, performing only individual comparisons is less favourable while covering different geographical regions and long time periods is the preferred approach. When using other space-borne sensor's data, their spatial relation with the SCIAMACHY results, i.e. the collocation, is one of the key parameters defining how well both data sets match. Some collocations tools are available from the World Wide Web, see e.g. <http://www.sat.ltu.se/projects/collocations/>. Unfortunately, they are either programmed using commercial languages or unsuited for our purpose of SCIAMACHY data product validation. Therefore a clear need for developing our own dedicated collocation tool together with our own database of ozone profiles measurements existed.

Ozone measurements database

Ozone profiles from the following sensors were used:

- SAGE III (from January 2003 to November 2005)
- HALOE (January 2003 to November 2005)
- LIDAR, Microwave and ozone sondes measurements performed in the frame of the Network for the Detection of Atmospheric Composition Change (NDACC). Geolocations and time periods of these measurements (LIDAR, microwave and ozone sondes) are listed in Table 2-2.

Station	Location	Latitude	Longitude	Data Period
LIDAR				
Andoya	Norway	69.3	16.0	01.2003 - 12.2007
Hohenpeissenberg	Germany	47.8	11.0	01.2003 - 03.2011
Observatoire Haute Provence	France	43.9	5.7	01.2003 - 03.2010
Tsukuba	Japan	36.1	140.1	01.2003 - 02.2010
Table Mountain	USA (California)	34.4	-117.7	01.2003 - 12.2010
Mauna Loa	USA (Hawaii)	19.5	-155.6	01.2003 - 12.2010
Lauder	New Zealand	-45.0	169.7	01.2003 - 04.2009
Microwave				
Mauna Loa	USA (Hawaii)	19.5	-155.6	01.2003 - 12.2010
Lauder	New Zealand	-45.0	169.7	01.2003 - 12.2009
Ozone Sondes				
Hilo	USA (Hawaii)	19.72	-155.0	01.2003 - 06.2010
Lauder	New Zealand	-45.0	169.7	01.2003 - 04.2009
McMurdo	Antarctica	-77.8	166.7	01.2003 - 10.2008
Natal	Brazil	-5.5	-35.3	01.2003 - 04.2007
Ny-Alesund	Norway (Spitzbergen)	78.9	12.0	01.2003 - 09.2010
Payerne	Switzerland	46.8	6.95	01.2003 - 12.2010
Samoa	Pacific	-14.2	-171.0	01.2003 - 06.2010

Table 2-2: Location and data availability of NDACC stations

Description of the tool

The modular collocation tool consists of individual modules, programmed using the Python language. While the tool runs on an user computer, each module communicates with the data server for reading, formatting and writing data. The ozone profiles measured by SCIAMACHY are the first products to be validated. To handle the different format and structure of the various sensors, separate reading functions had to be developed. They are all located in the module *readers.py*, whereas the *records.py* module contains an architecture of the file formats necessary for extracting the required information from a specific sensor.

The *GeoData.py* module extracts the geolocations, the time and the date of each individual measurement and saves this information into text files together with the input file name. One text file contains the geolocations from one month of measurements. These files are stored in a common directory where each sensor possesses its own subdirectory, e.g. all geolocations of the HALOE measurements performed in May 2005 could be found under */home/scia04/scia/Haloe/Geolocations/O3Haloe_2004_05.txt* file.

The *Geoloc.py* module searches for the collocated profiles. In order to be qualified as a collocation, the ozone profiles have to meet two criteria: The spatial distance between the profiles has to be less than 500 km with a temporal separation of less than 6 hours between the measurements. These criteria could be adjusted for each particular task. The collocation points are saved in text files with their time, date, latitude and longitude attributes, as well as the distance and the time difference between the two measurement points. The naming convention used for the collocation files is "YYYY MM SCIA SensorName.txt", e.g. collocations for SCIAMACHY and microwave stations for December 2004 could be found in */home/scia04/scia/GeoLoc/Results/2004_12_SCIA_MW.txt* file.

Finally the module *helpers.py* contains auxiliary functions required for the validation procedure, such as

- function *genSciaL1c*: Extracting calibrated radiances needed to retrieve ozone profiles by means of the SCIAMACHY scientific processor
- function *map2points*: Calculating a distance between two locations on the Earth's surface
- function *countLoc*: Counts number of collocation points

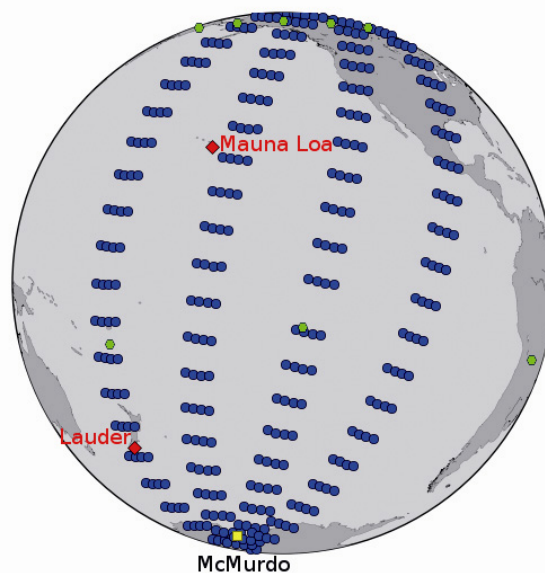


Fig. 2-3: Example of SCIAMACHY (blue circles) geolocations for September 23rd, 2003 with microwave stations at Mauna Loa, Hawaii and Lauder, New Zealand (red), HALOE satellite (green) and ozone sonde station at McMurdo, Antarctic (yellow).

It is planned to expand the tool by developing a graphical user interface, by adding plotting functionalities (Fig. 2-3) and by providing statistics options.

2.3 SCIAMACHY Operations Support

M. Gottwald, E. Krieg (TwIG), K. Reissig (IBR), J. How (TwIG), S. Noël (IUP-IFE), K. Bramstedt (IUP-IFE)

With the end of 2011 SCIAMACHY has finished its 10th year in orbit. Throughout this period the SCIAMACHY Operations Support Team (SOST), formed by personnel from IMF-AP and IUP-IFE/University of Bremen played a major role in making this mission a great success.

Together with colleagues from the Quality Working Group (SQWG) and ESA (flight operations at ESOC, post launch support at ESTEC and payload data segment at ESRIN) SOST ensured that the instrument performance remained at a very high level (Fig. 2-4 and 2-5). This includes the overall availability where only 160 orbits were lost due to one platform and 6 instrument anomalies. 4 of them were triggered by a ground segment deficiency while the rest was instrument related. All instrument related events could be attributed to Single Event Upsets (SEU), i.e. high energy particles impinging onto instrument electronic components. The overall availability reached, as in 2010, the high value of 97%.

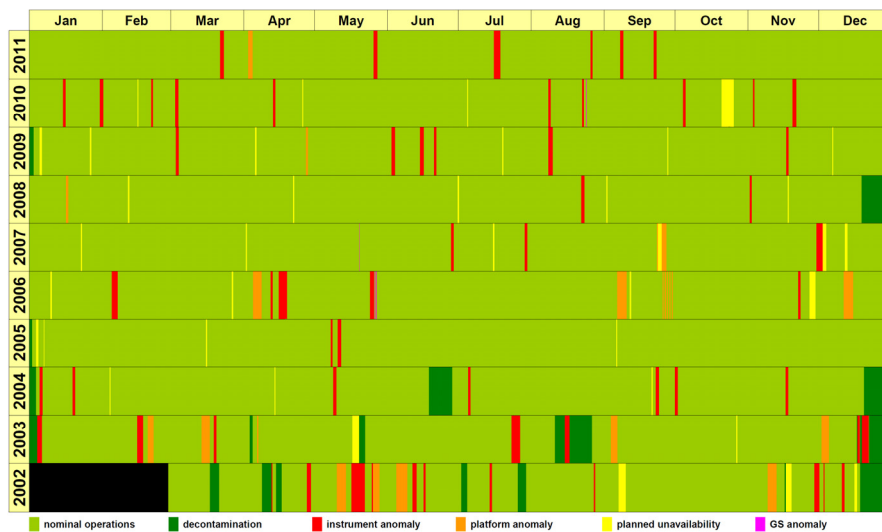


Fig. 2-4: Instrument availability since launch

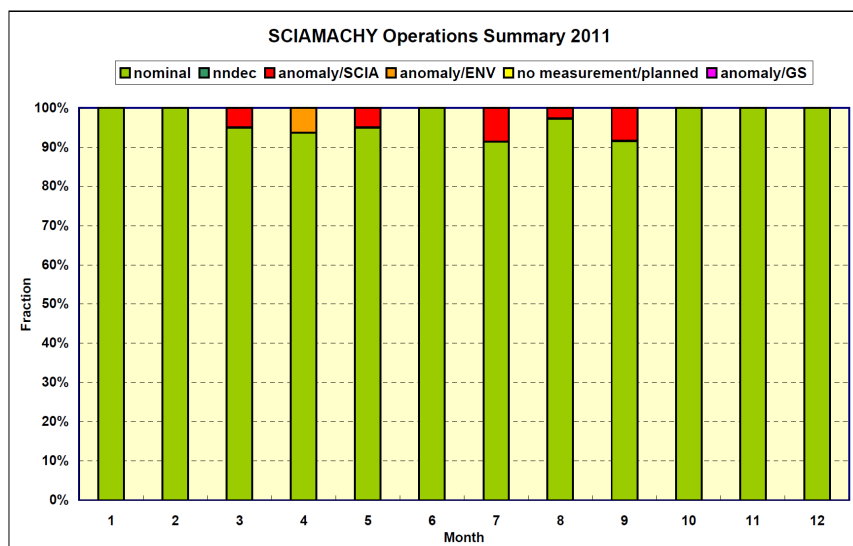


Abb. 2-5: Instrument availability in 2011 on a monthly basis

Operation Change Requests

Two *Operation Change Request (OCR)* had to be implemented. The first fine-tuned the final flight configuration parameter settings of the Basic Scan Profile table to fully comply with the orbit lowering executed in October 2010. The second targeted the bright planets Venus and Jupiter when they rose just in flight direction in early May 2011. Such a particular viewing geometry aimed at gaining not only scientific information about planetary atmospheres but also support line-of-sight studies. While Jupiter turned out to be too faint to be detected this OCR added another 3 minutes of Venusian atmospheric data to the SCIAMACHY record. This time the illuminated part of the disk of Venus amounted to more than 80% as compared to 3% and 50% in 2009.

Routine Operations

Routine operation execution continued as required and planned. Great care was put on the monitoring of instrument subsystems. In early 2011 the optical throughput in channels 1-5 began to recover. This trend was maintained throughout the year. No final conclusion about its cause exists yet. However this behaviour is a clear indication that careful monitoring is a must in long-duration space missions since unexpected phenomena may occur occasionally. All results were made available via the SOST webpages (<http://atmos.af.op.dlr.de/projects/scops/>).

Operations 2014+

The current mission extension phase terminates at the end of 2013. Since the ENVISAT platform together with the payload instruments still perform very well and the next generation of Europe's EO missions, e.g. the Sentinels, will only become operational in the not too near future, ESA is considering to operate ENVISAT even further (2014+). SOST has studied the present instrument performance (optical, thermal, LoS pointing, Life Limited Items and anomaly occurrence) and extrapolated the findings beyond 2014 until 2018. This investigation demonstrated that SCIAMACHY can provide valuable data well into the future for many more years to come. Particularly the unique limb and occultation viewing geometries, absent on the future atmospheric missions, should therefore be exploited as long as possible.

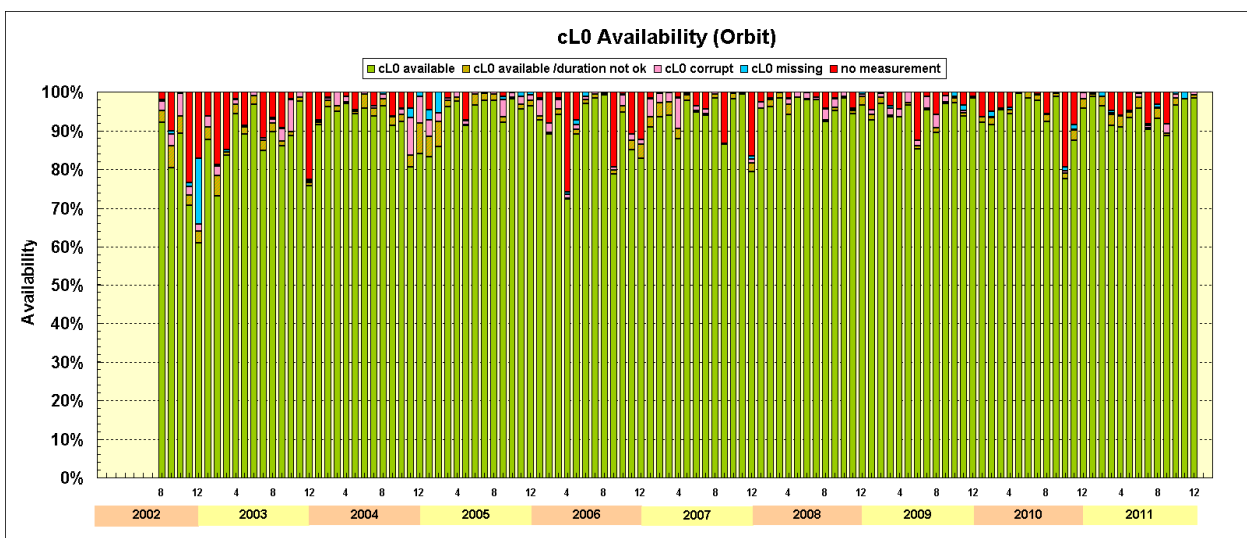


Fig. 2-6: cL0 statistics for the years 2002-2010 (final) and 2011 (preliminary).

Consolidated Level 0 Master Archive

Maintenance of the master archive of consolidated level 0 (cL0) data in the environment of the Data Information Management System (DIMS) of the German Remote Sensing Data Center (DFD) was continued. This archive serves as a cL0 reference and supports SCIAMACHY product debugging in ENVISAT's Payload Data Segment (PDS). Consolidated level 0 data are regularly transferred to DIMS once they passed a sequence of checking routines thus verifying the overall integrity of the cL0 products. By the end of 2011 more than 50000 cL0 products have been quality checked and transferred to DIMS. The statistics for the years 2002-2011 is displayed in Fig. 2-6. The detailed cL0 availability on single orbit level is given at the SOST website (<http://atmos.caf.dlr.de/projects/scops/>).

2.4 Hard Drive Encryption

D. Scherbakov, G. Lichtenberg, T. Trautmann

Recent advances in computer technology, increases in data transfer speed and certification of fast encryption algorithms like the Advanced Encryption Standard (AES) have enabled software and hardware solutions performing on-the-fly encryption of user data. Now every user has a possibility to protect all own data before being written to a hard drive without introducing a noticeable speed penalty.

Full disk encryption (DE) is aimed at protecting personal and company data from unauthorized access, e.g. when the Hard Disk Drive (HDD) gets stolen. It can be seen as an addition layer of protection with certain advantages and shortcomings. Under DE users mean that at least one partition or the whole hard drive is completely encrypted. In order to get access to the partition the user is required to have an access key which he supplies to an encryption/decryption software or hardware. In turn, this device or application performs all necessary operations in a way absolutely transparently to the user.

Available data encryption solutions

Available disk encryption options can be characterized by the following properties:

- software- or hardware-based
- implementation and maintenance cost
- solution performance
- location of a key file

In the following table 2-3 all options are combined side-by-side:

Encryption option	Number of keys	Approx. cost	Performance penalty	Key location	Reliability
Software-based disk volume encryption	many	free or cheap	moderate to none	inside or outside	C
Software-based whole disk encryption	one	free or cheap	moderate to none	outside	B-
Hardware-based outside storage device	one	very expensive	almost none	outside	B+
Hardware-based within storage device	one	expensive	none	outside	A

Table 2-3: Encryption options characteristics

Master Boot Record		
Partition 1	256 MB	Linux boot (/boot)
Partition 2	60 GB	Windows
Partition 3	2 GB	Linux swap
Partition 4	37 GB	Linux root (/)

Table 2-4: Laptop configuration for software-based disk volume encryption example (see text)

Software-based disk volume encryption

Under the assumption that all data and as much partitions as possible shall be encrypted with open-source freely available applications, for a laptop with a 100 GB hard drive having Windows and Linux installed (see table 2-4), implementation of a software-based disk volume encryption using open-source tools would require the steps listed below. Note that because of the two operating systems,

implementation of the encryption is required for both separately. Moreover, decryption software needs to be running before the system is booted.

For Linux, booting may either occur from an external device like USB stick or use the */boot partition*. In both cases the Linux kernel has to be setup for being able to read the encrypted partition. This setup step must usually happen in *initrd*. Otherwise the system will initialize, but will be unable to find a root partition to continue *boot phase*. In that situation either */boot* partition located on the hard drive or on the USB-stick must remain unencrypted, thus open for tampering, forcing us to implement additional protective measures for our secret encryption key. The following methods exist:

- *Password-protected secret key*: The secret key is protected by a password. One could encrypt it, e.g., with another symmetric key derived from a long pass-phrase. In this case security of our data relies solely on length and complexity of a pass-phrase.
- *Smart-card with PIN*: Keys are stored or derived using a smart-card. For gaining access to the encrypted partition, the user must not only obtain a laptop, but also the smart-card and the user defined PIN.
- *Biometric authentication*: Many modern laptops are quipped with a fingerprint reader, usually a very suitable solution for moderate security measures. However not all fingerprint readers are as secure as they should be. Moreover, fingerprints may easily be copied.
- *Using dongle*: This is a variant of an USB-stick. It is a very interesting solution under the assumption that the user can ensure that the dongle is not stolen or if the contents are encrypted or protected by a pass-phrase.
- *Using boot-time driver or the whole operating system that asks for password*: Security of this method relies on the security of a network location, where the boot image resides, and a security of the network transmitting the boot image to the user.
- *Using network interchange to recover key*: This is mainly a variation of the previous method, e.g. 802.1X authentication in Active Directory.
- *Using Trusted Platform Module to store the key*

Once an authentication method is chosen, the Linux root partition has to be encrypted:

- Boot a live CD and backup the root partition to the external hard drive.
- Fill the root partition with random data to overwrite contents and to randomize encrypted content.
- Setup the core of the Linux encryption – a special loop device. The encryption algorithm, underlying physical partition and an encryption key have to be specified.
- Create a partition on the loop device and mount it.
- Copy contents of the root partition on the encrypted loop device.
- Prepare */boot* partition and set it up according to manual.
- Reboot into Linux and verify that system boots and uses encrypted volume.
- Shred the contents of the root partition which had been copied to the external device.

After encryption of the Linux partition has been completed, one may start the Windows part. Almost the only available option for Windows OS is TrueCrypt. One of its requirements is that it must be installed into Master Boot Record (MBR) before any other software takes control of the hard drive. As outlined in the TrueCrypt manual, user authentication for TrueCrypt can only be a pass-phrase. As soon as TrueCrypt boots, it will ask for a password. If <Esc> is pressed, TrueCrypt will pass control to the next available boot partition – Linux, allowing dual-booting two encrypted systems on the same machine.

Implementation of drive encryption with password authentication seems to be more complex than it is in reality. TrueCrypt performs automatically and in Linux only the manual has to be followed.

Hardware-based disk encryption

A much preferred solution is to use a hard drive that supports encryption of user data within itself. In this case the hard drive will be protected by a key generated from a pass-phrase entered during BIOS initialization and encryption will be performed absolutely transparent for all operating systems installed. Drawbacks of this solution are that it is not supported by all BIOS versions and full-drive-encryption hard drives cost considerably more than normal ones.

A 'real world' example

In July 2008, several TrueCrypt-secured hard drives were seized from Daniel Dantas, who was suspected of financial crimes. The Brazilian National Institute of Criminology tried for five months to obtain access to TrueCrypt-protected disks owned by the banker without success, after which they enlisted the help of the FBI. The FBI used dictionary attacks against Dantas' disks for over 12 months, but were still unable to decrypt them.

3. Atmospheric Remote Sensing – Retrieval Methods

3.1 SCIAMACHY Methane Retrievals

S. Gimeno García (TUM), F. Schreier, G. Lichtenberg, M. Meringer, B. Aberle, S. Slijkhuis

Methane (CH₄) is the third most important greenhouse gas representing 1/5 of the whole radiative forcing of long-life well-mixed gases. Its concentration has increased by more than a factor of two since the pre-industrial era with a growth rate of roughly 1% per annum. Atmospheric methane is produced by anthropogenic activities, e.g., agriculture, fossil fuel combustion, etc; as well as by natural sources, for instance at wetlands and geological processes. The atmospheric methane life time is about 10 years and its concentrations present smooth spatial and temporal variations. Thus, methane variability is difficult to observe and, consequently, the required retrieval precision is much higher than in case of short- to medium-life gases such as nitrous oxide or carbon monoxide.

With passive atmospheric remote sensing, methane can be observed in several spectral regions, ranging from the thermal to the near infrared. CH₄ is a target species of several space-borne instruments: AIRS (Zhang *et al.* 2011), MOPITT, and TES (Payne *et al.* 2009) from NASA's nadir sounders aboard the EOS satellite series; MIPAS (Payan *et al.* 2007) and SCIAMACHY (Buchwitz *et al.* 2005, Frankenberg *et al.* 2006, Gloudemans *et al.* 2008) on ESA's ENVISAT mission. More recently, it has also been observed by IASI on MetOp (Razavi *et al.* 2009). Furthermore, it is one of the two target gases of the TANSO Fourier transform spectrometer onboard the GOSAT satellite (Kuze *et al.* 2009).

The retrieval code BIRRA (Beer InfraRed Retrieval Algorithm) has been developed for the operational level 1b-2 processing of SCIAMACHY data. BIRRA performs a (separable) nonlinear least squares fit of the measured radiance, where molecular concentration vertical profiles are scaled to fit the observed spectra. For methane retrievals, two microwindows in SCIAMACHY's channel 6 are selected: the interval 1629-1670 nm (5986-6139 cm⁻¹) which has CH₄ as the strongest absorber, and the interval 1557-1594 nm (6273-6419 cm⁻¹) which has carbon dioxide (CO₂) as the strongest one. Additionally, water vapor (H₂O) is included as an additional absorber in both windows. The instrumental response function is considered to be a Gaussian slit with HWHM fixed to 0.67 nm (2.45 cm⁻¹) in the first and to 0.66 nm (2.64 cm⁻¹) in the second window. Surface albedo is fitted to a second degree polynomial.

Scattering is neglected in the BIRRA forward model. Hence, the photon path corresponds to the geometrical path which solar light travels from the top of the atmosphere to the Earth's surface and which the reflected light travels from the surface up to the observer. However, the measured radiance has a high probability of having also a fraction coming from scattering events in the atmosphere, and consequently, having a photon path different from the pure geometrical one. In addition, the atmospheric conditions are set a-priori to climatological datasets but the actual meteorological conditions, e.g. pressure, temperature, at the time of the observations are unknown. Furthermore, the quality of the observed spectra has a considerable impact on the fitted scaling factors of the atmospheric constituents.

In order to account for these unconsidered effects, the results of the retrieved methane are presented as 'proxy'-normalized *column mixing ratios* instead of the direct retrieved *mixing ratios*. As proxy, it is typical to select a fit parameter which contains information about the unaccounted issues. A good candidate is CO₂. It is more homogeneous than methane, both vertically and horizontally. Moreover, the absorption signatures of the CH₄ and CO₂ species are of comparable magnitude in channel 6, and so are their retrieval altitude sensitivities. So the deviations of CO₂ concentrations from the a-priori can then be interpreted as the effect of the unconsidered processes and not due to CO₂ sources and sinks.

Considering the arguments presented above, the methane *dry-air column mixing ratio* can be defined as

$$XCH4 = q_{CH4}^{prior} \times \frac{a_{CH4}}{a_{CO2}}$$

where q_{CH4}^{prior} is the a-priori column mixing ratio of CH₄, a_{CH4} and a_{CO2} are the scaling factors of CH₄ and CO₂, respectively.

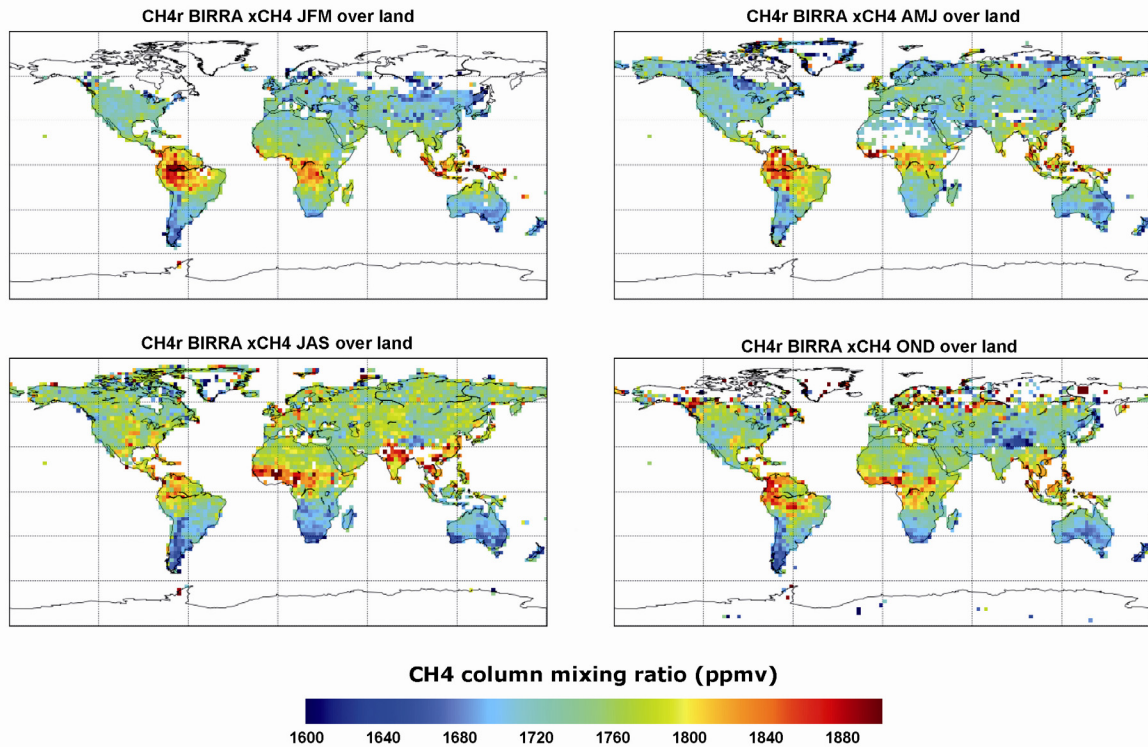


Fig. 3-1: Quarterly means of the year 2004 of methane column mixing-ratio (ppmv). In view of the reduced signal over oceans, methane is only plotted over land. The methane data was gridded into a $2^\circ \times 2^\circ$ scheme.

Fig. 3-1 illustrates trimonthly averages of methane column mixing ratios in the year 2004. Regions of strong emissions, e.g. the northern South America and the equatorial region of Africa are clearly visible and reflect patterns found by, e.g. *Frankenberg et al. 2006*, *Schneising et al. 2009*. The increased CH₄ emissions in South Eastern Asia during the period July-August-September, mainly due to rice cultivation, is evident. Furthermore, the plot shows the seasonal shift of methane emissions over wetlands from the southern to northern African intratropical region, and back.

References

Buchwitz M., de Beek R., Noël S., Burrows J.P., Bovensmann H., Bremer H., Bergamaschi P., Korner S., and Heimann M.: Carbon monoxide, methane and carbon dioxide columns retrieved from SCIAMACHY by WFM-DOAS: year 2003 initial data set, *Atm. Chem. Phys.*, 5, 3313–3329, doi:10.5194/acp-5-3313-2005, 2005

Frankenberg C., Meirink J.F., Bergamaschi P., Goede A.P.H., Heimann M., Korner S., Platt U., van Weele M., and Wagner T.: Satellite cartography of atmospheric methane from SCIAMACHY on board ENVISAT: Analysis of the years 2003 and 2004, *J. Geophys. Res.*, 111, D07 303, doi:10.1029/2005JD006235, 2006

Gloudemans A., de Laat A., Schrijver H., Aben I., Meirink J., and van der Werf G.: SCIAMACHY CO over land and oceans: 2003-2007 interannual variability, *Atm. Chem. Phys.*, 9, 3799–3813, doi:10.5194/acp-9-3799-2009, 2009

Kuze A., Suto H., Nakajima M., and Hamazaki T.: Thermal and near infrared sensor for carbon observation Fourier-transform spectrometer on the Greenhouse Gases Observing Satellite for greenhouse gases monitoring, *Appl. Opt.*, 48, 6716-6733, doi:10.1364/AO.48.006716, 2009

Payan, S., Camy-Peyret C., Oelhaf H., Wetzell G., Maucher G., Keim C., Pirre M., Huret N., Engel A., Volk M., et al.: Validation and data characteristics of methane and nitrous oxide profiles observed by mipas and processed with version 4.61 algorithm, *Atmospheric Chemistry and Physics Discussions*, 7 (6), 18,043–18,111, 2007

Payne V.H., Clough S.A., Shephard M.W., Nassar R., and Logan J.A.: Information-centered representation of retrievals with limited degrees of freedom for signal: Application to methane from the Tropospheric Emission Spectrometer, *J. Geophys. Res.*, doi:10.1029/2008JD010155, 2009

Razavi A., Clerbaux C., Wespes C., Clarisse L., Hurtmans D., Payan S., Camy-Peyret C., Coheur P., et al.: Characterization of methane retrievals from the iasi space-borne sounder, *Atmospheric Chemistry and Physics*, 9(20), 7889-7899, 2009

Schneising O., Buchwitz M., Burrows J.P., Bovensmann H., Bergamaschi P., and Peters W.: Three years of greenhouse gas column-averaged dry air mole fractions retrieved from satellite – Part 2: Methane, *Atm. Chem. Phys.*, 9, 443–465, doi:10.5194/acp-9-443-2009, 2009

Zhang X., Bai W., Zhang P., and Wang W.: Spatiotemporal variations in mid-upper tropospheric methane over china from satellite observations, *Chinese Science Bulletin*, 1-7, 2011

3.2 Assessment of Independent Macrophysical Cloud Properties in the Oxygen A-Band

O. Schüssler, D. Loyola, A. Doicu, R. Spurr (RTS)

Precise information about clouds is rather important for the retrieval of atmospheric trace gases, especially in the troposphere. Therefore we investigated the number of independent macrophysical cloud properties that can be retrieved from the O₂ A-band, in the context of trace gas retrievals.

The cloud parameter retrieval assumes a single homogeneous cloud layer characterized by fractional cloud cover (CF), cloud-top height (CTH), cloud geometrical thickness (CGT) and cloud optical thickness (COT). Additional information required for the retrieval of cloud properties includes the surface properties, the viewing geometry and the pressure and temperature distribution.

To assess the retrieval feasibility, we use a set of simulated spectra in the wavelength range of 758-770 nm, for different combinations of cloud, surface and geometry parameters. The inversion is performed by using Tikhonov regularization with an *a priori* parameter choice method. Values of the condition number, defined as the ratio between the largest and the smallest values of the Jacobian matrix, are analyzed and the degree of ill-posedness is evaluated for retrievals involving multiple (four, three and two parameters) and a single cloud parameter.

Simulations and results

In the ideal case the goal is simultaneous retrieval of all four parameters describing the cloudy atmosphere. The condition number values and the absolute errors of the retrieval for each parameter are depicted in the Fig. 3-2.

High values of condition number indicate that a small change in the measurement leads to large changes in the solution of the retrieval problem. From the Fig. 3-2 (right) it can be seen that all four retrieved parameters have too high errors, as information, contained in the O₂ A-band spectra, is not enough to extract all of them simultaneously.

For the next step we assume that the cloud fraction value is known and consider the retrieval problem for cloud-top height, cloud geometrical thickness and cloud optical thickness. The condition number values for this problem and corresponding absolute errors of the retrieved parameters are shown in the Fig. 3-3. As condition number values for this retrieval problem are also very high, this retrieval problem is also highly ill-posed. The retrieved values of cloud optical thickness are of acceptable accuracy, but the errors of the cloud geometrical thickness and cloud top height are excessively high.

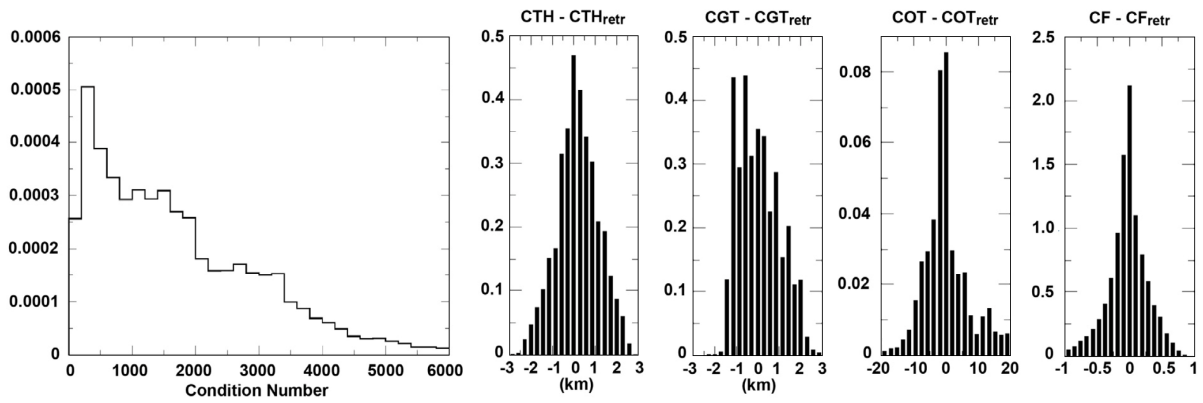


Fig. 3-2: Condition number values for the CTH, CGT, COT and CF retrieval (left) and retrieval errors for CTH, CGT, COT and CF (right).

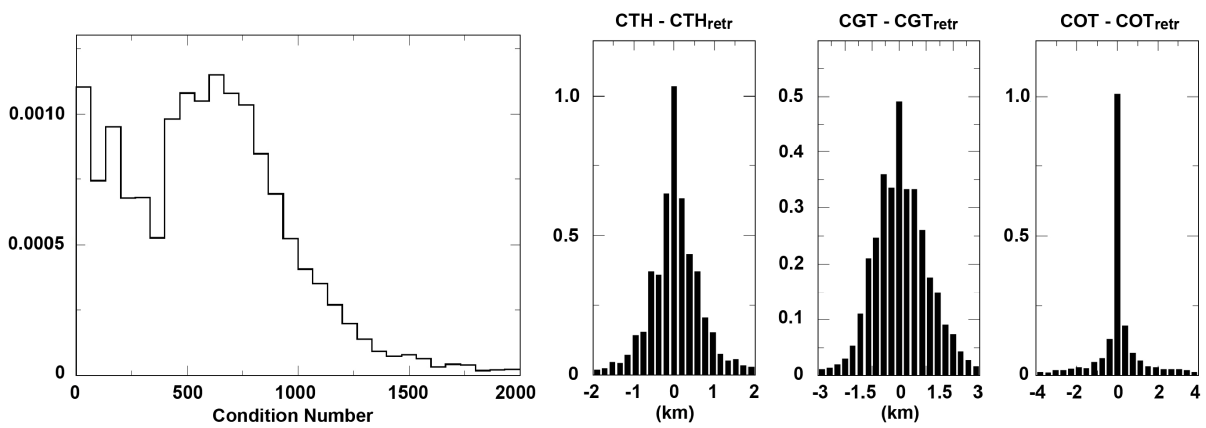


Fig. 3-3: Condition number values for the CTH, CGT and COT retrieval (left) and retrieval errors for CTH, CGT and COT (right).

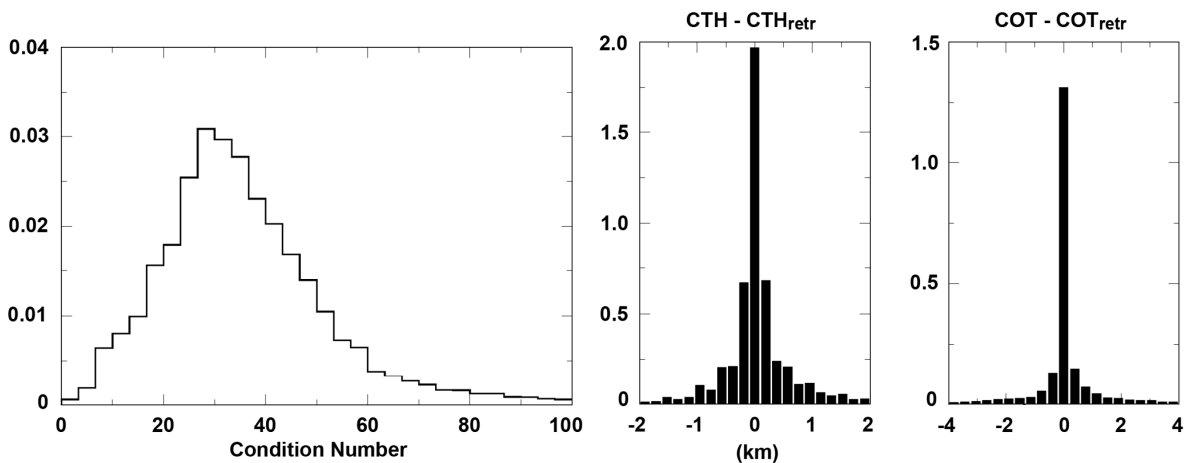


Fig. 3-4: Condition number values for the CTH and COT retrieval (left) and retrieval errors for CTH and COT (right).

In the next step we retrieve two parameters. Condition number values and retrieval errors for CTH and COT are depicted in the Fig. 3-4. Condition number values indicate that the retrieval problem is slightly ill-posed and needs a little amount of regularization. The errors of the retrieval are acceptable.

For the retrieval of CTH and CF the condition number values and corresponding retrieval errors are shown in the Fig. 3-5. As in the case of CTH and COT retrieval, the problem is slightly ill-posed and the retrieval of the CTH and CF is of acceptable accuracy.

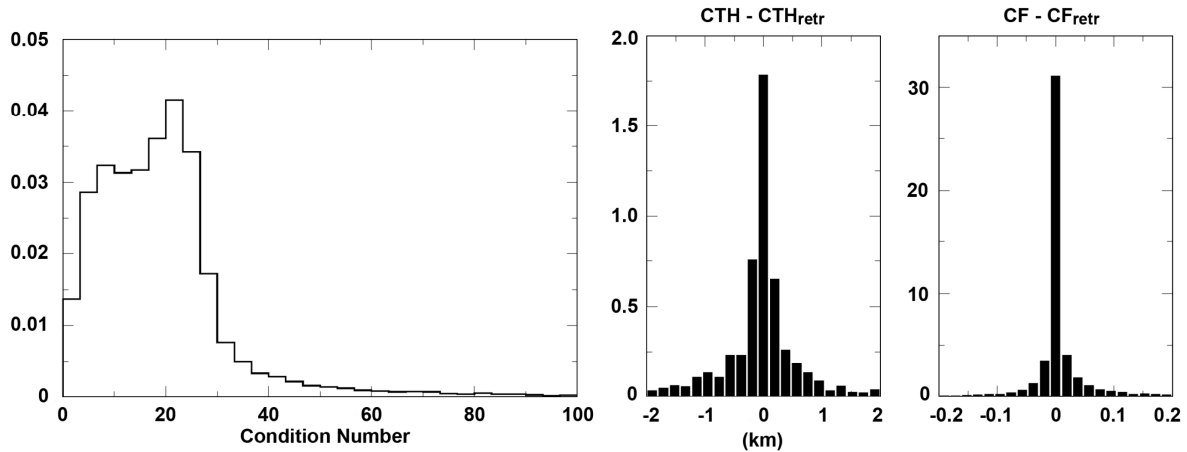


Fig. 3-5: Condition number values for the CTH and CF retrieval (left) and retrieval errors for CTH and CF (right).

Conclusions

In summary our analysis confirmed that the number of independent macrophysical cloud properties that can be retrieved from the O_2 A-band simultaneously is limited. The information contained in the O_2 A-band spectra is sufficient for retrieving only two independent cloud parameters. Best results are obtained for the joint retrieval of cloud-top height and cloud fraction, or of cloud top height and cloud optical thickness.

3.3 Multi-Dimensional Radiative Transfer

A. Doicu and T. Trautmann

The upcoming GMES (Global Monitoring for Environment and Security) atmospheric satellite mission Sentinel 5 Precursor will detect atmospheric trace gases with a considerably enhanced spatial resolution of $7 \times 7 \text{ km}^2$ at sub-satellite point. Despite the fact that the spatial resolution will be much higher than with current spectrometric sensors, for the atmospheric column over each pixel the chances will increase that neighboring cloudy pixels will also contribute light due to lateral light transport. Thus, for developing enhanced trace gas retrieval methods the need to complement the widely used one-dimensional radiative transfer models with information on multi-dimensional radiative transfer (RT) effects becomes obvious.

The approaches for solving the multi-dimensional radiative transfer equation (RTE) can be divided into deterministic and stochastic methods. From the class of deterministic methods we distinguish direct methods, based on the differential form of the RTE, and iterative methods, based on integral form of the RTE.

Direct deterministic methods for solving the RTE

The first category includes methods that treat the horizontal variables directly or via the Fourier transform. For the methods in which the horizontal variable is treated directly, the finite difference scheme is used to approximate the partial derivatives. The spatial part of the radiance field is represented with a discrete grid. For the angular part of the field, discrete ordinate representation or a spectral approach, such as the spherical harmonic spatial grid method, are employed. In the *Fourier-Ricatti* method, the partial differential equation is converted to a set of ordinary differential equations by Fourier transforming the horizontal variable dependency to the spectral domain. The DLR multi-dimensional RT code is based on the finite element method. The main steps of the finite element method can be summarized as follows:

- discretize the domain of analysis with simple preselected finite element-grid generations
- derive the element or the cell equation from the governing equation
- assemble the element equations to obtain the algebraic system of the entire problem
- impose the boundary conditions
- solve the assembled system of equations

In the case of atmospheric radiative transfer, the discretization process consists in a discretization of the spatial domain using rectangular cells and a discretization of the angular domain using discrete ordinates. The cell equation is obtained by using the *Galerkin* method or the integral and finite difference form of the RTE. The assembled system of equations relates the radiances at the lower and upper boundary of the domain. This technique reduces the computation time versus the global system solution. The assembling of cell equations consists in a simple addition of each equation. For the solution of the assembled system of equations, direct or iterative methods can be used.

Iterative methods for solving the RTE

The integral equation of the RT problem is exploited by the *Picard* iterative method. This method, which is a successive order of scattering solution method, computes the radiance field on a discrete spatial grid with the angular distribution represented along discrete ordinates or in a spherical harmonic series. One of the most efficient computer programs used to model general three-dimensional atmospheric radiative transfer is based on the Spherical Harmonic's Discrete Ordinate Method (SHDOM). The following peculiarities of the SHDOM can be evidenced:

- The RT source function is computed on a discrete spatial grid with the angular distribution represented in a spherical harmonic series. The spherical harmonic representation saves memory because with the adaptive series truncation only the required number of spherical harmonics is stored at each grid point.
- The iterative solution method
 - 1) transforms the source function to discrete ordinates
 - 2) integrates the source function along the discrete ordinates to compute the radiance field
 - 3) transforms the discrete ordinate radiance to spherical harmonics
 - 4) computes the source function from the radiance field in spherical harmonics.
- The radiance and source function are initialized before the solution iterations with an Eddington RT solution on independent columns of the base grid.
- An acceleration method is implemented to speed convergence in optically thick, scattering media.
- An adaptive grid is implemented to add grid points where they are most needed during the solution iterations.

Additional features for the SHDOM method

The DLR multi-dimensional RT code incorporates the SHDOM method and contains some additional features:

- In step 2) of the iterative process, the radiance field can be computed by using finite-difference schemes, or by employing the *Galerkin* method. As compared to the source function integration method, these techniques reduce the computer time for optically thin media.
- The radiance and source function are initialized with a discrete ordinate solution based on matrix exponential formalism.
- Several acceleration methods as for example, Anderson mixing, biconjugate gradient, conjugate gradients squared and Bi-CGSTAB have been implemented.
- The code enables the computation of an independent column solution in which the direct solar radiation is treated in an inhomogeneous atmosphere, the base grid values of the radiance and sources are computed on independent columns by using the discrete ordinate method with matrix exponential, while the output radiances are computed by employing the source integration technique in an inhomogeneous atmosphere.

3.4 Current Status and Recent Results of TELIS Retrievals

J. Xu, F. Schreier, A. Doicu, P. Vogt (IMF-EV), T. Trautmann

TELIS (TErahertz and submillimeter Limb Sounder) is a balloon-borne cryogenic heterodyne spectrometer. It was mounted on a stratospheric balloon gondola together with the MIPAS-B (Michelson Interferometer for Passive Atmospheric Sounding – Balloon) instrument. TELIS has completed three successful scientific flights in Kiruna from 2009 to 2011. Thus, we have developed a retrieval code PILS (Profile Inversion for Limb Sounding) dedicated to high resolution infrared (IR)/microwave radiative transfer calculation and reliable inversion strategy with the aim of retrieving the vertical distribution of trace gases from the TELIS measurements.

The ambitious spectral coverage of the instrument is accomplished by use of three channels being provided by three scientific facilities: 500 GHz (RAL), 480-650 GHz (SRON), and 1.8 THz (DLR). Based on preliminary tests on the DLR channel, the main systematic component of the retrieval error was found to be the neglect of the non-linearity of the radiometric gain in the calibration procedure. It can lead to a retrieval error up to 30 % without non-linearity correction. Currently, the calibration with non-linearity correction has been implemented on the measurements of the SRON channel for the 2010 flight.

Regarding the multi-profile inversion, we utilize Tikhonov regularization for ill-posed nonlinear least squares problems. The regularization parameter is defined as a set of local parameters $\alpha = [\alpha_1, \alpha_2, \dots, \alpha_n]^T$ in connection with each fit target, such enabling to constrain every target properly and to obtain a physically meaningful solution. Consequently, the global regularization matrix will be expressed as

$$H = \begin{bmatrix} \sqrt{\alpha_1} L_1 & 0 & \dots & 0 \\ 0 & \sqrt{\alpha_2} L_2 & \dots & 0 \\ \vdots & \vdots & \ddots & \vdots \\ 0 & 0 & \dots & \sqrt{\alpha_n} L_n \end{bmatrix}$$

We make use of a sequence of spectra in one limb scan measured by the SRON channel on January 24, 2010. The main target species of this microwindow are O₃, HCl, ClO, and H₂O. In addition, a baseline polynomial is retrieved for each spectrum to remove radiance offsets. In order to investigate the performance of PILS, we select MIPAS-B, SMILES, and MLS (Microwave Limb Sounder) retrievals as reference profiles.

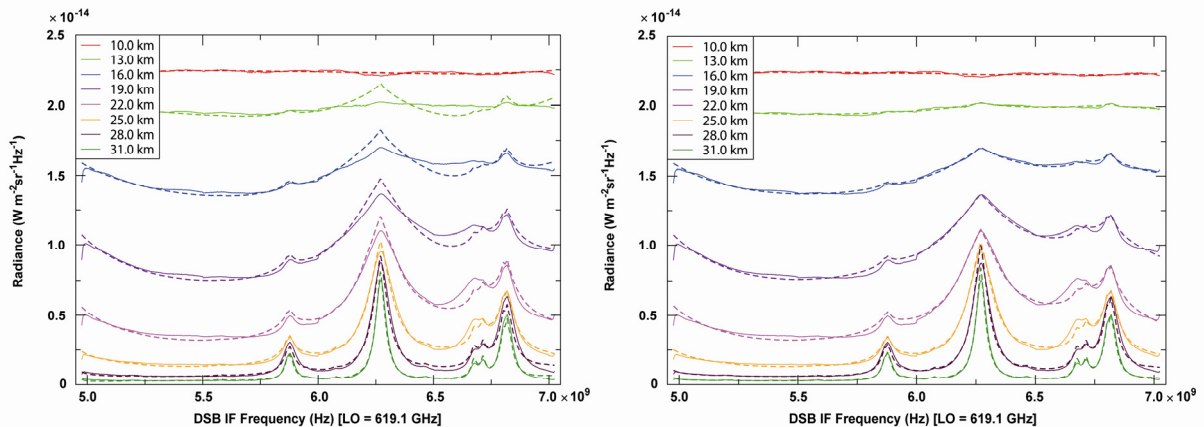


Fig. 3-6: Comparisons of model spectra after retrieval (dash) with actual measurements (solid). The left/right displays are explained in the text.

Greybody effect

Water vapor has a large number of very strong spectral lines in the millimeter and submillimeter spectral range. Even if one assumes that the water vapor profile is exactly known, the error introduced by the uncertainty in the continuum model creates a fairly large error in the retrieval of other species. In order to compute simulated limb sounding spectra with more precise continuum information, an additional

artificial molecule, so-called *greybody*, can be achieved accounting for the continuum-like part at each retrieval altitude. The left plot in Fig. 3-6 illustrates the comparisons of model spectra after retrieval without greybody fitting with the TELIS measurements, while the right one demonstrates that the high bias over the ozone lines at lower tangent altitudes can be removed by joint-fitting of this greybody.

Temperature error propagation

In our case the assumed model temperature profile has limited accuracy and may therefore introduce a considerable error. The temperature profile is therefore taken from the MIPAS-B retrievals, and the ozone retrieval result is shown in Fig. 3-7 (top). Besides, we compare the result with those obtained by

using the subarctic winter model temperature, and a model temperature decreased by 10 K. The dashed horizontal line serves as an indication of the observation height of the instrument.

Pointing offset

In general the uncertainty in the pointing of the instrument contributes significantly to the error budget in limb retrievals, hence it is necessary inspecting its impact on the retrieval. In our case, the estimated offset is up to 6 arcmin downwards. As displayed in Fig. 3-7 (bottom), the ozone retrieval seems to be decreased by 15-30 %, and the effect on the retrieval is highest for the altitude of 22 km.

Summary

Based on these results, PLS appears to generate reasonable retrieval results from the TELIS measurements. However, consolidation of the instrument parameters, such as sideband ratios, pointing information, and instrumental line shape is still required. An intercomparison of retrieval results between SMILES and TELIS is currently ongoing. In future, the calibrated measurements of the DLR channel will be used to study the concentrations of other trace species, such as CO and OH.

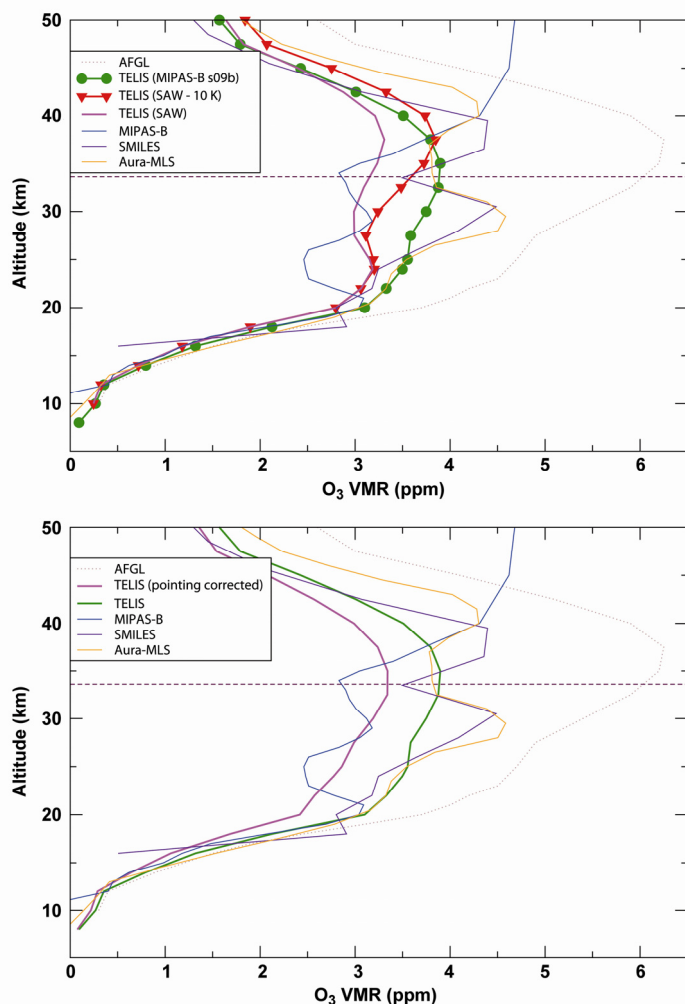


Fig. 3-7: Comparisons of O₃ retrievals with different temperature profiles to reference profiles (top). The bottom figure shows comparisons of O₃ retrievals with pointing correction to reference profiles.

3.5 Intercomparison of the GARLIC and PIRATES IR Radiative Transfer Codes

F. Schreier, C. Köhler (IMF-AP and IMF-EV)

Modeling of atmospheric radiative transfer is essential for the analysis of a growing number of ultraviolet, infrared, and microwave remote sensing instruments. Because the quality of retrieval products critically depends on the accuracy of the radiative transfer codes used as forward model in the inversion, verification and validation of these codes is crucial. Accordingly, several code intercomparisons have been performed in the past. Here we present an intercomparison of two Line-by-Line (LbL) codes developed independently at IMF-AP for simulation and/or analysis of high resolution infrared spectra. These are

- GARLIC: The Generic Atmospheric Radiation Line-by-Line Infrared Code (a Fortran 2003 reimplementations of the Fortran 77 code MIRART/SQURRL) has been designed for far and mid IR applications, arbitrary observation geometries, instrumental field of view and spectral response functions. MIRART/SQURRL has been verified in extensive intercomparisons (see annual report 2003); furthermore, the code was used successfully to model observations of the Venus transit 2004 made by the Tenerife Vacuum Tower Telescope or for assessments of exoplanet biosignatures (see chapters 4.5 and 4.6 of this report).
- PIRATES: The Programmers Interface to Radiative Transfer Algorithms has been developed in the framework of a PhD thesis on interpretation and analysis of ground-based radiation measurements in the thermal infrared during the SAMUM-2 campaign (see annual report 2010). Modularity has been a key design feature for PIRATES; furthermore, thorough documentation, shared memory parallel processing capabilities, and re-usability of implemented routines were important aspects in the development phase. PIRATES is written in (object oriented) C++ and combines LbL high spectral resolution cross section capabilities with multiple scattering radiative transfer solvers (see annual report 2009).

For the intercomparison of GARLIC and PIRATES a thermal infrared atmospheric sounding scenario by means of a ground-based, uplooking spectrometer has been considered. More specifically atmospheric data (pressure, temperature, and molecular concentration profiles) available from the CIRC (Continual Intercomparison of Radiation Codes) web site (<http://circ.gsfc.nasa.gov/>) covering a wide range of atmospheric conditions such as e.g., humidity were used as input. Profiles of temperature and humidity up to about 20 km are based on radiosonde information acquired in the context of the Atmospheric Radiation Measurement (ARM) program, while climatological profiles are used above. Spectra were calculated for four standard clear sky CIRC cases in the wavenumber range from 800 to 1200 cm^{-1} covering the shortwave wing of the strong CO_2 ν_2 band and the ozone band around 9.6 μm . In addition to these two molecules, absorption by water, methane and nitrous oxide has been considered. Absorption due to continua, nb. water, is included besides the contribution described by line-by-line cross sections using the most recent HITRAN 2008 as input.

Fig. 3-8 illustrates an intercomparison of the GARLIC and PIRATES modeled spectra together with an observed AERI (Atmospheric Emitted Radiance Interferometer) spectrum for the low humidity 'Case 4'. Compared to the measured spectrum both model spectra display a small, slowly varying offset that can be attributed to an imperfect continuum model. Note that GARLIC uses version 2.0 of the so-called 'CKD water continuum', whereas in PIRATES the more recent MT-CKD continuum has been implemented. Furthermore differences between the model spectra can be expected due to differences in discretization of the wavenumber regime, the temperature conversion of line strengths, or integration of the path integrals along the line-of sight (numerical quadrature schemes, Curtis-Godson approximation).

In order to understand the origin of the discrepancies between the models further investigations are planned, e.g., intercomparisons of intermediate quantities such as cross sections, absorption coefficients, and optical depths. This will help to uncover potential bugs and to identify code segments or algorithms to be improved, finally leading to better and more reliable radiative transfer codes.

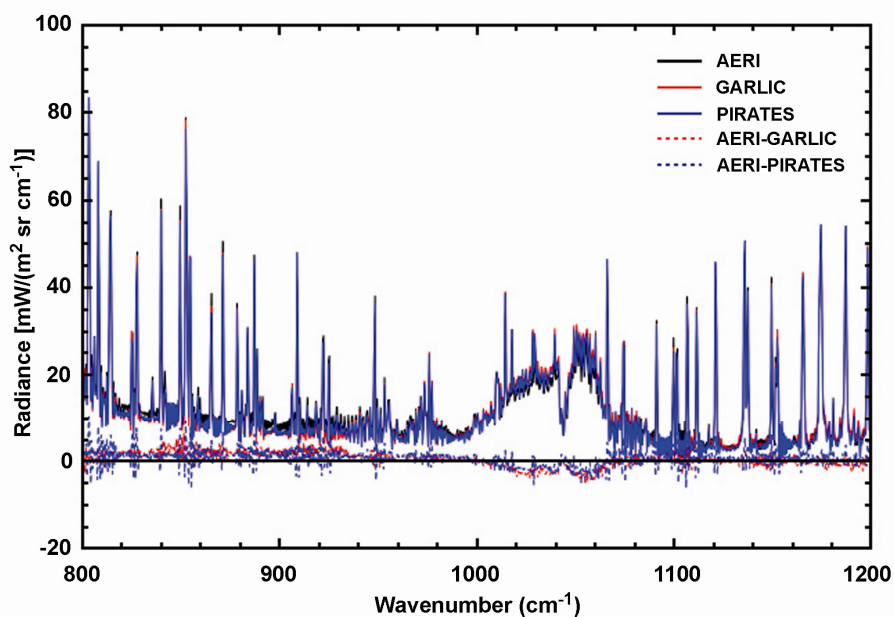


Fig. 3-8: Spectra modelled with GARLIC and PIRATES in comparison with a measured spectrum (AERI). For details see text.

3.6 A Case Study on the Reciprocity in Light Scattering Computations

K. Schmidt, M. Yurkin (Institute of Chemical Kinetics and Combustion SB RAS), M. Kahnert (SMHI)

In the past, a variety of different methods have been developed to describe the scattering of electromagnetic waves on single nonspherical particles. In general, they differ in the approaches used, and, consequently, in their capabilities to compute the scattering behaviour of various particle classes. Corresponding computer programs are sophisticated, tested, and partly publicly available. However, they may lead to slightly different numerical results for a given scattering problem. This can be also the case for various implementations of the same method or even for different versions of the same program. The differences may become larger and larger when approaching the limits of the algorithms. On the other hand there are cases where only one single method exists for treating special types of scatterers such that no comparative calculations with alternative methods are possible for verifying the results obtained. In all these cases it is up to the user to finally judge the accuracy and correctness of the findings. This is, e.g., important in remote sensing applications. Different scattering models can lead to different results in the data processing and finally to different conclusions.

There are various criteria to test the results of a given scattering program and to gain confidence in them. One of these criteria is the fulfilment of the reciprocity condition (e.g. *van de Hulst 1957*). It means that the source and the observation point of a certain scattering configuration can be interchanged without changing the result. In the present study, the suitability of this criterion is investigated in more detail for some publicly available programs applied to defined scatterers and configurations. The programs considered were either T-matrix method implementations [*mieschka (Wauer et al. 2004)*, *scsmfo1b (Mackowski et al., made available for free download in the late 1990s)*, and *mstm (Mackowski and Mishchenko 2011)*] or Discrete Dipole Approximation (DDA) implementations [*ADDA, (Yurkin and Hoekstra 2011)* and *DDSCAT (Draine and Flatau 2010)*]. Prolate and oblate spheroids, circular cylinders, touching bispheres, Chebyshev particles, and cubes have been taken into account as particles shapes. They have been characterized by the following parameters:

- volume equivalent size parameter of 3 and 15
- aspect ratio of the prolate spheroids and the circular cylinders of 1.5
- aspect ratio of the oblate spheroids of 0.67
- orders of the Chebyshev particles of 5 and 45
- deformation parameter of the Chebyshev particles of 0.05
- complex refractive index of $(1.313, 5.889 \times 10^{-10})$ and $(1.6, 0.0005)$

Note that not all chosen programs can handle all above particle shapes. To check the reciprocity, the following two configurations have been considered in most cases:

- Eulerian angles ($\alpha=0^\circ$, $\beta=0^\circ$, $\gamma=180^\circ$) and a scattering angle $\theta=90^\circ$
- Eulerian angles ($\alpha=0^\circ$, $\beta=90^\circ$, $\gamma=180^\circ$) and a scattering angle $\theta=270^\circ$

The hh- and vv-polarized differential scattering cross sections (DSCS) have been computed for these configurations and compared with each other. The difference between the cross sections of two reciprocal configurations (relative reciprocity error) represents a measure for the reciprocity fulfilment.

The main results obtained so far are summarized hereafter. Program *mieschka* with a predefined accuracy of 5% in computing the DSCS yields, in most cases, a relative reciprocity error less than 5%. The error goes even down to about $3 \times 10^{-4}\%$ for the Chebyshev particle having a size parameter of 3, an order of 45, and a refractive index of $(1.313, 5.889 \times 10^{-10})$. The only exception is the circular cylinder with a size parameter of 15 and a refractive index of $(1.6, 0.0005)$. In the vv-polarization, the error amounts to about 15%. This relatively large error results from the fact that the DSCS values are located near deep down spikes for both configurations. Convergence of the differential scattering behaviour is, however, not tried to be achieved in such regions according to the convergence strategy of *mieschka*. Since it is hard to ensure convergence in deep spikes for most of the scattering programs, investigations in such angular ranges should be, therefore, avoided by an adequate choice of the corresponding reciprocal configurations. This becomes, in particular, more important for particles having larger size parameters and/or refractive indices. Furthermore, a correlation between the relative reciprocity error and the error in gaining relative convergence of the DSCS has been found for *mieschka*. If the DSCS start to converge with an increasing number of series expansion terms, then the reciprocity fulfilment improves at the same time unless no numerical problems arise. So the improvement of both, the relative convergence of the DSCS and the fulfilment of the reciprocity condition, represents an indication for the accuracy and correctness of the final *mieschka* results.

The programs *scsmfo1b* and *mstm*, developed to compute the scattering behaviour of ensembles of spheres, yield comparable relative reciprocal errors for the bispheres when using their default convergence parameters. They vary from about $1 \times 10^{-2}\%$ to 6%. Test computations have shown a behaviour of *mstm* similar to *mieschka*. An increase of the number of field expansion terms has led, in general, to an improvement of the relative convergence of the DSCS, again unless no numerical problems arise. At the same time, a better fulfilment of the reciprocity condition has been obtained. So the conclusion drawn above for *mieschka*, can be generalized as follows: The reciprocity fulfilment together with the DSCS relative convergence indicate that the results obtained by scattering programs, which are based on field expansions such as above T-matrix methods, seem to be reasonable.

The behaviour of the programs *ADDA* and *DDSCAT* depends strongly on the polarizability model chosen. This model characterizes the small volume elements (dipoles) which are used to replace a given scatterer. If the polarizability model does not depend on the propagation and polarization direction of the incident electric field then the reciprocity condition is a priori fulfilled by *ADDA* and *DDSCAT*, respectively. This is due to the fact that the solutions of the linear equation system within the DDA formulation are the same for the reciprocal configurations, in this case. And this is, in turn, a consequence of the symmetry $G(\mathbf{r}_i, \mathbf{r}_j) = G(\mathbf{r}_j, \mathbf{r}_i)$ ($(i, j) = 1 \dots N$, $i \neq j$, N – number of dipoles) of the Green function $G(\mathbf{r}_i, \mathbf{r}_j)$ present in the equation system. Therefore, the numerical accuracy of the reciprocity fulfilment is solely determined by the solution scheme applied to the DDA equation system. In this way, the relative reciprocity error is often smaller than those obtained by the T-matrix methods considered. It can decrease down to about $5 \times 10^{-9}\%$ by *ADDA* for the cube with a size parameter of 3 and a refractive index of $(1.6, 0.0005)$, for instance. Additional comparisons of the corresponding DSCS with reference data generated by the program *mieschka* have shown that there is no correlation between the relative reciprocity error and the DSCS quality. Consequently, a reciprocity check is, in this case, not appropriate to evaluate the scattering behaviour of a given particle.

On the other hand, if the polarizability model depends on the propagation and polarization direction of the incident field then the reciprocity condition is not a priori fulfilled. There are, however, particle shapes and scattering configurations which lead to the situation described above. This can, e.g., happen if either the propagation or the polarization direction is along a coordinate axis. But the other cases, showing a direction dependence, are more interesting. Here the reciprocal error ranges between about 2% to 156% by *ADDA* for the cubes in the vv-polarization, or between $1 \times 10^{-2}\%$ to 284% by *DDSCAT*.

It has been observed, in general, that particles with lower size parameters and/or refractive indices exhibit smaller reciprocity errors and, concurrently, a better agreement of the DSCS compared to *mieschka* results than particles having larger size parameters and/or refractive indices. This indicates that there is a certain correlation between the quality of the DSCS (i.e. the agreement with reference values) and the fulfilment of the reciprocity. So checks of the latter are appropriate to test DDA results, but only in cases in which this criterion is not a priori fulfilled.

References

Draine B.T., and Flatau P.J.: User guide to the Discrete Dipole Approximation code DDSCAT 7.1, <http://arXiv.org/abs/1002.1505v1>, 2010

Mackowski D.W., Fuller K., and Mishchenko M.I.: Codes for calculation of scattering by clusters of spheres, <ftp://ftp.eng.auburn.edu/pub/dmckwski/scatcodes/index.html>

Mackowski D.W., and Mishchenko, M.I.: A multiple sphere T-matrix Fortran code for use on parallel computer clusters, *J. Quant. Spectrosc. Radiat. Transfer*, 112, 2182-2192, 2011

van de Hulst H.C.: *Light Scattering by Small Particles*, New York: John Wiley & Sons, 1957

Wauer J., Schmidt K., Rother T., Ernst T. and Hess M.: Two software tools for the plane-wave scattering on nonspherical particles in the German Aerospace Center's virtual laboratory, *Appl. Opt.*, 43, 6371-6379, 2004

Yurkin M.A., and Hoekstra A.G.: The discrete-dipole-approximation code ADDA: capabilities and known limitations, *J. Quant. Spectrosc. Radiat. Transfer*, 112, 2234-2247, 2011

3.7 Dust/Urban Aerosol Radiative Forcing Based on Surface Aerosol Measurements

K. Alam (University of Salzburg) and T. Trautmann

Owing to the fact that there is still incomplete knowledge of both aerosol physical and chemical properties as well as the spatial and temporal distribution of the atmospheric aerosol, aerosol radiative forcing (ARF) recently has been discussed as one of the main uncertainties in climate radiative forcing. Dust particles influence the transport of shortwave and longwave radiation through scattering, absorption and emission processes. If one considers an atmospheric column, aerosols can either lead to a cooling (negative forcing) or a heating (positive forcing) effect depending on the net radiative fluxes entering the atmospheric column from above and from below. The ARF is commonly defined with respect to the clear aerosol-free atmosphere. The magnitude and sign of radiative heating or cooling is determined by different aerosol types, their size distribution and chemical composition. The direct ARF is the difference in the net fluxes (down minus up) with and without aerosols in that layer. Here we report on the determination of aerosol optical properties in the megacity of Karachi employing a GRIMM model 1.109 optical particle counter (OPC) which was operated during a short campaign at Karachi in March 2010.

The GRIMM OPC is a standard instrument to measure the number concentration of near-surface aerosols, the associated size-dependent aerosol mass loading and the total suspended aerosol matter. The GRIMM OPC is a portable, lightweight, battery-operated optical particle counter, which registers the particles into 31 different size bins in the diameter range between 0.25 μm and 32 μm . The optical detection of the aerosol particles is based on single particle counts due the light scattering of a laser light source located within the OPC.

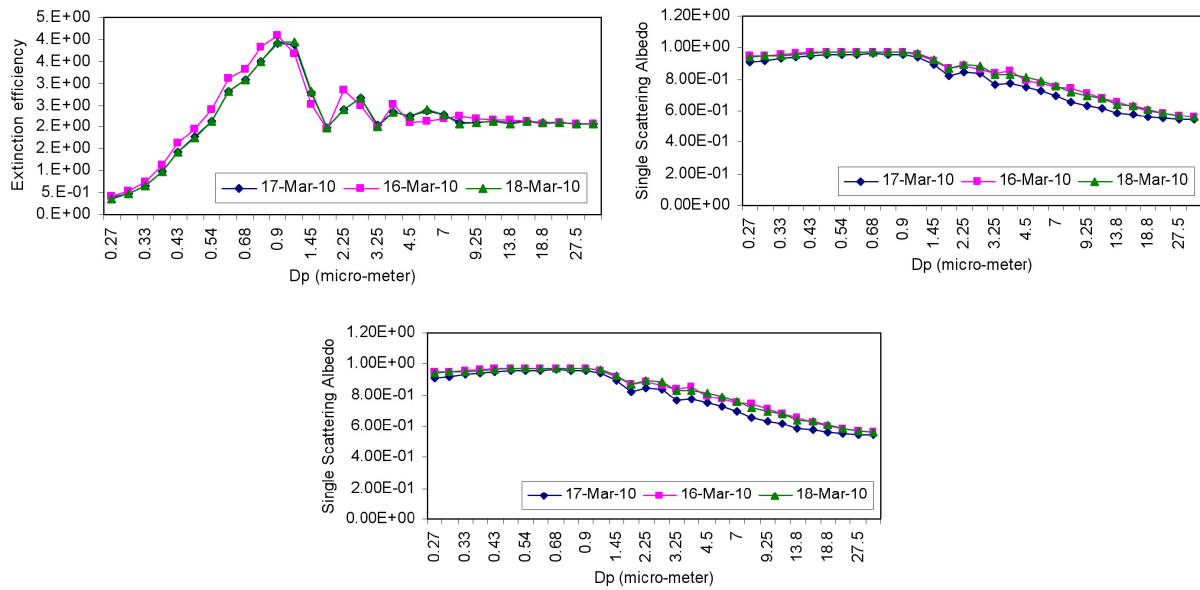


Fig. 3-9: Aerosol optical properties at the wavelength 676 nm on 16, 17, and 18th March 2010: (top left) extinction efficiency, (top left) single scattering albedo, (bottom) asymmetry parameter.

From the GRIMM spectrometer size distribution measurements, the following quantities have been calculated via Mie theory by using additional information on particle composition from other sources: The Mie efficiencies for extinction and absorption, the single scattering albedo and the asymmetry parameter of the scattering phase function, see Fig. 3-9. For specifying the real and imaginary part of the refractive index of the aerosol the AERONET Inversion Data Product (2010 inversion, level 1.5) for the station Karachi has been used. For estimating the spectrally dependent aerosol extinction coefficient as input for the radiative transfer simulations, we assumed that the planetary boundary layer is well-mixed from the surface up to 1000 m altitude.

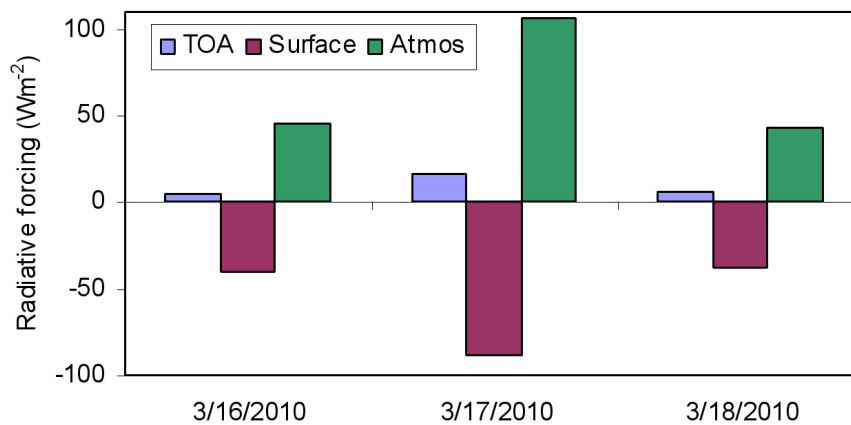


Fig. 3-10: Direct solar aerosol radiative forcing effect for Karachi at the surface, at TOA and within the atmosphere computed with SBDART.

For the radiative transfer computations in the solar spectral range the SBDART model (*Ricchiazzi et al. 1998*) has been used in this study which employs the so-called DISORT method (*Stamnes et al. 1988*) as solver for the plane-parallel radiative transfer equation. Within the wavelength range from 0.3 to 4.0 μm the net radiative fluxes are computed at the top of the atmosphere (TOA) and at the surface separately, both with and without aerosols. Finally, these net fluxes have been integrated over the entire solar range (0.3-4 μm). For estimating the direct ARFs the clear sky days 16, 17, and 18th March 2010 have been considered by running SBDART for every full hour of the day. In this manner the integrated average solar radiative forcings were estimated on the basis of prevailing weather conditions and measured parameters (cf. columnar water vapor and ozone contents from sun/sky radiometers and NASA's AURA satellite, respectively). Fig. 3-10 shows the direct solar ARFs for Karachi. For example, for

17th March 2010 the mean atmospheric ARF was found to be 105 Wm^{-2} , which suggests that a considerable amount of solar radiation is absorbed within the atmosphere. This can have a substantial effect on local atmospheric stability and dynamics.

References

Alam K., Blaschke T., Madl P., Mukhtar A., Hussain M., Trautmann T. and Rahman S.: Aerosol size distribution and mass concentration measurements in various cities of Pakistan, *Journal of Environmental Monitoring*, 13, 1944-1952, DOI: 10.1039/c1em10086f, 2011

Alam K., Trautmann T. and Blaschke T.: Aerosol optical properties and radiative forcing over mega-city Karachi. *Atmospheric Research*, 101. Elsevier. DOI: 10.1016/j.atmosres.2011.05.007, 2011

Ricchiazzi P., Yang S., Gautier C., and Sowle D.: *SBDART*: A research and teaching software tool for plane-parallel radiative transfer in the earth's atmosphere. *Bull. Amer. Meteorol. Soc.* 79, 2101-2114, 1998

Stamnes K., Tsay S.-C., Wiscombe W., and Jayaweera K.: Numerically stable algorithm for discrete-ordinate-method radiative transfer in multiple scattering and emitting layered media, *Appl. Opt.*, 27, 2502-2509, 1988 – for the source code see ftp://climate1.gsfc.nasa.gov/wiscombe/Multiple_Scatt/

3.8 Light Scattering of 3D Chebyshev Particles

T. Rother, M. Kahnert (SMHI)

Particles with a small-scale surface roughness are encountered in many types of natural and anthropogenic aerosols in planetary atmospheres (terrestrial but also e.g. dust storms in the Martian atmosphere), as well as in mineral particles in interplanetary and interstellar regions. Having appropriate models for the light scattering properties of such particles is therefore required when applying remote sensing methods or analyzing astrophysical observations. Developing such algorithms is a challenging task, especially if a realistic 3D roughness must be taken into account. For particles with a smooth boundary surface, and if large compared to the wavelength, we can apply the Geometric Optics (GO) approximation. However this method fails if an additional small-scale roughness on the smooth surface of the order of the wavelength has to be accounted for. Therefore, more rigorous methods are needed to solve such scattering problems. We have developed such a method by combining a group theoretical approach with an iterative solution of the Lippmann-Schwinger equation related to Waterman's T-matrix approach. Tests have been performed for 2D and 3D Chebyshev particles with a refractive index of $m=3.0+0.1i$ (i.e. for higher absorption), which is typical for hematite at visible wavelengths (Fig.3-11).

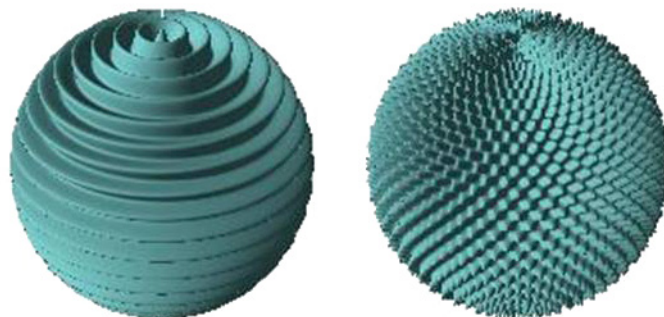


Figure 3-11: 2D (left) and 3D (right) Chebyshev particle with $l=45$ and $\epsilon = 0.05$.

The surface of a 3D Chebyshev particle with an underlying spherical base geometry of radius r is described by

$$r(\theta, \phi) = r[1 + \varepsilon \cdot \cos l\phi \cdot \cos l\theta]$$

where $-1 \leq \varepsilon \leq 1$ is the deformation parameter, and l is the order of the Chebyshev polynomial. It was already shown that, for lower deformation parameters and higher order Chebyshev particles, the phase function becomes independent of l , even though the phase function is distinctly different from that of the underlying sphere (Rother et al. 2006). 3D Chebyshev particles can be considered as a compromise between the computationally efficient 2D Chebyshev particle and a real irregular particle with small-scale surface roughness. Moreover, 3D Chebyshev particles exhibit a higher degree of symmetry, thus facilitating the computations by using group theory (Kahnert 2005). Such group theoretical approaches can be combined with an iterative solution of the T matrix method if we consider only lower deformation parameters. Thus we have to reformulate the T matrix equation in terms of an appropriate Lippmann-Schwinger equation (Rother and Wauer 2010). The developed method allows us to calculate the scattering properties of 3D Chebyshev particles for size parameters up to 70. The method was tested against well-established existing codes, and by employing the principle of reciprocity which is a highly sensitive method.

Perhaps the most remarkable result obtained is the large difference in the backscattering cross-section computed for spheres and 3D Chebyshev particles with higher absorption, as shown in Fig. 3-12. This difference may have important consequences for e.g. interpreting lidar measurements.

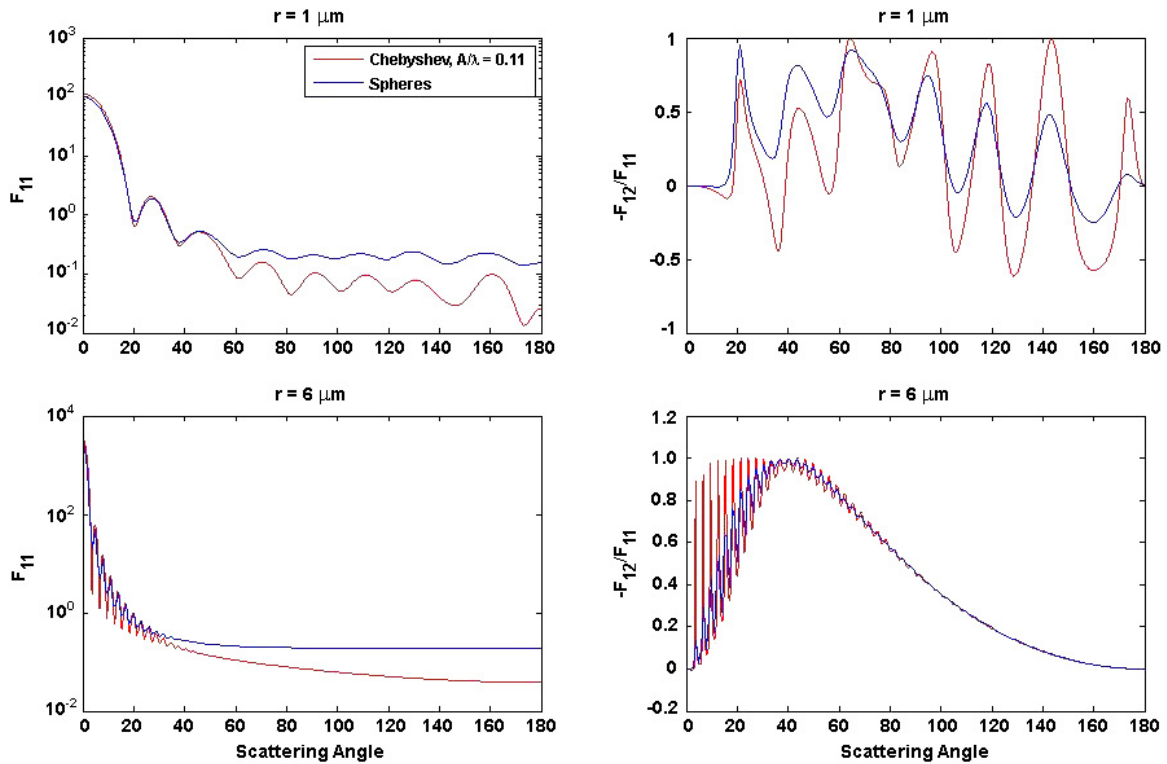


Figure 3-12: F_{11} element (left column) and F_{12}/F_{11} element (right column) of the Müller matrix of a 3D Chebyshev particle (red) and a sphere (blue) with a refractive index of $m = 3 + 0.1i$. Calculations have been performed for two different radii ($r = 1 \mu\text{m}$ and $r = 6 \mu\text{m}$ correspond to size parameters of approximately 10 and 60).

References

Kahnert M.: Irreducible representations of finite groups in the T matrix formulation of the electromagnetic scattering problem, J. Opt. Soc. Am. A 22, 1187-1199, 2005

Rother T., Schmidt K., Wauer J., Shcherbakov V., Gayet J.-F.: Light scattering on Chebyshev particles of higher order, Appl. Opt. 45, 6030-6037, 2006

Rother T. and Wauer J.: Case study about the accuracy behaviour of three different T matrix methods, Appl. Opt. 49, 5746-5756, 2010

3.9 New Database Interfaces for the WDC-RSAT

M. Hess (RASCIN) and F. Schreier

The World Data Center for Remote Sensing of the Atmosphere (WDC-RSAT) contains, in addition to the remote sensing data themselves, also a number of auxiliary scientific software and data, which can be used for interpretation of the satellite data. Two web interfaces to such auxiliary databases have already been presented before, namely the interfaces to the molecular spectroscopic databases HITRAN and GEISA, as well as to the database OPAC (Optical Properties of Aerosols and Clouds) – see Annual Report 2006. Two additional interfaces have been added recently.

Global Aerosol Data Set (GADS)

The Global Aerosol Data Set provides a global climatological distribution of aerosol microphysical and optical data on a 5×5 degree grid. Data are available for winter and summer (Fig. 3-13). Microphysical data are the total number density, the mixing ratios of aerosol components, and the type of aerosol height profile used for calculating optical depths. The optical properties of aerosol components are extracted from the Optical Properties of Aerosols and Clouds (OPAC) database and combined to the total aerosol optical properties using the GADS component mixing ratios. Optical properties comprise extinction, scattering and absorption coefficients, single scattering albedo, asymmetry parameter, lidar ratio and optical depth for 60 wavelengths between 0.25 and 40 μm , and for 8 values of relative humidity (Koepke et al. 1997). Output of GADS are the global fields as text files or global plots (Fig. 3-14).

Collection of Aerosol Refractive Indices

For calculating optical properties of atmospheric particles, information on the particle's size, shape and refractive index is needed. This collection gives the complex refractive indices of the OPAC aerosol model (Hess et al. 1998), the Shettle and Fenn model (Shettle and Fenn 1979), of water vapour and ice and of a number of minerals present in desert aerosol (Köhler et al. 2011). Data may be extracted as text files or visualised as plots. Additional information, for instance on data origin and genesis or mixing rules is given (Fig. 3-15, Fig. 3-16).

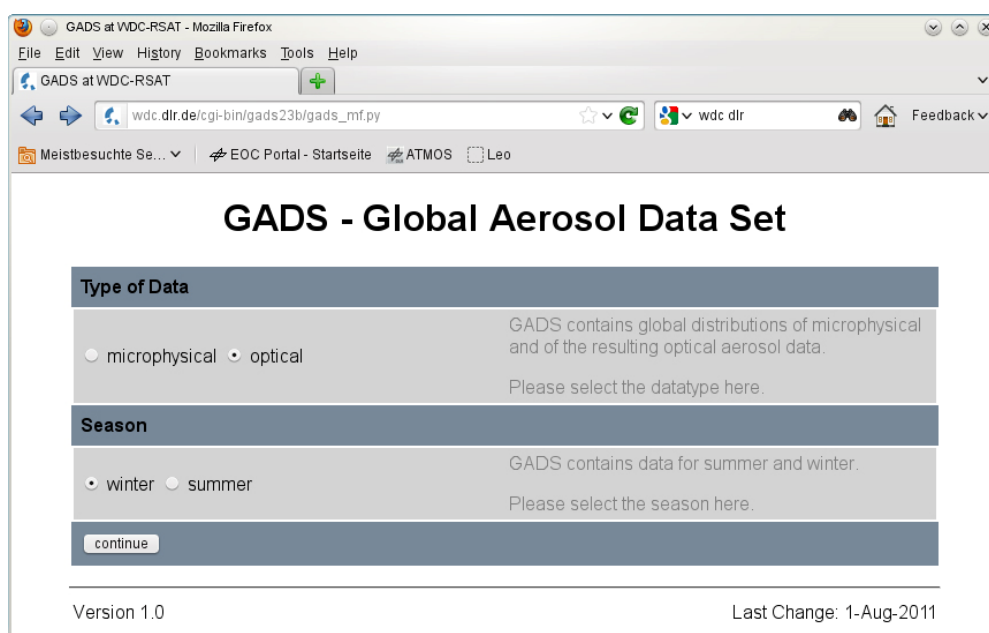


Fig. 3-13: WDC-RSAT GADS interface

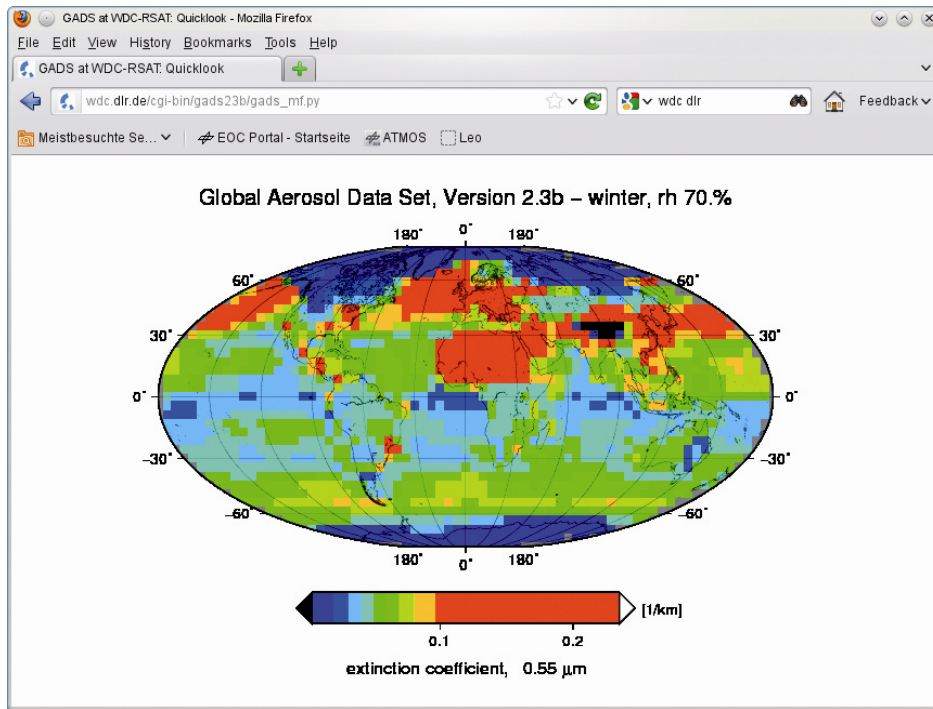


Fig. 3-14: Quicklook of retrieved WDC-RSAT GADS

aerosol material	references
<ul style="list-style-type: none"> • OPAC (Optical Properties of Aerosols and Clouds) <ul style="list-style-type: none"> <input type="radio"/> watersoluble <ul style="list-style-type: none"> <input type="radio"/> 0% <input type="radio"/> 50% <input checked="" type="radio"/> 70% <input type="radio"/> 80% <input type="radio"/> 90% <input type="radio"/> 95% <input type="radio"/> 98% <input type="radio"/> 99% - rel. hum. <input type="radio"/> insoluble <input type="radio"/> soot <input type="radio"/> sea salt <ul style="list-style-type: none"> <input type="radio"/> 0% <input type="radio"/> 50% <input type="radio"/> 70% <input type="radio"/> 80% <input type="radio"/> 90% <input type="radio"/> 95% <input type="radio"/> 98% <input type="radio"/> 99% - rel. hum. <input type="radio"/> mineral <input type="radio"/> sulfate_stratospheric(75% H2SO4) <ul style="list-style-type: none"> <input type="radio"/> 0% <input type="radio"/> 50% <input type="radio"/> 70% <input type="radio"/> 80% <input type="radio"/> 90% <input type="radio"/> 95% <input type="radio"/> 98% <input type="radio"/> 99% - rel. hum. • Shettle and Fenn Aerosol Models <ul style="list-style-type: none"> <input type="radio"/> rural <ul style="list-style-type: none"> <input type="radio"/> 0% <input type="radio"/> 50% <input type="radio"/> 70% <input type="radio"/> 80% <input type="radio"/> 90% <input type="radio"/> 95% <input type="radio"/> 98% <input type="radio"/> 99% - rel. hum. <input checked="" type="radio"/> urban <ul style="list-style-type: none"> <input type="radio"/> 0% <input type="radio"/> 50% <input type="radio"/> 70% <input type="radio"/> 80% <input type="radio"/> 90% <input type="radio"/> 95% <input type="radio"/> 98% <input type="radio"/> 99% - rel. hum. <input type="radio"/> oceanic <ul style="list-style-type: none"> <input type="radio"/> 0% <input type="radio"/> 50% <input type="radio"/> 70% <input type="radio"/> 80% <input type="radio"/> 90% <input type="radio"/> 95% <input type="radio"/> 98% <input type="radio"/> 99% - rel. hum. 	<p>Hess, M., P. Koepke, and I. Schult (1998): Optical Properties of Aerosols and Clouds: The software package OPAC, Bull. Am. Met. Soc., 79, 831-844.</p> <p>Shettle, E.P. and W. Fenn (1979): Models of the Aerosols of the Lower Atmosphere and the Effects of Humidity Variations on their Optical Properties, AFGL-TR-79-0214, 94pp</p>

Version 0.1 last update: 19-Sep-2011

Fig. 3-15: WDC-RSAT aerosol refractive indices interface

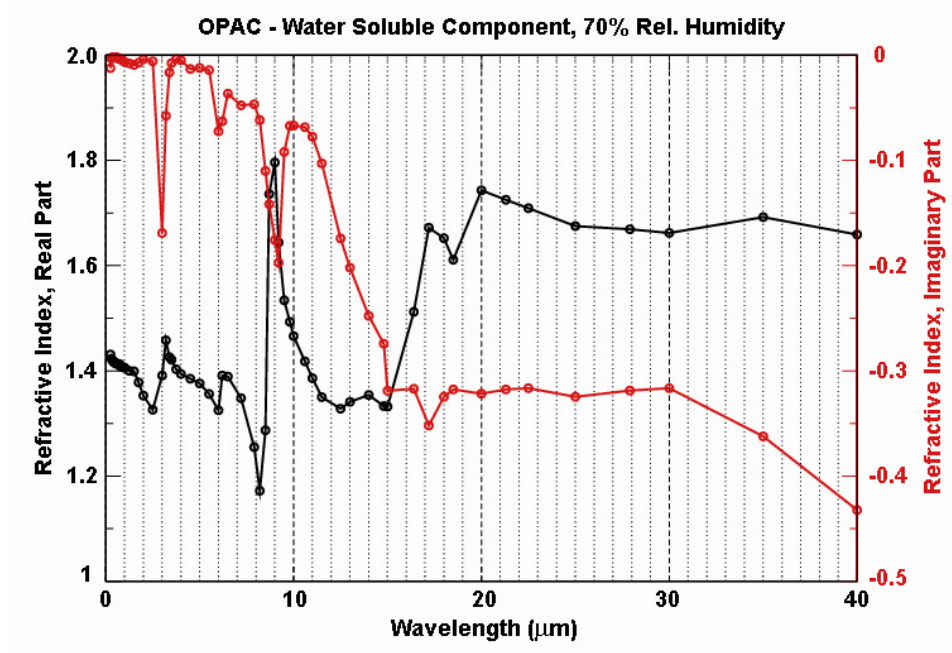


Fig. 3-16: Example of OPAC output – water soluble component (70% relative humidity)

References

Hess M., Koepke P., and Schult I.: Optical Properties of Aerosols and Clouds: The software package OPAC, Bull. Am. Met. Soc., 79, 831-844, 1998

Koepke, P., Hess M., Schult I., and Shettle E.P.: Global Aerosol Data Set, Report No. 243, Max-Planck-Institut für Meteorologie, Hamburg, 1997

Köhler C.H., Trautmann T., Lindermeier E., Vreeling W., Lieke K., Kandler K., Weinzierl B., Gross S., Tesche M. and Wendisch M.: Thermal IR radiative properties of mixed mineral dust and biomass aerosol during SAMUM-2. Tellus B, 63: 751-769. doi: 10.1111/j.1600-0889.2011.00563.x, 2011

Shettle E.P., Fenn R.W.: Models for the aerosols of the lower atmosphere and the effects of humidity variations on their optical properties, AFGL-TR-79-0214, 94, 1979

4. Atmospheric Remote Sensing – Applications

4.1 DLR Science Award 2011: Global Long-term Environmental Satellite Data for Climate Monitoring

D. Loyola, M. Coldewey-Egbers, M. Dameris (DLR-PA)

A team from DLR-IMF and DLR-PA received the DLR science award 2011 for its work about *Global long-term environmental satellite data for climate monitoring*. At the ceremony it was stated that with “The creation of long-term time series of stratospheric parameters such as ozone from homogenized satellite measurements is an extremely important and essential contribution for climate research”. This is the first time that the Remote Sensing Technology Institute received this award, the most important science prize from DLR.

Towards a Total Ozone Essential Climate Variable

The DLR work on atmospheric composition missions started almost two decades ago. DLR is responsible for the operational products of GOME/ERS-2 (1995-2011) and SCIAMACHY/ENVISAT (since 2002) on behalf ESA, as well as total column and cloud products of the GOME-2/MetOp-A (since 2006) as member of EUMETSAT O3M-SAF. The scientific activities related to retrieval algorithms are being performed in very close collaboration with partner institutes from

- Belgium: Belgisch Instituut for Ruimte-Aëronomie (BIRA)
- Greece: Aristotle University of Thessaloniki (AUTH)
- USA: RT Solutions (RTS)
- Germany: Institute for Environmental Physics / Institute for Remote Sensing, University of Bremen (IUP-IFE) and Max Planck Institute for Chemistry (MPIC)

The Global Climate Observing System (GCOS) identified a number of so called *Essential Climate Variables (ECV)* required to support the work of the climate research community. The ECVs largely depend upon satellite observations from several missions covering different domains of the Earth system: atmospheric, oceanic, and terrestrial.

Today European satellite missions provide sixteen years of atmospheric composition data. Using these, a first version of an homogenized global ECV from the European space-borne sensors GOME, SCIAMACHY and GOME-2 was created, a first comparison with ground-based measurements occurred, and an initial evaluation of coupled climate-chemistry model was carried out, see *Loyola et al. 2009*.

The GOME/SCIAMACHY/GOME-2 total ozone data starting in June 1995 has been combined with NASA data starting in 1979. Fig. 4-2 illustrates the evolution of the ozone hole over Antarctica as measured by the TOMS sensor onboard the Nimbus 7 satellite between 1979 to 1992, TOMS data



Fig. 4-1: Prof. Wörner (right), Chairman of the Board of DLR, awards the DLR science prize 2011 to Diego Loyola, Andrea Stenke, Martin Dameris and Melanie Coldewey-Egbers during the DLR annual general meeting in Stuttgart (photo: DLR).

from the Meteor satellite between 1993 to 1994, GOME data from ERS-2 for the period 1995-2002, SCIAMACHY data from ENVISAT between 2003 and 2006, and GOME-2 data from MetOp-A between 2007 and 2010. The average ozone from 1st to 3rd October is plotted for each year with the exception of 1993 and 2002 where data from 23rd to 25th September are used.

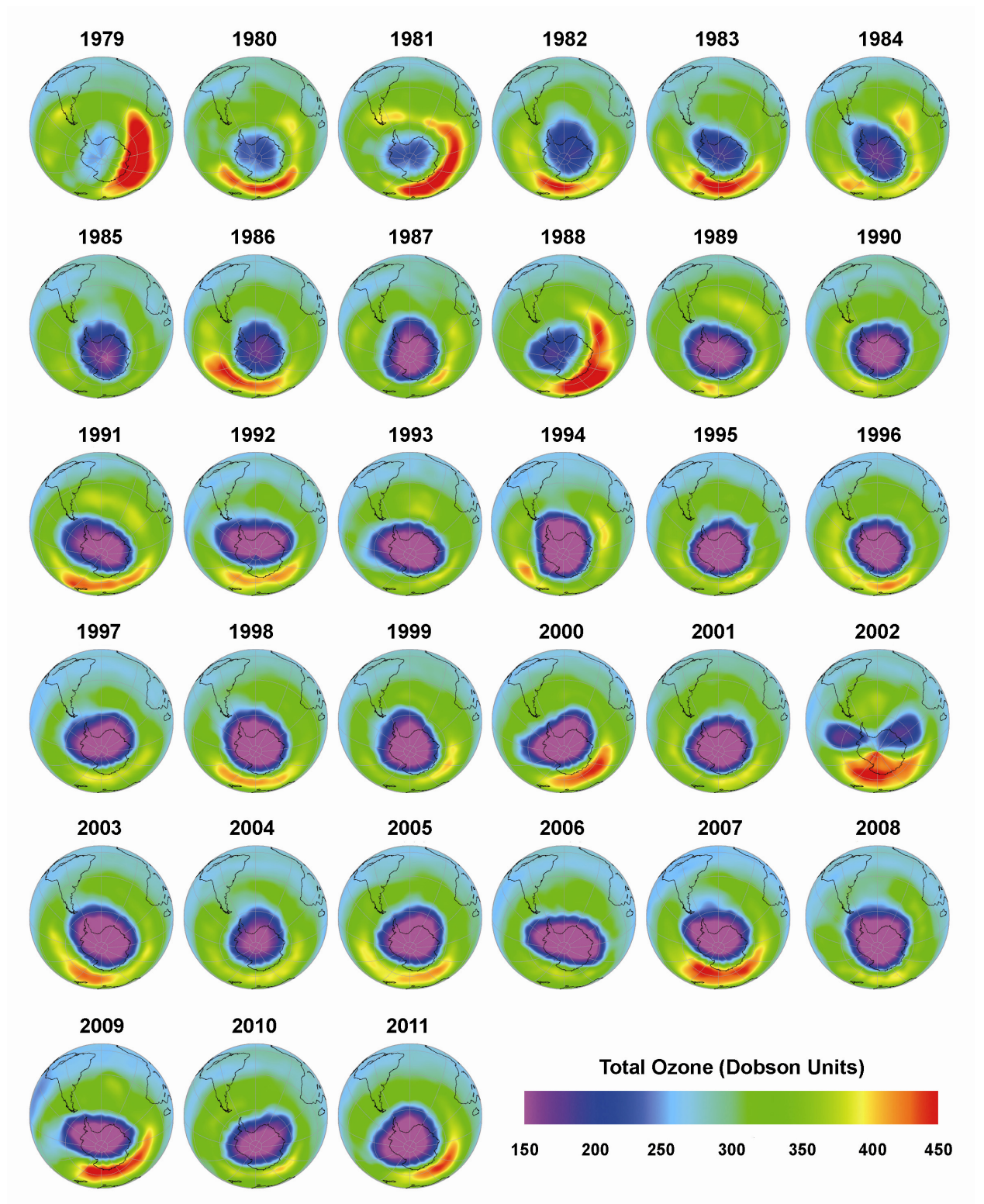


Fig. 4-2: Evolution of the ozone hole over Antarctica derived from satellite measurements from early October 1979 until 2010 (adapted from Fig. 4 in *Dameris and Loyola 2011*).

Confronting chemistry-climate model results with satellite observations

The evaluation of results derived from numerical modelling with observations provides indications about the quality of the applied model which partly reflects our current understanding of atmospheric processes, their causes and how interactions lead to changes in atmospheric behaviour (see *Dameris and Loyola 2011*).

The evolution of the total ozone column in the atmosphere and respective standard deviation as a function of latitude and time derived from GOME/SCIAMACHY/GOME-2 satellite measurements and the E39C-A R2 model simulation are presented in Figure 4-3. It is obvious that the overall variations of total ozone with latitude and time are well reproduced by E39C-A.

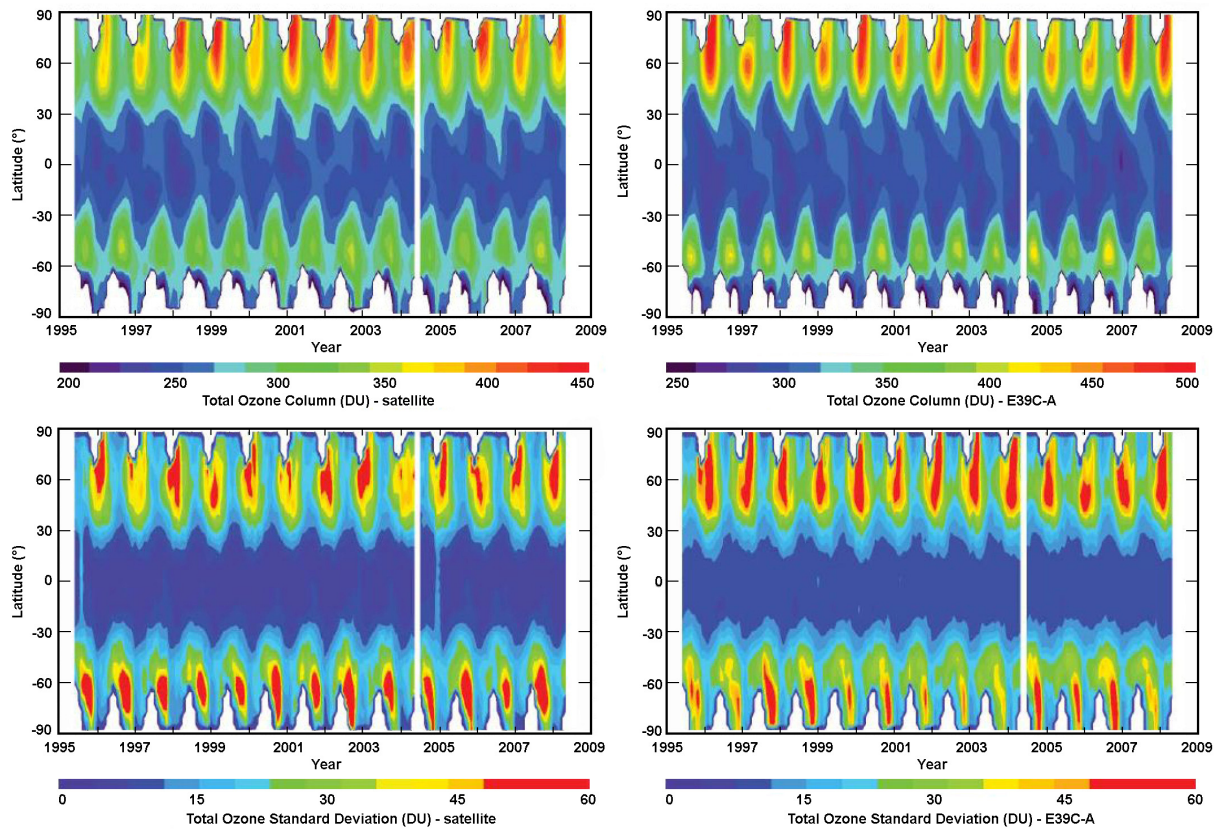


Fig. 4-3: Latitudinal evolution of total ozone (top) and standard deviation (bottom) from June 1995 to May 2008. GOME/SCIAMACHY/GOME-2 satellite data are presented on the left side (top and bottom) and E39C-A model on the right side (top and bottom). Satellite measurements from April 2004 are not available; the corresponding model data are therefore neglected as well (adapted from Fig. 8 in *Loyola et al. 2009*).

Fig. 4-4 provides a more detailed evaluation of the absolute accuracy of total column ozone values as derived from E39C-A simulations. Here, seasonal mean values of total ozone retrieved from space-borne measurements and E39CA are once again presented for the time period from June 1995 to May 2008. Note that the colour bars here are also different for satellite and model data since E39C-A total ozone values have a positive bias.

Fig. 4-5 shows seasonal means of the standard deviation of total ozone, again for satellite data and model results. The overall seasonal change and the hemispheric patterns of the standard deviation in the model follow quite well the respective values from observations. However some deviations in fine structure are still persistent.

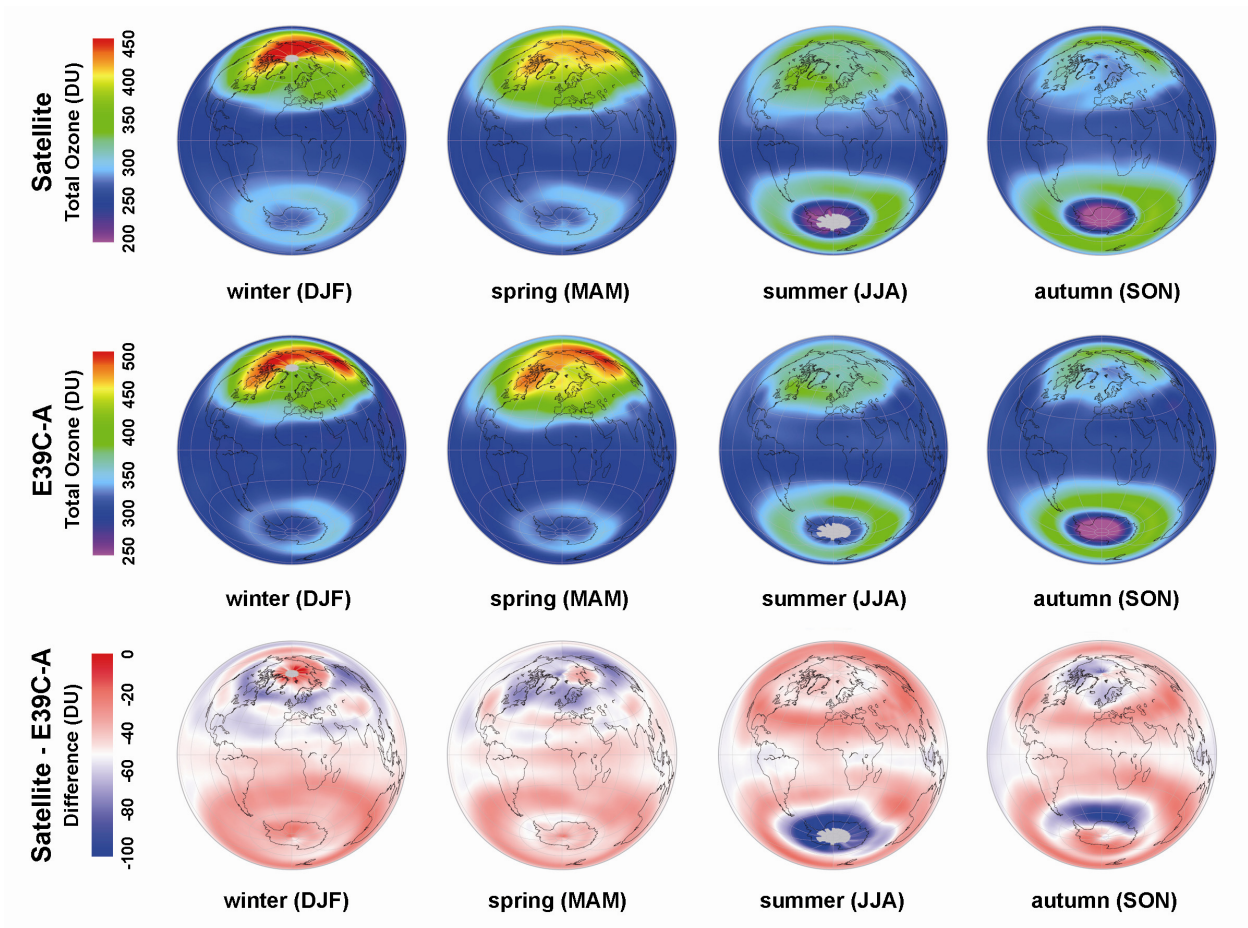


Fig. 4-4: Seasonal mean values of total ozone (June 1995 to May 2008) from GOME/SCIAMACHY/GOME-2 satellite instruments (top), the E39C-A simulation (middle), and the difference between satellite measurements and model results (bottom) (adapted from Fig. 6 in *Loyola et al. 2009*).

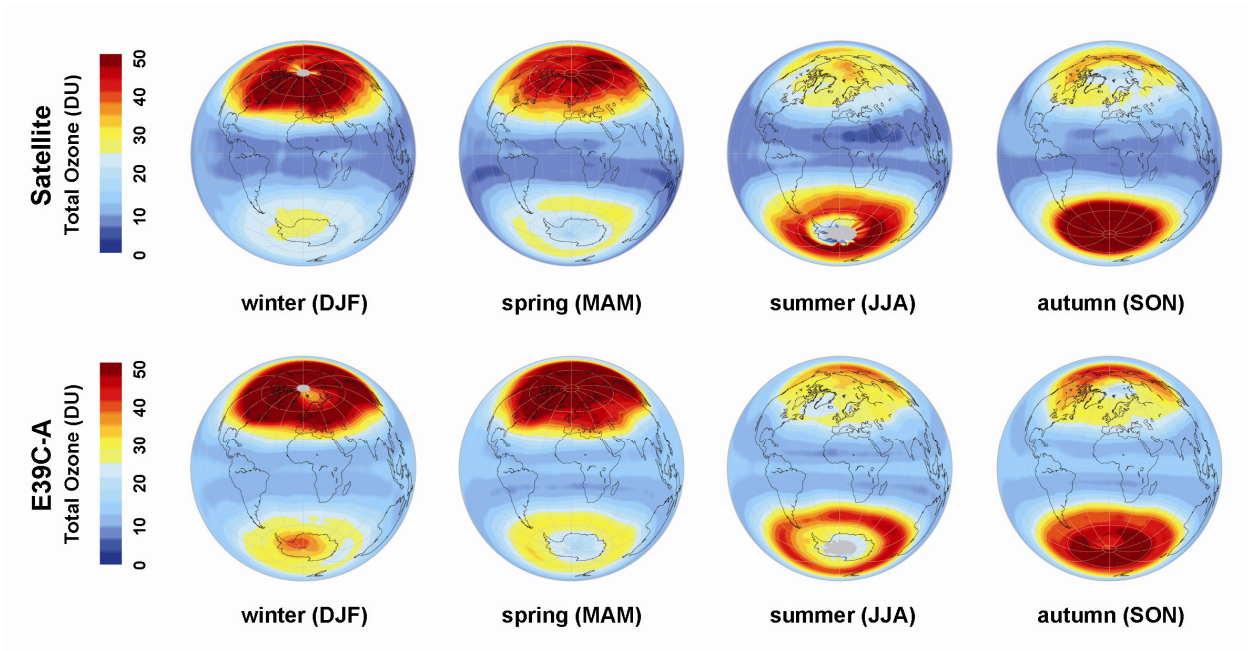


Fig. 4-5: Seasonal mean values of total ozone standard deviations (June 1995 to May 2008) from GOME/SCIAMACHY/GOME-2 satellite instruments (top) and the E39C-A simulation (bottom) (adapted from Fig. 7 in *Loyola et al. 2009*).

Total ozone: past evolution and future projection

Based on prognostic studies with climate models it is expected that the ozone layer will build up again in the next decades and that the ozone hole over Antarctica will be closed (see *Dameris and Loyola 2011*). Fig. 4-6 shows an example of the temporal evolution of total ozone deviations regarding a mean ozone value (1995-2009) for the near global mean, i.e. global mean values neglecting polar regions. For the past it is obvious that the E39C-A model is able to reproduce seasonal and interannual fluctuations in a sufficient manner, although the amplitudes of ozone anomalies are slightly underestimated.

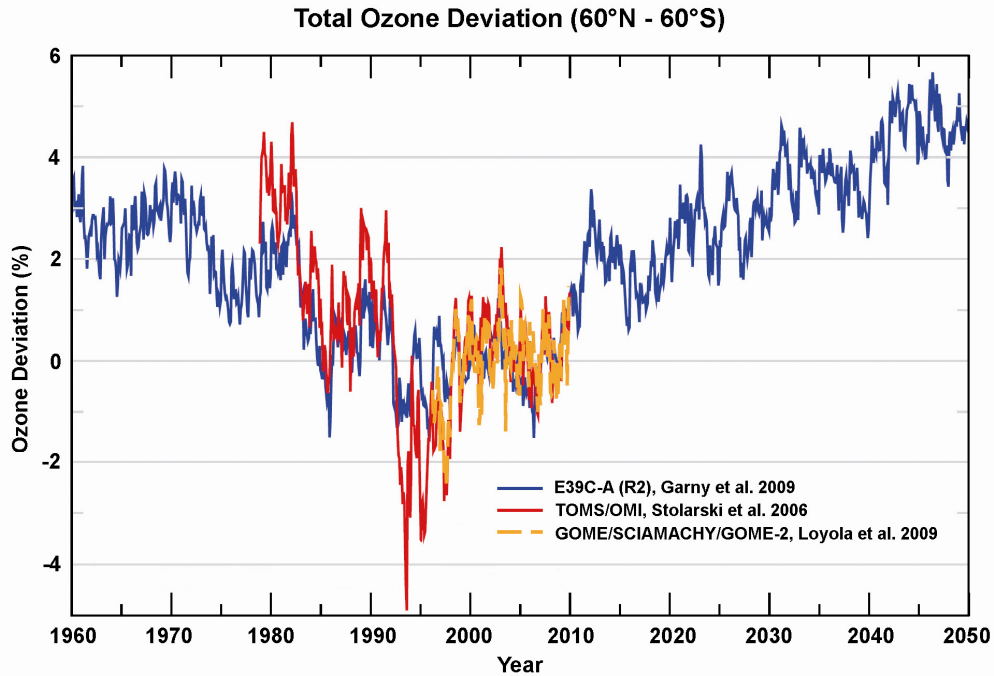


Fig. 4-6: Average deviations of the total ozone column (in %) with the orange and red curves representing data obtained from space-borne instruments (TOMS, GOME, SCIAMACHY and GOME-2). The blue curve shows results from a numerical simulation (R2) using a chemistry-climate model (adapted from Fig. 10 in *Dameris and Loyola 2011*).

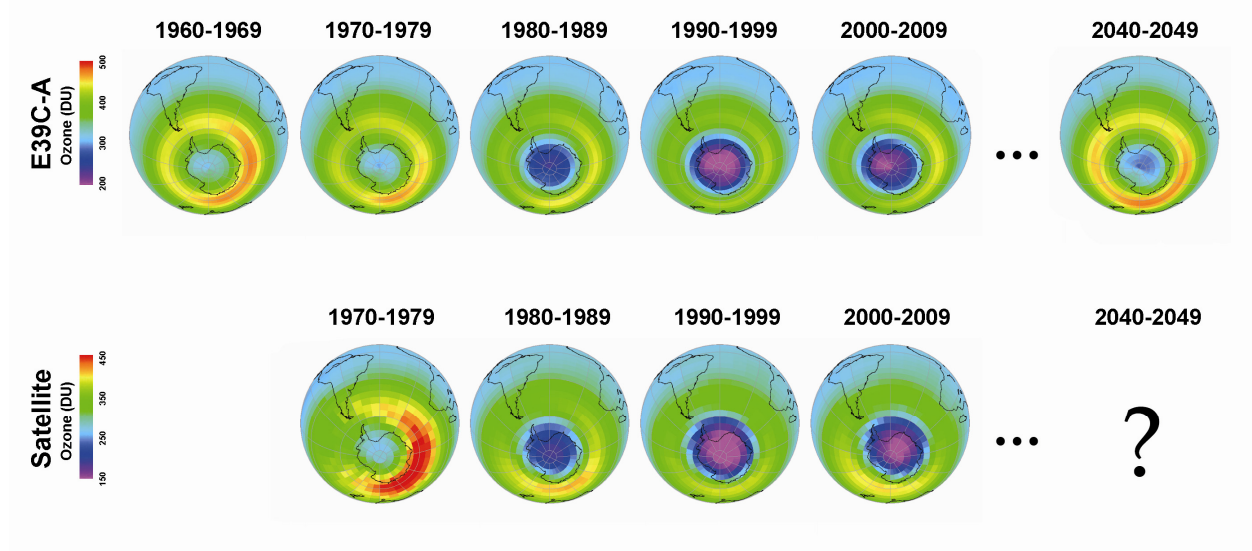


Fig. 4-7: Decadal evolution of the ozone hole in October (monthly mean value) derived from satellite measurements (TOMS, GOME, SCIAMACHY, GOME-2) from 1970 to 2009 and the simulation with the climate model E39C-A from 1960 until 2049 (adapted from Fig. 12 in *Dameris and Loyola 2011*).

Figure 4-7 illustrates the decadal mean total ozone values over Antarctica for October derived from a climate model and satellite observations. These images of simulated total ozone columns also indicate that the closure of the ozone hole will be delayed with respect to the prescribed temporal decrease of the stratospheric chlorine content, i.e. we expect that it will be not completed before 2050 (see *Dameris and Loyola 2011*).

References

Loyola D., Coldewey-Egbers M., Dameris M., Garny H., Stenke A., Van Roozendaal M., Lerot C., Balis D., Koukouli M.: Global long-term monitoring of the ozone layer – a prerequisite for predictions. *International Journal of Remote Sensing*, 30, 15-16, 4295–4318, 2009

Dameris M., Loyola D.: Chemistry-Climate Connections – Interaction of Physical, Dynamical, and Chemical Processes in Earth Atmosphere, in *Climate Change - Geophysical Foundations and Ecological Effects*, J. Blanco, H. Kheradmand (Eds), InTech, ISBN 978-953-307-419-1, 1-26, 2011

4.2 Tropospheric Trace Gas Products from GOME-2

P. Valks, N. Hao, D. Loyola and W. Zimmer

The tropospheric NO₂ and O₃ column products for GOME-2 are being developed by IMF-AP in the framework of EUMETSAT's Satellite Application Facility on Ozone and Atmospheric Chemistry Monitoring (O3M-SAF). The tropospheric NO₂ column product is generated operationally at DLR using the GOME Data Processor (GDP) version 4.4 (*Valks et al. 2011a*) since 2008, and is available for the users in near real time, i.e. within two hours after sensing. In 2011, a prototype algorithm for the retrieval of the tropospheric ozone column for the (sub)-tropical region has been developed for GOME-2.

Tropospheric NO₂ product

Nitrogen dioxide (NO₂) plays a key role in tropospheric chemistry. It is an important air pollutant affecting human health and ecosystems and one of the most important ozone precursors. The main anthropogenic sources of nitrogen oxides are combustion of fossil fuels and biomass burning, the most important natural sources are microbial production in soils, wildfires and lightning. The DOAS method is used to determine NO₂ slant column densities from calibrated GOME-2 (ir)radiance data in the 425–450 nm wavelength range (*Valks et al. 2011b*). Initial total Vertical Column Densities (VCD) are computed using an air mass factor based on a stratospheric NO₂ profile climatology. To separate the tropospheric and stratospheric NO₂ component, a spatial filtering approach is used, which is shown to be an improvement on the Pacific reference sector method. For the tropospheric air mass factor computation, monthly average NO₂ profiles from the MOZART-2 chemistry transport model are used, determined for the satellite overpass time. Furthermore, GOME-2 derived cloud properties, determined with the OCRA and ROCINN algorithms are exploited to calculate the air mass factors for scenarios in the presence of clouds.

Fig 4-8 shows the tropospheric NO₂ columns from GOME-2 for the period 2007-2010 over Europe. Remarkable features are the high tropospheric NO₂ concentrations above large urban and industrial areas of Europe, such as the Po Valley, the Benelux, South-East England and Germany's Ruhr area. Also the 'city-size' polluted areas around Paris, Madrid and Moscow are clearly visible.

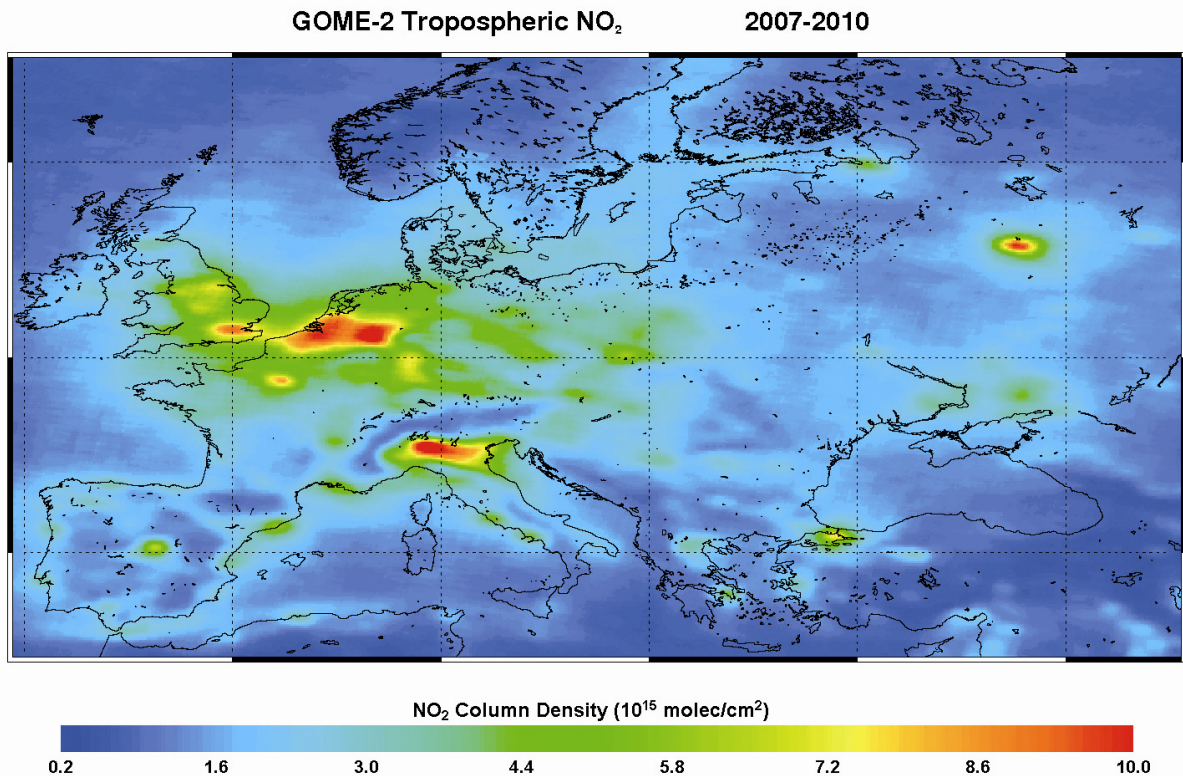


Fig. 4-8: Average tropospheric NO₂ columns measured by GOME-2 over Europe for 2007-2010.

Tropospheric O₃ product

A prototype algorithm has been developed for the retrieval of the tropospheric ozone column for the (sub)-tropical region using the convective-cloud-differential (CCD) method (Valks *et al.* 2003). The GOME-2/CCD method uses both ozone column and cloud measurements from GOME-2. The OCRA and ROCINN algorithms (Loyola *et al.* 2007) are used for obtaining GOME-2 cloud information: OCRA provides the cloud fraction using the broad-band polarization measurements, and ROCINN provides cloud-top height and cloud-top albedo from measurements in and adjacent to the oxygen A-band around 760 nm.

By combining the cloud information with GOME-2 ozone column measurements, monthly-mean values of the tropospheric ozone columns, below 200 hPa, have been determined. Fig. 4-9 shows a schematic illustration of the GOME-2/CCD technique. In the first step, cloudy GOME-2 measurements with cloud fraction $f \geq 0.8$, cloud albedo $a_c \geq 0.8$, and cloud top pressure $p_c \leq 300$ hPa are used to determine the above-cloud ozone column (above ~200 hPa, including the ozone column in the stratosphere and the tropical transition layer), as shown on the left of Fig. 4-9. The cloudy GOME-2 pixels are selected from tropical measurements over the highly convective eastern Indian Ocean and the western Pacific (70°E – 170°W), where the greatest frequency of high level clouds is found. It is assumed that the ozone column above 200 hPa is independent of longitude in a given latitude band.

In the second step, cloud-free GOME-2 measurements ($f \leq 0.1$) are used to determine the total ozone column, as shown on the right of Fig. 4-9. In the case of cloud-free pixels, GOME-2 is able to detect both ozone in the stratosphere and in the troposphere. The total ozone columns are monthly averaged on a $1.25^\circ \times 2.5^\circ$ latitude-longitude grid between 20°N and 20°S. In a last step, the ozone column above 200 hPa is subtracted from the gridded total ozone values, resulting in the monthly-averaged tropical tropospheric ozone column (TTOC) below 200 hPa.

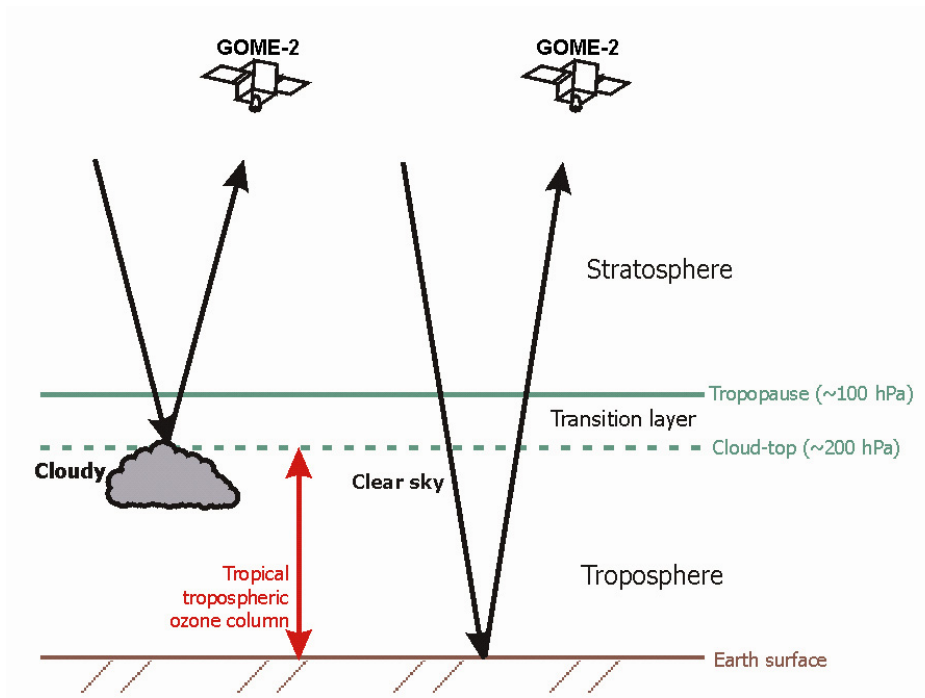


Fig. 4-9: Schematic illustration of the GOME-2/CCD technique for the (sub)-tropics. Cloudy GOME-2 measurements with cloud fraction ≥ 0.8 , cloud top albedo ≥ 0.8 and cloud top pressure ≤ 300 hPa, which are used to determine the above-cloud ozone column, are shown on the left. Cloud-free GOME-2 measurements (cloud fraction ≤ 0.1) are shown on the right. The result is a tropical tropospheric ozone column below 200 hPa.

The effect of biomass burning on the tropical tropospheric NO_2 and ozone column distribution is illustrated in Fig. 4-10. The top right figure displays the southern hemisphere biomass burning hot spots as measured by ATSR in September 2007. The biomass burning produced large amounts of NO_2 over Southern Africa and South America as can be seen in this figure (top left). The largest increases in ozone are found over the southern Atlantic as shown in Fig. 4-10 (bottom), and are a result of the biomass burning emissions and large-scale transport.

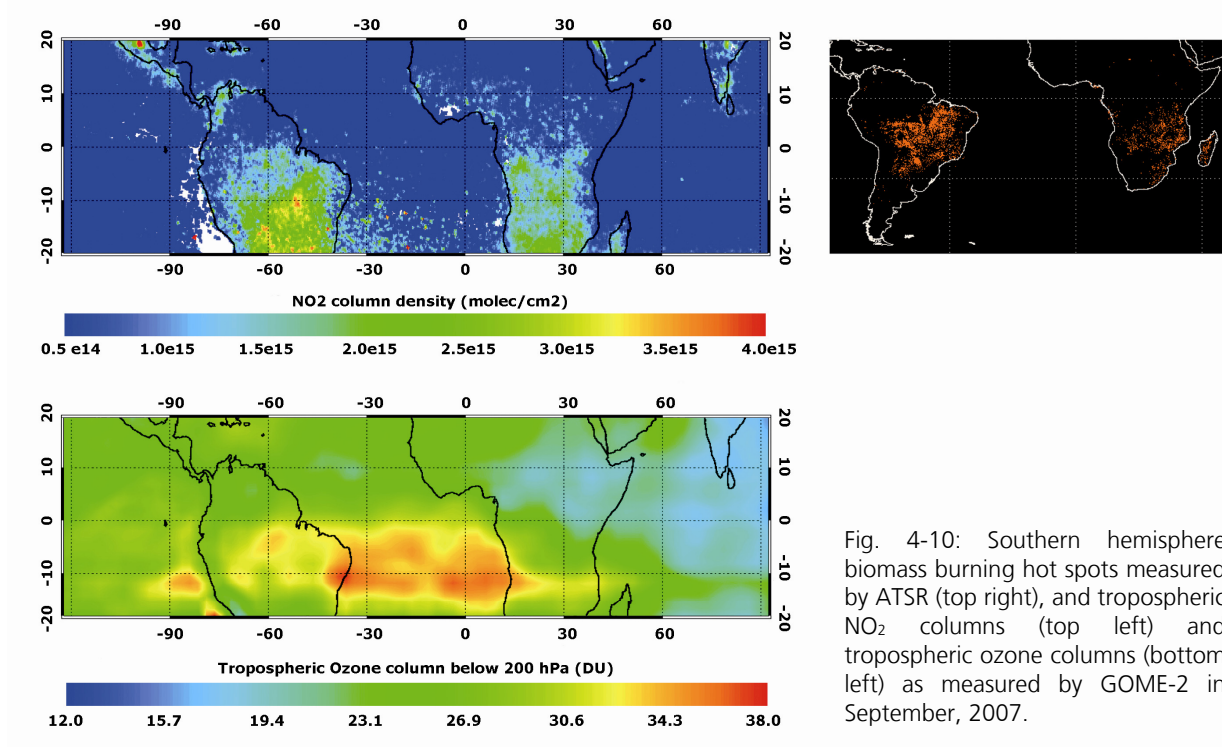


Fig. 4-10: Southern hemisphere biomass burning hot spots measured by ATSR (top right), and tropospheric NO_2 columns (top left) and tropospheric ozone columns (bottom left) as measured by GOME-2 in September, 2007.

References

Loyola D., Thomas W., Livschitz Y., Ruppert T., Albert P., and Hollmann R.: Cloud properties derived from GOME/ERS-2 backscatter data for trace gas retrieval, *IEEE Transactions on Geoscience and Remote Sensing*, 45/9, 2747-2758, 2007

Valks P.J.M., Koelmeijer R.B.A., van Weele M., van Velthoven P., Fortuin J.P.F., and Kelder H.: Variability in tropical tropospheric ozone: Analysis with Global Ozone Monitoring Experiment observations and a global model, *J. Geophys. Res.*, 108, 4328, 2003

Valks P., Loyola D., Hao N., Rix M., and Slijkhuis S.: Algorithm Theoretical Basis Document for GOME-2 Total Column Products of Ozone, Minor Trace Gases and Cloud Properties (GDP 4.4 for O3M-SAF OTO and NTO), DLR/GOME-2/ATBD/01, Iss./Rev.: 2/D, 2011a, available at: <http://o3msaf.fmi.fi>

Valks P., Pinardi G., Richter A., Lambert J.-C., Hao N., Loyola D., Van Roozendael M., and Emmadi S.: Operational total and tropospheric NO₂ column retrieval for GOME-2, *Atmos. Meas. Tech.*, 4, 1491-1514, doi:10.5194/amt-4-1491-2011, 2011b

4.3 Spaceborne Measurements of Air Quality During the World Expo 2010 in Shanghai

N. Hao, P. Valks, D. Loyola, W. Zimmer

Shanghai (31.2° N, 121.5° E), one of the largest cities in China, held the World Exposition 2010 (Expo) from May 1 to October 31, 2010. Its fast growing economy, long history of industrial development and rapid industrialization in neighboring provinces pose large challenges to the air quality in the Shanghai area. The air quality during the Expo in Shanghai was a major concern for the local government, similarly to the Olympic Games in Beijing. For improving the air quality during the Expo, Shanghai municipal government pursued many emission control measures (ECMs) focusing on energy, industry, transport and construction (UNEP, 2010). As during the Beijing Olympic Games, several high polluting enterprises such as coking and cement industries were ordered to reduce their operating capacities and all construction activities in the city were suspended during the Expo. Although no very strict traffic control measures were implemented during the Expo period because of its longer duration, such as removing half of the cars from the road as implemented during Beijing 2008 Olympic Games, it was estimated that the NO_x emissions from vehicles would decrease by about 10% (*Shanghai Environmental Protection Bureau 2010*). In addition, joint pollution prevention and control measures were carried out in the surrounding provinces because air pollutants from the surrounding areas could also affect the air quality in Shanghai under certain meteorological conditions.

We used satellite measurements to monitor the evolution of major air pollutants, i.e. NO₂, aerosol loading and CO, in Shanghai and surrounding areas. Their changes during and after the Expo were tracked using data from three satellite instruments: the Global Ozone Monitoring Experiment 2 (GOME-2), Terra's Measurements of Pollutants in the Troposphere (MOPITT) and Aqua's Moderate Resolution Imaging Spectroradiometer (MODIS). The six-month duration of the Expo provided a unique opportunity to examine the effectiveness of ECMs on air quality over Shanghai and surrounding provinces and to demonstrate the ability of satellite observation to monitor and quantify these changes. In order to analyze the effect of the ECMs on the air quality during the Expo 2010, two periods were defined: the Expo period (May to October 2010) when all the ECMs had been in effect and the post-Expo period (November 2010 to April 2011) when short-term ECMs had been lifted. May to October 2007-2009 served as a reference for the Expo period. Similarly, November to April 2007-2010 served as a reference for the post-Expo period.

GOME-2 tropospheric NO₂ columns for the Expo and the post-Expo periods were compared with those for the reference periods over Shanghai (see Fig. 4-11). The ratios of NO₂ columns between 2010 and the reference period showed a reduction of NO₂ during the Expo period over Shanghai. Compared to previous years, tropospheric NO₂ columns over Shanghai decreased about 8% during the Expo period. Fig. 4-11 also displays that the tropospheric NO₂ columns increased about 20% during the post Expo period, compared to its reference period. In-situ NO₂ measurements derived from NO₂ air pollution index (API) for the period May 2009 to April 2011 have been used for the comparison with the GOME-2

measurements. A high correlation (correlation coefficient up to 0.83) between satellite and in-situ measurements was found.

	GOME-2					In-situ Measurements				
	2007-2009		2010		Diff (%)	2007-2009		2010		Diff (%)
	Mean	σ	Mean	σ		Mean	σ	Mean	σ	
Expo	14.3	3.5	13.1	3.7	-8	46.3	6.3	41.6	6.2	-10
Post-Expo	22.9	3.3	27.5	4.2	20	57	8.6	65.3	7.8	15

Table 4-1: Tropospheric NO₂ columns (10¹⁵ molec/cm²) and 1- σ standard deviation over Shanghai (30.7° -31.5° N, 120.9°-121.9° E, see box in Fig. 4-13) as measured by GOME-2. In-situ NO₂ concentrations ($\mu\text{g}/\text{m}^3$) and 1- σ standard deviation over Shanghai as measured by the Shanghai Environmental Monitoring Center (SEMC). Tropospheric NO₂ columns and in-situ NO₂ concentrations are given for the periods: May to October 2010 (Expo), November 2010 to April 2011 (post-Expo) as well as the reference period (2007-2009).

Table 4-1 lists the average NO₂ concentrations and columns observed by in-situ and satellite measurements for the Expo, the post-Expo and the corresponding reference periods. The in-situ measurements indicated that NO₂ concentrations decreased by about 10% during the Expo and increased by about 15% after the Expo. Both from satellite and in-situ measurements it could be inferred that the short-term ECMs implemented in Shanghai were effective in reducing the NO_x concentrations during the Expo. The lift of short-term emission control measures after the Expo resulted in a rebound of NO_x pollution.

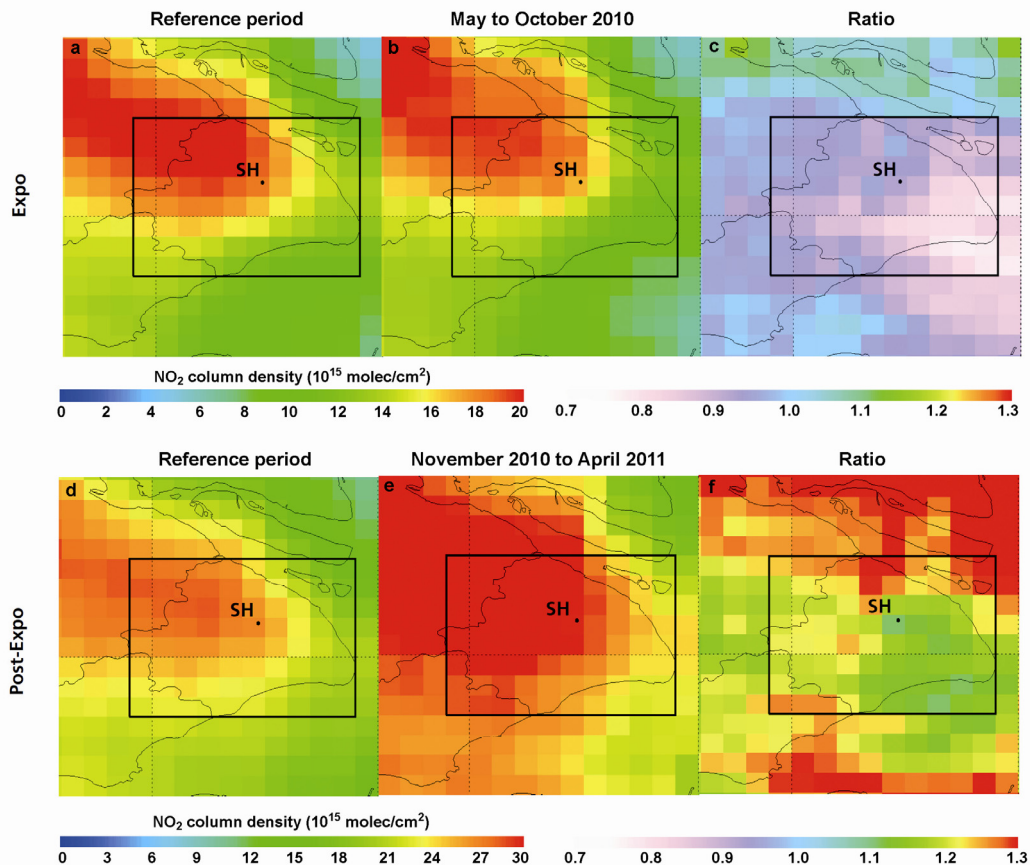


Fig. 4-11: Average tropospheric NO₂ columns during the Expo period (b) and the post-Expo period (e). 18-month averages of tropospheric NO₂ columns for the corresponding reference of the Expo period (a, May to October 2007-2009) and the post-Expo period (d, November to April 2007-2010) are also shown. The ratio of NO₂ columns between the Expo, post-Expo and the reference are shown in c and f. The ratio less than 1 indicates larger NO₂ in the reference period. During the Expo period, significant NO₂ reduction (c) is found around Shanghai (SH).

To estimate the effect of ECMs on the aerosol loading over Shanghai, average Aqua/MODIS Aerosol Optical Thickness (AOT) during the Expo period and the corresponding reference period are compared in Fig. 4-12. During the Expo period, the AOT decreased by about 14% over Shanghai (circle in Fig. 4-12) compared to the reference period. Similar reductions in the Particulate Matter 10 (PM₁₀) concentrations in Shanghai during the Expo period were reported by a Mid-Expo Air Quality Report (CAI-Asia 2010). The observed reduction in aerosol is most likely related to the short-term ECMs implemented over Shanghai during the Expo period.

Shanghai's neighboring provinces Zhejiang and Jiangsu, which are rapidly industrialized and highly urbanized, have large impacts on the air quality in Shanghai (UNCP 2010). Therefore, joint pollution prevention and emission control measures based on the cooperation platform of Shanghai and surrounding provinces were in effect during the Expo period. To check the effect of these joint ECMs, an analysis domain (29°-32° N, 120°-122° E) including Shanghai and neighboring provinces was defined (box in Fig. 4-12). AOT over this domain for the Expo and the post-Expo were compared with those during the same months in the reference period. AOT reduction during the Expo period is about 21% and AOT increase after the Expo amounts to about 18%, relative to the reference period. This might be a consequence of joint ECMs implemented in Shanghai and surrounding provinces during the Expo period.

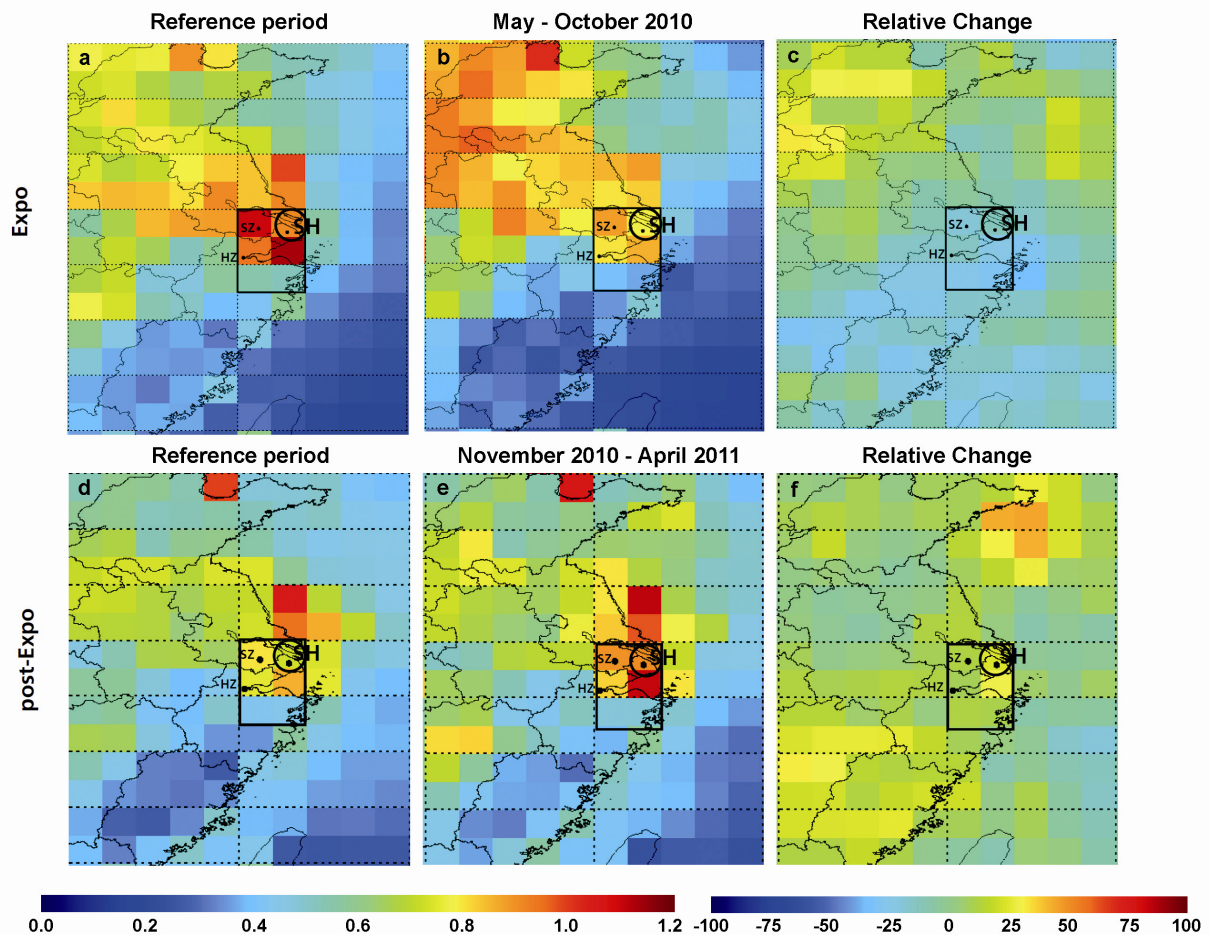


Fig. 4-12: Mean AOT during the Expo (b) and the post-Expo period (e) as measured by MODIS. 18 month averages of AOT for the reference of the Expo period (a, May to October 2007-2009) and the post-Expo period (d, November to April 2007-2010) are also shown. During the Expo period, significant AOT reduction (c) is found around Shanghai (SH), Suzhou (SZ) and Hangzhou (HZ). The relative change is given in %; negative values indicate a larger AOT in the reference period. The circle represents Shanghai while the box indicates Shanghai and surrounding areas.

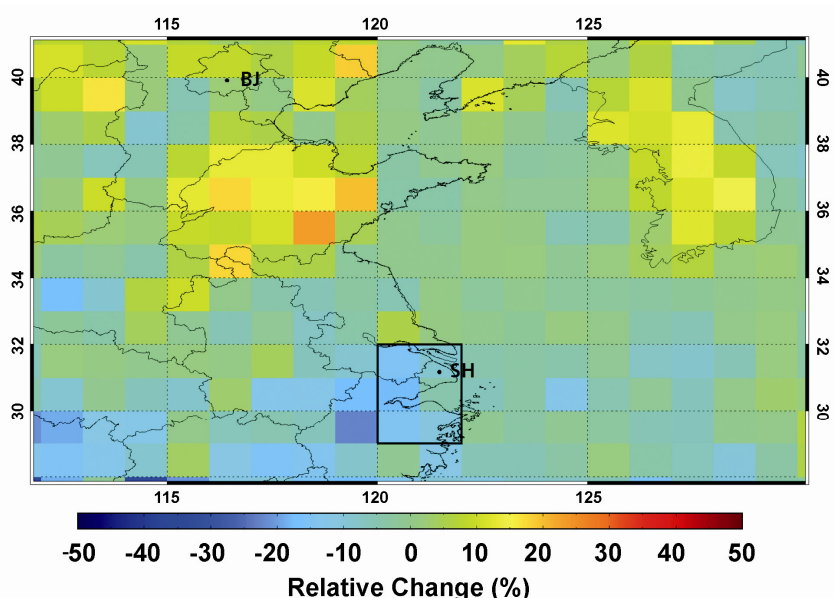


Fig. 4-13: Relative changes in CO concentrations (in %) between the Expo period (May-October 2010) and the reference period (2007-2009) for Shanghai and surrounding areas (box). SH represents Shanghai and BJ represents Beijing.

CO has longer chemical lifetimes in the troposphere and enhanced concentrations may be found further away from the emission sources (*Witte et al. 2009*), therefore a larger region (29°-32° N, 120°-122° E) including Shanghai and neighboring areas is used for the Expo analysis. The relative changes in CO concentrations between the Expo period and the reference period are shown in Fig. 4-13. CO concentrations over Shanghai and neighboring areas (box in Fig. 4-13) decreased about 12% during the Expo period, compared to the reference years. It is interesting to mention that in contrast to Shanghai, the large urban areas located in the north of China (i.e. Beijing and vicinity) where no ECMs were implemented showed an increase in the CO concentrations.

	Expo		
	Reference Period	2010	Climatological Data*
Mean Temperature (°C)	25.2 ± 3.3	24.9 ± 4.5	23.2
Relative Humidity	70 ± 4.2	69 ± 3.6	79
Mean Precipitation (mm/month)	158 ± 78	120 ± 55	131
Mean Number of Rainy Days (per year)	71	69	69
Prevailing Wind Direction	SE SSE	SE SSE	SE
Wind Speed (km/h)	11.0 ± 1.3	10.7 ± 0.8	10.3

* Precipitation data come from China Meteorological Administration. Other data come from Solar and Wind Energy Resource Assessment (SWERA)

Table 4-2: Meteorological data at Hongqiao airport, Shanghai (31.2° N, 121.3° E). Mean temperature, relative humidity, mean precipitation amount per month, prevailing wind direction, wind speed (including 1-σ standard deviation) and mean number of rainy days per year are given for the Expo period (May to October 2010) as well as the reference period (2007-2009). The 30 years (1971-2000) climatological data are also listed.

To investigate the effect of meteorological conditions on the changes in NO₂, aerosol loading and CO as described above, precipitation, temperature and wind data for Shanghai's Hongqiao airport during the Expo period and the reference period had been used. In addition, 30 years (1971-2000) climatological data for the Shanghai area are also listed in Table 4-2. It shows that meteorological conditions including

prevailing wind direction, mean precipitation per month and mean number of rainy days per year during the Expo and the reference period in Shanghai were typical when compared to the climatological data in the 30 year period. A number of studies (*Ding et al. 2009*) found that between May and August the East Asian summer monsoons (EASM) affects the air quality over eastern China by influencing transport, chemical reactions and deposition of air pollutants. To investigate the potential effect of the EASM strength on interannual variations of air pollutants over Shanghai, the EASM index from 2007 to 2010 was used (*Li and Zeng 2005*). A high aerosol pollution over East China was expected due to a relative weak summer monsoon in 2010. In addition, satellite retrieved precipitation data showed that the total precipitation amount (about 720 mm) during the Expo period was smaller than for the same months in 2007 (about 1200 mm). Improved air quality in Shanghai during the Expo period was found although a lower relative humidity and rainfall rate occurred which are both favourable for air pollutants accumulation. Thus it could be concluded that meteorological conditions had no significant impact on the improved air quality in Shanghai during the Expo period.

References

- Clear Air Initiative for Asian Cities (CAI-Asia) Center*: Blue Skies at Shanghai Expo 2010 A Mid-Expo Air Quality Report. Pasig City Philippines, 2010
- Shanghai Environmental Protection Bureau*: The implement of National Stage IV Motor Vehicle Emission Standard and vehicle emission control measures during the Expo (in Chinese), 2010
- United Nations Environment Programme (UNEP)*: Environmental assessment: EXPO 2010-Shanghai China U.N. Environ. Programme Nairobi 00100 Kenya, 2010
- Witte J.C., Schoeberl M.R., Douglass A.R., Gleason J.F., Krotkov N.A., Gille J.C., Pickering K.E., Livesey N.* : Satellite observations of changes in air quality during the 2008 Beijing Olympics and Paralympics. *Geophys. Res. Lett.*, 36, L17803, doi: 10.1029/2009GL039236, 2009
- Ding A.J., Wang T., Thouret V., Cammas J.-P., and Nédélec P.*: Tropospheric ozone climatology over Beijing: analysis of aircraft data from the MOZAIC program *Atmos. Chem. Phys.* 8 1-13, 2008
- Li J. and Zeng Q.*: A new monsoon index, its interannual variability and relation with monsoon precipitation. *Climatic and Environmental Research*, 10(3): 351-365, 2005

4.4 The Light Scattering Laboratory within the DLR_School_Lab Neustrelitz

K. Schmidt, T. Rother, A. Weidemann (LS-SL NZ), S. Simon (Contractor), K. Prehn (FH Neubrandenburg)

The DLR_School_Labs represent high-tech student laboratories in DLR research institutions aiming at providing students with capabilities for doing their own experiments, well matched to the age level of the participants. The experiments reflect the entire range of DLR activities in the fields of aeronautics, space, transportation, energy, and security. In this way, young people and students have an opportunity to actively discover the fascinating world of research and technology. There are also special programmes for highly gifted young people to motivate them to choose, in future, a relevant course of studies or a professional career. But also teaching personnel can benefit from the DLR_School_Labs. The laboratories offer support for planning modern and interesting courses. In addition they provide access to sophisticated equipment and facilities usually unavailable at schools. By demonstrating practical applications of research results, corresponding curricula may be improved accordingly. Meanwhile nine DLR_School_Labs, located at various DLR premises or partner universities welcome and coach some 20,000 students every year (*Kratzenberg-Annies and Tegen 2011*).

One of the DLR_School_Labs is hosted at DLR in Neustrelitz. The department for *Atmospheric Processors* (IMF-AP) has been involved in developing and installing a light scattering laboratory. The basic idea behind this lab is to demonstrate and explain phenomena caused by sunlight scattering on small atmospheric particles such as the blue and red sky, the sky polarization, rainbows, and halos. This helps to better understand the underlying physical processes. Conceptually the lab is based on our long-time experience in the field of light scattering modelling on non-spherical particles with applications to

remote sensing of the Earth's atmosphere. Useful instructions for some of the experiments have also been found in existing literature, e.g. *Vollmer (2006)*.

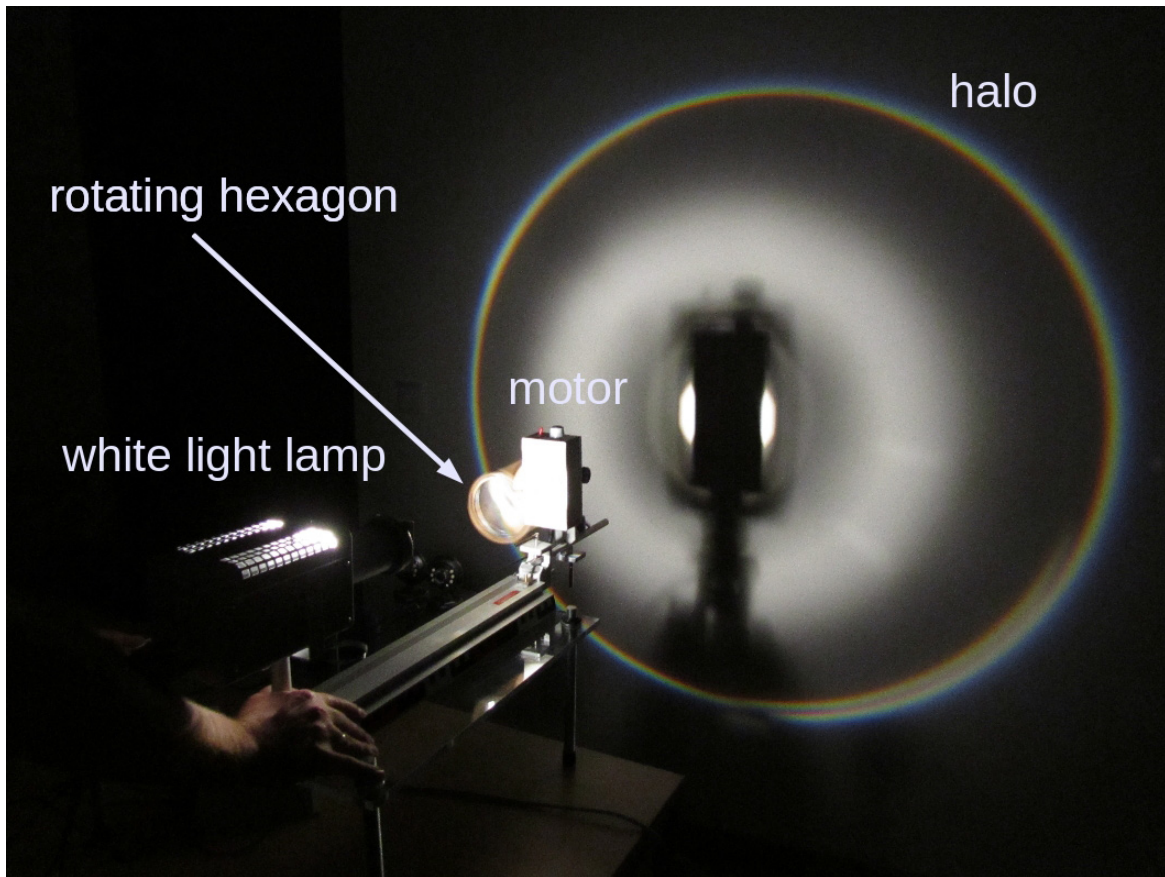


Fig. 3-13: Demonstration of the 22° halo. The cylindrical axis of the hexagon is perpendicularly oriented against the incident light direction.

Most of the phenomena are related to the fact that white sunlight is a mixture of different colours. This is demonstrated by means of a prism. Some of these colours can be observed as dawn, afterglow, and blue sky. They are caused by sunlight scattering on the air molecules (Rayleigh scattering). The same mechanism is also responsible for the sky polarization. A simple indoor experiment allows simulating such phenomena. A bin containing a turbid medium such as a milk powder solution represents the atmosphere, while a white light lamp serves as the sun. The polarization state of the scattered light can be demonstrated by means of a filter at an angle of about 90° with respect to the incident light propagation direction thus permitting studies of polarization effects. For investigating the conditions leading to the occurrence of rainbows, water spray and glass spheres are used. Halo phenomena are generated by means of a rotating hexagonal plexiglass cylinder (Fig. 3-13). Since it is possible to operate lasers at different wavelengths instead of a white light lamp, the students are able to perform frequency dependent investigations. Weather permitting, all the experiments may even be conducted outside.

References

Kratzenberg-Annie V., and Tegen C.: The DLR_School_Labs. Out of the classroom - into the lab!, DLR (ed.), Köln, 2011. <http://www.dlr.de/dlrschoollab>.

Vollmer M.: Lichtspiele in der Luft - Atmosphärische Optik für Einsteiger, Elsevier, München, 2006

4.5 Spectroscopic Characterization of the Atmospheres of Potentially Habitable Planets: GL 581d as a Model Case Study

F. Schreier, P. von Paris (DLR-IPF und LAB), J. Cabrera (DLR-IPF), M. Godolt (TUB-ZAA), J.L. Grenfell (TUB-ZAA), P. Hedelt (LAB), H. Rauer (DLR-IPF und TUB-ZAA), B. Stracke (DLR-IPF)

Up to January 2012 more than 700 extrasolar planets have been detected. Among these are a few dozen terrestrial exoplanets with masses $1 m_E < m < 10 m_E$, i.e. 'Super-Earths', meanwhile discovered due to more sophisticated instrumentation. Clearly the characterization of terrestrial planets located in the habitable zone around their central star is a challenging yet exciting prospect, since these objects are good candidates for the search of extraterrestrial life. The Habitable Zone is defined as the shell around a star at orbital distances permitting moderate temperatures with liquid water on the planets surface to be present. The potential habitability of a planet is critically dependent on atmospheric (pressure, temperature and composition) and surface conditions, hence estimation of these quantities is crucial.

The red dwarf Gliese 581 is one of our closest galactic neighbors at a distance of only 20 light years. It has attracted increasing attention because at least three potentially low-mass planets have been detected orbiting this M star, one of which, GL 581d, could be a habitable Super-Earth with a mass of approx. $7 m_E$. It orbits the central star at a distance of about 0.22 Astronomical Units (AU).

Observations of transiting planets are a superior means to characterize planetary atmospheres: transmission spectroscopy during the primary transit is more practical at ultraviolet (UV), visible and near-infrared (IR) wavelengths, whereas emission spectroscopy during the secondary eclipse is easier in the mid-IR. Hence both methods provide complementary results. Although GL 581d is unlikely to transit its central star, GL 581d was used as an analogue of similar, transiting systems anticipated to be found in the near future. Thus we studied potential spectroscopic signatures of a transiting GL 581d using profiles obtained in a previous atmospheric modeling investigation of habitability in the Gliese 581 system. Using a 1D radiative-convective climate model, key parameters such as surface pressure and atmospheric temperature and composition had been varied to investigate their influence on resulting surface conditions. The stellar input spectrum was based on a synthetic spectrum in the visible and NIR combined with satellite observations in the UV. Atmospheres were assumed to be composed of N_2 , CO_2 , and H_2O , and the surface albedo was set to 0.13 (corresponding to the Earth surface albedo). For massive CO_2 atmospheres (5 or more bar surface pressure with CO_2 concentrations of 95%, 20 bar with 5% CO_2), the surface temperatures exceeded 273 K and could be as high as 357 K. Furthermore, the model runs indicated that for medium CO_2 concentrations (5% Volume Mixing Ratio as for the young Earth), habitable conditions could be found on GL 581d. In contrast, for scenarios with less CO_2 , the planet was found to be uninhabitable.

Pressure, temperature, and concentration profiles of atmospheric model scenarios of GL 581d with moderate surface temperatures were used to calculate high-resolution synthetic emission and transmission spectra. The line-by-line computations were performed with the MIRART/SQUIRRL code (the Fortran 77 precursor of the GARLIC code). These spectra were used to calculate contrast, effective tangent height, and signal-to-noise ratio (SNR) estimates assuming a spectral resolution of $R=10$ and a *James Webb Space Telescope* set-up. The existence of an atmosphere including water and carbon dioxide could be inferred from the spectra for the cases of 20 bar 95% CO_2 and 1 bar 95% CO_2 . Furthermore, in the 1 bar high CO_2 case some spectral windows would allow estimating the surface temperature, whereas the 20 bar high CO_2 atmosphere is optically too thick to permit any surface temperature estimates.

For the search of extraterrestrial life the identification of biosignatures is mandatory. Biosignatures are features in the observed spectra attributable to molecules suggesting some biological activity, e.g., oxygen O_2 , ozone O_3 , nitrous oxide N_2O . In this context the possibility of false-positive or false-negative detection of biomarkers is especially important. Fig. 3-14 shows that without careful examination the CO_2 absorption band at $9.5 \mu m$ (near the $9.6 \mu m$ band of ozone) could be erroneously interpreted as an evidence of O_3 . Likewise, the CO_2 bands around 7.5 and $8 \mu m$ are near the methane band at $7.7 \mu m$, emphasizing again the need for careful spectral analysis. Note that these three CO_2 bands are also present in the transmission spectra, so the possibility of false-positive biomarker detection has to be considered for both emission and transmission spectroscopy.

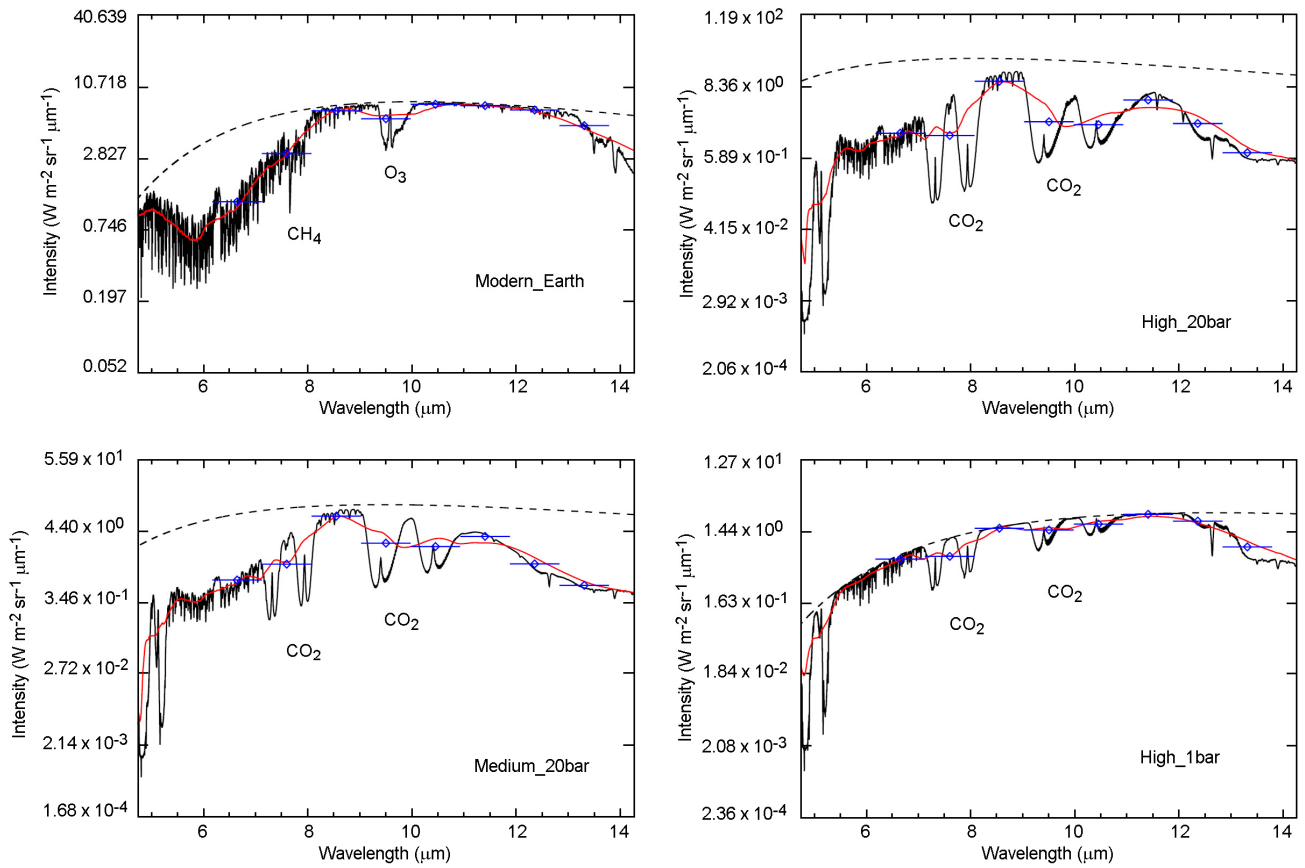


Fig. 3-14. Possibility of a false-positive biomarker detection for different scenarios. Planck curves of corresponding surface temperatures as dashed lines. Smoothed (red) and binned spectra (blue) are for a spectral resolution of 10. Note that the GL 581d spectra were calculated for a pure $\text{N}_2\text{-H}_2\text{O-CO}_2$ atmosphere.

References

von Paris P, Gebauer S, Godolt M, Grenfell J. L., Hedelt P, Kitzmann D., Patzer A.B. C., Rauer H., and Stracke B.: The extrasolar planet Gliese 581d: a potentially habitable planet?, *Astronomy & Astrophysics*, 522, A23, 2010

von Paris P, Gebauer S, Godolt M, Rauer H., and Stracke B.: Atmospheric studies of habitability in the Gliese 581 system, *Astronomy & Astrophysics*, 532, A58, 2011

von Paris P, Cabrera J, Godolt M, Grenfell J, Hedelt P, Rauer H, Schreier F, and Stracke B.: Spectroscopic characterization of the atmosphere of potentially habitable planets: GL 581d as a model case study, *Astronomy & Astrophysics*, 534, A26, 2011

4.6 High Resolution Infrared Emission Spectra of Earth-like Planets Influenced by Clouds

M. Vasquez, F. Schreier, D. Kitzmann (TUB-ZAA), S. Gimeno García (TUM), T. Trautmann, B.A.C. Patzer (TUB-ZAA), H. Rauer (DLR-IPF)

Study

Clouds have an impact on the radiative transfer in planetary atmospheres by changing the intensities and shapes of the planetary spectra due to extinction events. Thereby, they can influence the atmospheric and surface temperatures and can also generate false-negative biomarker signatures.

We studied the thermal emission spectrum of Earth-like planets at high resolution in the presence of low (~ 1 km) and high-level (~ 10 km) clouds. Four different cloud coverage percentages had been considered in the radiative transfer modeling: 0%, 30%, 70% and 100%. Accurate high resolution spectra were modeled using GARLIC, a line-by-line radiative transfer model that has been extended to take into account multiple scattering calculations. The atmospheric profiles (Fig. 4-15), which were required as input in GARLIC, were calculated with a radiative convective climate model (Kitzmann *et al.* 2010).

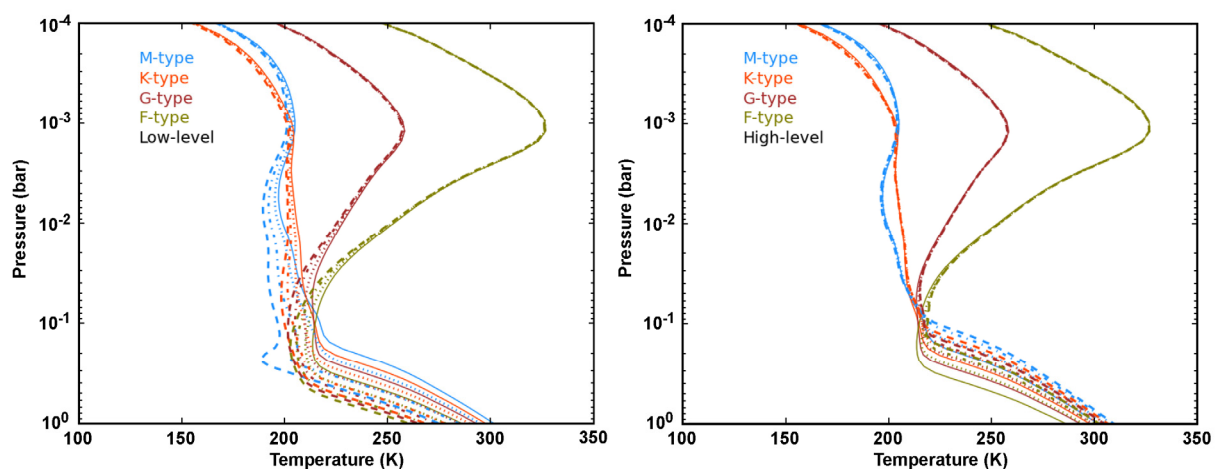


Fig. 4-15: Pressure-temperature profiles of planets influenced by low and high clouds for four different coverages: 0% (solid lines), 30% (dotted lines), 70% (dash-dot lines) and 100% (dashed lines). Planets are modeled around typical M (blue), K (orange), G (brown), and F-type (olive green) stars.

Results

The new extended version of the GARLIC model was successfully tested with respect to the consistency to the low resolution radiative transfer spectra calculated by Kitzmann *et al.* (2011). The modeled spectra for a cloud-free atmosphere (0%) show that the spectrum changes in the presence of different star types. The highest emission flux appears for the planet orbiting the M star. The resulting spectra in the presence of clouds indicate that they have a great impact on the radiative transfer of Earth-like planets by decreasing the depth of the absorption bands and changing their shape (Fig. 4-16). CO₂ bands at 4.3 and 15 μ m in the F star planet show an emission shape in the absence and presence of clouds. This is due to the temperature inversion found in the stratosphere of the planet. The upper stratosphere, where CO₂ still absorbs, reaches temperatures that are even larger than the surface temperature of the planet.

The H₂O and O₃ molecular bands resulted to be the most affected ones in the different planetary cases. In the planet orbiting the F star, the O₃ band is almost indistinguishable. The reason behind this is that the cloud deck of the low and high-level cloud in the F star planet is at a temperature that is comparable to that of the stratospheric altitudes, where O₃ is absorbing strongly.

Conclusion

The spectra of Earth-like planets have been analyzed in the presence of different cloud conditions. In general, high and low cloud types have different effects on the temperatures of the planets. The low-level cloud cooled down the tropospheric temperatures, while the high-level cloud warmed them up. Moreover, clouds may also impact the spectral signatures. The H₂O and O₃ bands were highly reduced for the 100% cloud coverage, clearly indicating that clouds may produce false-negative detection.

Clouds also affected the possibility to estimate the surface temperature of the planets. The difficulty of obtaining this temperature increased with larger percentage of cloud cover, especially in the presence of high-level clouds.

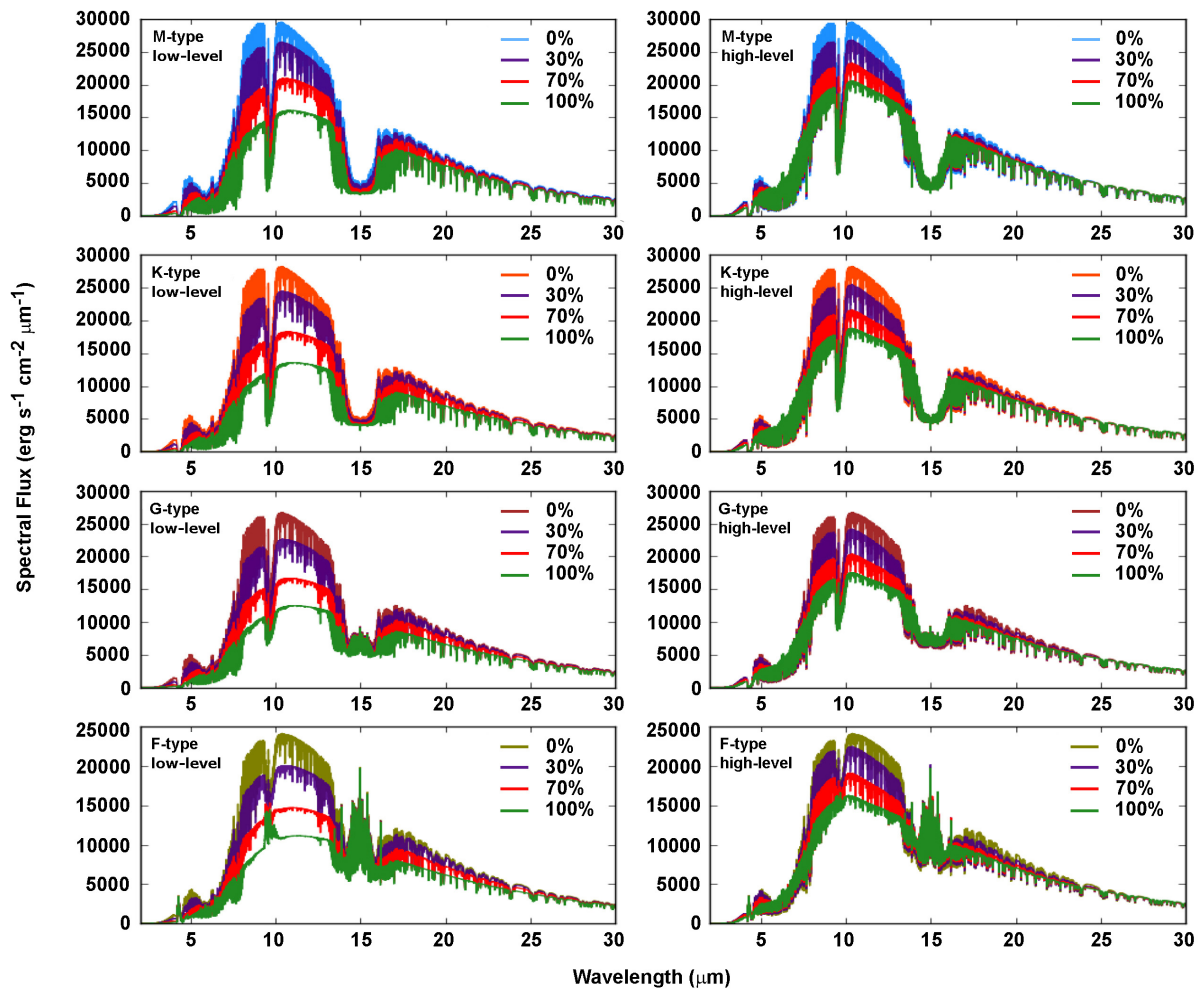


Fig. 4-16: Infrared emission spectra of Earth-like planets for two types of clouds (high ice clouds and low water clouds) with four different percent coverages.

References

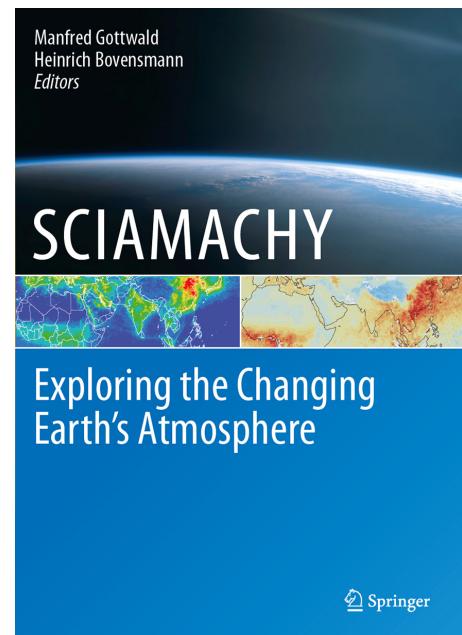
Kitzmann D., Patzer B., von Paris P., Godolt M., Rauer H.: Clouds in the atmospheres of extrasolar planets. II. Thermal emission spectra of Earthlike planets influenced by low and high-level clouds, *Astronomy and Astrophysics*, 531, A62, 2011

Kitzmann D., Patzer A., von Paris P., Godolt M., Stracke B., Gebauer S., Grenfell J., Rauer H.: Clouds in the atmospheres of extrasolar planets I. Climatic effects of multi-layered clouds for Earth-like planets and implications for habitable zones. *Astronomy & Astrophysics* 511, A66, 2010

4.7 Textbook SCIAMACHY – Exploring the Changing Earth’s Atmosphere

M. Gottwald, H. Bovensmann (IUP-IFE)

In March 2002 the atmospheric science instrument SCIAMACHY was launched on-board ESA’s ENVISAT mission into low-Earth orbit. It was, and is still, one of the major current Earth Observation undertakings of Germany, The Netherlands and Belgium, accomplished in cooperation with the European Space Agency (ESA). In 2006 a first version of a book describing the SCIAMACHY mission had been published as a common effort of the participating science community. It was issued by the space agencies DLR, NIVR and ESA. This edition had quite successfully described the entire SCIAMACHY mission from the very first ideas to the exciting current results. Meanwhile the mission had progressed well. It was therefore considered justified to prepare a new version of the book. Contrary to the 2006 issue, the new version was not printed as a space agency undertaking but was published by Springer (ISBN 978-90-481-9895-5) as a first edition in the series of Earth Sciences books in January 2011 under the title *SCIAMACHY – Exploring the Changing Earth’s Atmosphere*. The targeted readership is not only the existing and potentially new SCIAMACHY data users from undergraduate student level up to researchers new in the fields of atmospheric chemistry and remote sensing but anyone who is keen to learn about SCIAMACHY’s efforts to study the atmosphere and its responses to both, natural phenomena and anthropogenic effects.



Chapter 1 explains why it is necessary to make measurements from low-Earth orbit for studying the atmosphere. The global views from an altitude of 800 km open new windows to observe large-scale phenomena which are of prime importance to understand today’s changing atmosphere and climate. Having summarized why SCIAMACHY was selected to be launched into space, **chapter 2** takes a closer look at the ENVISAT mission, which hosts SCIAMACHY. The purpose of chapter 2 is to describe those aspects of ENVISAT being of relevance to the SCIAMACHY mission. The location on and the environment of the platform, together with the ENVISAT orbit, determines many aspects of the instrument’s design and operation. Similarly the concepts for data downlink and handling in the ground segment specify how measurement data is received, processed and disseminated in general.

A detailed description of the instrument concept is the subject of **chapter 3**. It permits insight into optical, thermal and electronic subsystems. Main emphasis is given to the optical paths since they collect and generate the spectral signals containing the information on geophysical parameters. In order to provide the reader with an idea about the challenges of instrument development, chapter 3 also outlines the history of how SCIAMACHY was built. Without a flexible operations concept however, all the sophisticated instrument functionalities would have been useless. How SCIAMACHY is operated in-orbit can be found in **chapter 4**. The chosen operations approach allows, despite the instrument complexity, full exploitation of its capabilities in a well structured operations environment thus supporting the need for long, stable measurements as required in atmospheric and climate research. In **chapter 5**, the various steps necessary to calibrate the instrument, on-ground and in-orbit, are presented. Calibration is required to fully characterize the optical paths. Additionally, chapter 5 also addresses optical performance monitoring which permits quantification of the degradation of optical components. Calibration and monitoring together ensure that the recorded signals are transformed into well calibrated spectra – a prerequisite for retrieving geophysical parameters with high accuracy over the full mission lifetime.

Chapter 6 describes SCIAMACHY’s in-orbit mission lifetime, starting with the launch and the Commissioning Phase and illustrates more than 8 years of routine measurements. Various instrument characteristics, derived from the monitoring activities, are presented and show the excellent in-orbit behaviour. It also outlines how in-orbit degradation, a phenomenon common to each long duration

space mission, impacts SCIAMACHY's measurements and demonstrates how it can be corrected or compensated.

With **Chapter 7** the science related information is introduced by summarizing the principles and methods for the derivation of geophysical parameters from the measured spectra. While in the early years of the mission the retrieval methods were mostly relying on standard algorithms, the scientific ingenuity has meanwhile generated a wealth of novel techniques permitting the retrieval of geophysical parameters beyond the original ideas.

Operational and scientific data products are the subject of **chapter 8**. The reader learns which products are generated under ESA responsibility and which are provided by research institutions involved in SCIAMACHY. For the ESA generated products, the strict requirements and implementations of the operational processing environment are outlined. As every geophysical parameter retrieval requires well calibrated measurements, we also report on how calibration and monitoring information is used to derive earthshine, extraterrestrial radiance and irradiance data products from the raw signals.

Retrieved geophysical parameters do not necessarily immediately translate into atmospheric science results. It has to be proven first that the data products are of sufficient quality. This process of product validation, subject of **chapter 9**, was an enormous effort in the first years of the mission and is required, at an adequate level, throughout the mission and even beyond to create long-term datasets of known and reliable quality relevant for environmental, atmospheric and climate change research. Chapter 9 explains the selected validation procedures, associated teams and summarizes results acquired so far.

Chapter 10 concludes the publication by presenting SCIAMACHY's unique view of the changing Earth's environment. The capabilities of the instrument permit studying phenomena ranging from the atmospheric layer where we are living in, i.e. the lower troposphere, up to the mesosphere and lower thermosphere where solar-terrestrial interactions begin to prevail. However SCIAMACHY does not at all stop at the bottom or top of the atmosphere. Even Earth surface parameters like vegetation or phytoplankton properties are now within reach as well as monitoring the solar activity. Finally SCIAMACHY has proven surprisingly successful in acquiring spectral signals from the atmosphere of our neighbour Venus. The content of chapter 10 nicely illustrates the success achieved up to now and justifies continuing investments in the SCIAMACHY mission and data usage.

The Atmospheric Science Librarians International (ASLI), an international professional association for atmospheric science librarians, institutions, and organizations involved in atmospheric research, has selected *SCIAMACHY – Exploring the Changing Earth's Atmosphere* as the '2011 ASLI Choice' in the fields of meteorology, climatology and atmospheric sciences for its 'comprehensive summary of the milestone SCIAMACHY mission from its initial conception to most recent results' (<http://aslionline.org/wp/2011-asli-choice-awards-winners/>). The award was presented by ASLI at the New Orleans annual meeting of the American Meteorological Society (AMS) in January 2012.

5. Documentation

5.1 Books and Book Contributions

Bovensmann, H., Doicu, A., Stammes, P., Van Roozendaal, M., von Savigny, C., Penning de Vries, M., Beirle, S., Wagner, T., Chance, K., Buchwitz, M., Kokhanovsky, A., Richter, A., Rozanov, A., Rozanov, V.: From Radiation Fields to Atmospheric Concentrations - Retrieval of Geophysical Parameters. Chapter 7 in: *SCIAMACHY - Exploring the Changing Earth's Atmosphere*, Earth and Environmental Science. Springer Dordrecht Heidelberg London New York, ISBN 978-90-481-9895-5

Bovensmann, H., Aben, I., Van Roozendaal, M., Köhl, S., Gottwald, M., von Savigny, C., Buchwitz, M., Richter, A., Frankenberg, C., Stammes, P., de Graaf, M., Wittrock, F., Sinnhuber, M., Sinnhuber, B.M., Schönhardt, A., Beirle, S., Gloudemans, A., Schrijver, H., Bracher, A., Rozanov, A., Weber, M., Burrows, J.P.: SCIAMACHY's View of the Changing Earth's Atmosphere. Chapter 10 in: *SCIAMACHY - Exploring the Changing Earth's Atmosphere*, Earth and Environmental Science. Springer Dordrecht Heidelberg London New York, ISBN 978-90-481-9895-5

Dameris, M., Loyola, D.: Chemistry-climate connections – Interaction of physical, dynamical, and chemical processes in Earth atmosphere. In *Climate Change - Geophysical Foundations and Ecological Effects*, Open Access Book, InTech, 3-24, ISBN 978-953-307-419-1

Doicu, A., Trautmann, T., Schreier, F.: Regularization of inverse problems in atmospheric remote sensing. In *Polarimetric Detection, Characterization and Remote Sensing*, NATO Science for Peace and Security Series C: Environmental Security, 79-116, Springer, DOI: 10.1007/978-94-007-1636-0_4, 2011

Gottwald, M., Bovensmann, H. (eds): *SCIAMACHY - Exploring the Changing Earth's Atmosphere*, Earth and Environmental Science. Springer Dordrecht Heidelberg London New York, ISBN 978-90-481-9895-5

Gottwald, M., Diekmann, F.J., Fehr, T.: ENVISAT - SCIAMACHY's Host. Chapter 2 in: *SCIAMACHY - Exploring the Changing Earth's Atmosphere*, Earth and Environmental Science. Springer Dordrecht Heidelberg London New York, ISBN 978-90-481-9895-5

Gottwald, M., Hoogeveen, R., Chlebek, C., Bovensmann, H., Carpay, J., Lichtenberg, G., Krieg, E., Lützow-Wentzky, P., Watts, T.: The Instrument. Chapter 3 in: *SCIAMACHY - Exploring the Changing Earth's Atmosphere*, Earth and Environmental Science. Springer Dordrecht Heidelberg London New York, ISBN 978-90-481-9895-5

Gottwald, M., Moore, A., Noël, S., Krieg, E., Mager, R., Kröger, H.: Instrument Operations. Chapter 4 in: *SCIAMACHY - Exploring the Changing Earth's Atmosphere*, Earth and Environmental Science. Springer Dordrecht Heidelberg London New York, ISBN 978-90-481-9895-5

Gottwald, M., Bramstedt, K., Snel, R., Krijger, M., Lichtenberg, G., Slijkhuis, S., von Savigny, C., Noël, S., Krieg, E.: SCIAMACHY In-orbit Operations and Performance. Chapter 6 in: *SCIAMACHY - Exploring the Changing Earth's Atmosphere*, Earth and Environmental Science. Springer Dordrecht Heidelberg London New York, ISBN 978-90-481-9895-5

Lichtenberg, G., Eichmann, K.-U., Lerot, C., Snel, R., Slijkhuis, S., Noël, S., van Hees, R., Aberle, B., Kretschel, K., Meringer, M., Scherbakov, D., Weber, H., von Barga, A.: Processing and Products. Chapter 8 in: *SCIAMACHY - Exploring the Changing Earth's Atmosphere*, Earth and Environmental Science. Springer Dordrecht Heidelberg London New York, ISBN 978-90-481-9895-5

Snel, R., Lichtenberg, G., Noël, S., Krijger, M., Slijkhuis, S., Bramstedt, K.: Chapter 5: Calibration and Monitoring. Chapter 5 in: *SCIAMACHY - Exploring the Changing Earth's Atmosphere*, Earth and Environmental Science. Springer Dordrecht Heidelberg London New York, ISBN 978-90-481-9895-5

5.2 Journal Papers

Alam, K., Blaschke, T., Madl, P., Mukhtar, A., Hussain, M., Trautmann, T., Rahman, S.: Aerosol size distribution and mass concentration measurements in various cities of Pakistan. *Journal of Environmental Monitoring*, 13, 944-1952, doi: 10.1039/c1em10086f, 2011

Alam, K., Trautmann, T., Blaschke, T.: Aerosol optical properties and radiative forcing over mega-city Karachi. *Atmospheric Research*, 101, doi: 10.1016/j.atmosres.2011.05.007, 2011

Antón, M., Loyola, D., Clerbaux, C., López, M., Vilaplana, J.M., Bañón, M., Hadji-Lazaro, J., Valks, P., Hao, N., Zimmer, W., Coheur, P.F., Hurtmans, D., Alados-Arboledas, L.: Validation of the MetOp-A total ozone data from GOME-2 and IASI using reference ground-based measurements at the Iberian Peninsula. *Remote Sensing of Environment*, 115 (6), 1380-1386. DOI: 10.1016/j.rse.2011.01.018, 2011

Antón, M., Loyola, D.: Influence of cloud properties on satellite total ozone observations. *Journal of Geophysical Research*, 116 (116). DOI: 10.1029/2010JD014780, 2011

Antón, M., Bortoli, D., Kulkarni, P.S., Costa, M.J., Domingues, A.F., Loyola, D., Silva, A.M., Alados-Arboledas, L.: Long-term trends of total ozone column over the Iberian Peninsula for the period 1979–2008. *Atmospheric Environment*, 45(35), 6283-6290. DOI: 10.1016/j.atmosenv.2011.08.058, 2011

Bauer, S., Bierwirth, E., Esselborn, M., Petzold, A., Macke, A., Trautmann, T., Wendisch, M.: Airborne spectral radiation measurements to derive solar radiative forcing of Saharan dust mixed with biomass burning smoke particles. *Tellus B - Chemical and Physical Meteorology*, 63, 742-750. DOI: 10.1111/j.1600-0889.2011.00567.x, 2011

Gimeno García, S., Schreier, F., Lichtenberg, G., Slijkhuis, S.: Near infrared nadir retrieval of vertical column densities: methodology and application to SCIAMACHY. *Atmospheric Measurement Techniques*, 4 (12), 2633-2657, Copernicus Publications. DOI: 10.5194/amt-4-2633-2011, 2011

Hao, N., Valks, P., Loyola, D., Cheng, Y., Zimmer, W.: Space-based measurements of air quality during the World Expo 2010 in Shanghai. *Environmental Research Letters*. DOI: 10.1088/1748-9326/6/4/044004, 2011

Hedelt, P., Alonso, R., Brown, P., Collados, M., Rauer, H., Schleicher, H., Schmidt, W., Schreier, F., Titz-Weider, R.: Venus transit 2004: Illustrating the capability of exoplanet transmission spectroscopy. *Astronomy and Astrophysics*, 533 (A136), 8 pages, EDP Sciences . DOI: 10.1051/00046361201016237, 2011

Kahnert, M. and Rother, T.: Modelling optical properties of particles with small-scale surface roughness: combination of group theory with a perturbation approach. *Optics Express* 19, 11138–11151, 2011

Kniffka, A. and Trautmann, T.: Combining the independent pixel and point-spread function approaches to simulate the actinic radiation field in moderately inhomogeneous 3D cloudy media. *Journal of Quantitative Spectroscopy and Radiative Transfer*, 112 (8), DOI: 10.1016/j.jqsrt.2011.01.026, 1383-1393, 2011

Köhler, C.H., Trautmann, T., Lindermeir, E., Vreeling, W., Lieke, K., Kandler, K., Weinzierl, B., Gross, S., Tesche, M., Wendisch, M.: Thermal IR radiative properties of mixed mineral dust and biomass burning aerosol during SAMUM-2. *Tellus B - Chemical and Physical Meteorology*, 63 (4), 751-769, Blackwell Publishing Ltd. DOI: 10.1111/j.1600-0889.2011.00563.x, 2011

Kohlert, D., Schreier, F.: Line-by-Line Computation of Atmospheric Infrared Spectra With Field Programmable Gate Arrays. *IEEE Journal of Selected Topics in Applied Earth Observations and Remote Sensing*, 4 (3), 701-709. IEEE. DOI: 10.1109/JSTARS.2010.2098395, 2011

Loyola, D., Koukouli, M.L., Valks, P., Balis, D., Hao, N., Van Roozendael, M., Spurr, R., Zimmer, W., Kiemle, S., Lerot, C., Lambert, J.-C.: The GOME-2 total column ozone product: Retrieval algorithm and ground-based validation. *Journal of Geophysical Research*, 116 (D07302). DOI: 10.1029/2010JD014675, 2011

Meringer, M., Reinker, S., Zhang, J., Muller, A.: MS/MS Data Improves Automated Determination of Molecular Formulas by Mass Spectrometry. *MATCH Communications in Mathematical and in Computer Chemistry*, 65 (2), 259-290, 2011

Otto, S., Meringer, M.: Positively homogeneous functions in atmospheric radiative transfer theory. *Journal of Mathematical Analysis and Applications*, 376(2), 588-601, Elsevier, DOI: 10.1016/j.jmaa.2010.10.068, 2011

Otto, S., Trautmann, T., Wendisch, M.: On realistic size equivalence and shape of spheroidal Saharan mineral dust particles applied in solar and thermal radiative transfer calculations. *Atmospheric Chemistry and Physics*, 11, 4469-4490. Copernicus Publications. DOI: 10.5194/acp-11-4469-2011, 2011

von Paris, P., Cabrera, J., Godolt, M., Grenfell, J.L., Hedelt, P., Rauer, H., Schreier, F., Stracke, B.: Spectroscopic characterization of the atmospheres of potentially habitable planets: GL 581 d as a model case study. *Astronomy and Astrophysics*, 534, DOI: 10.1051/00046361/201117091, 2011

Rauer, H., Gebauer, S., von Paris, P., Cabrera, J., Godolt, M., Grenfell, J.L., Belu, A., Selsis, F., Hedelt, P., Schreier, F.: Potential Biosignatures in Super-Earth Atmospheres I. Spectral appearance of super-Earths around M dwarfs. *Astronomy and Astrophysics*, 529, DOI: 10.1051/0004-6361/201014368, 2011

Rix, M., Valks, P., Hao, N., Loyola, D., Schlager, H., Huntrieser, H., Flemming, J., Koehler, U., Schumann, U., Iness, A.: Volcanic SO₂, BrO and plume height estimations using GOME-2 satellite measurements during the eruption of Eyjafjallajökull in May 2010. *Journal of Geophysical Research*, AGU, DOI: 10.1029/2011JD016718, 2011

Roazanov, A., Kühl, S., Doicu, A., McLinden, C., Puķīte, J., Bovensmann, H., Burrows, J., Deutschmann, T., Dorf, M., Goutail, F., Grunow, K., Hendrick, F., von Hobe, M., Hrechanyy, S., Lichtenberg, G., Pfeilsticker, K., Pommereau, J.P., Van Roozendael, M., Stroh, F., Wagner, T.: BrO vertical distributions from SCIAMACHY limb measurements: comparison of algorithms and retrieval results. *Atmospheric Measurement Techniques*, 4, 1319-1359, DOI: 10.5194/amt-4-1319-2011, 2011

Schreier, F.: Optimized implementations of rational approximations for the Voigt and complex error function. *Journal of Quantitative Spectroscopy and Radiative Transfer*, 112 (6), 1010-1025, DOI: 10.1016/j.jqsrt.2010.12.010., 2011

Schymanski, E.L., Meringer, M., Brack, W.: Automated Strategies To Identify Compounds on the Basis of GC/EI-MS and Calculated Properties. *Analytical Chemistry*, 83 (3), 903-912, ACS Publications, DOI: 10.1021/ac102574h, 2011

Schuessler, O., Loyola, D.: Parallel Training of Artificial Neural Networks Using Multithreaded and Multicore CPUs. In: *Adaptive and Natural Computing Algorithms Lecture Notes in Computer Science*, 6593, 70-79, 2011

Thomas, W., Loyola, D.: Satellite remote sensing of reactive trace gases: How does it work?. *WMO-GAW Letter - Deutscher Wetterdienst*, 54, 2011

Valks, P., Pinardi, G., Richter, A., Lambert, J.-C., Hao, N., Loyola, D., Van Roozendael, M., Emmadi, S.: Operational total and tropospheric NO₂ column retrieval for GOME-2. *Atmospheric Measurement Techniques*, 4 (7), 1491-1514, DOI: 10.5194/amt-4-1491-2011, 2011

5.3 Conference Proceeding Papers and Presentations

Alam, K., Hussain, M., Mukhtar, A., Madl, P., Rehman, S., Trautmann, T., Blaschke, T.: Measurement of Atmospheric aerosol size distribution, mass concentration and lung deposition in four cities of Pakistan. European Aerosol Conference, Manchester, United Kingdom, 2011

Alam, K., Trautmann, T., Blaschke, T.: Ground-based Aerosol Optical Properties and radiative forcing over Karachi Pakistan. European Aerosol Conference, Manchester, United Kingdom, 2011

Antón, M., Bortoli, D., Kulkarni, P.S., Costa, M.J., Domingues, A.F., Loyola, D., Silva, A.M., Alados-Arboledas, L.: Analysis of total ozone trends in the Iberian Peninsula using satellite data. Global Conference on Global Warming, Lisbon, Portugal, 2011

Coldewey-Egbers, M., Loyola, D., Zimmer, W., Van Roozendaal, M., Lerot, C., Dameris, M., Garny, H., Braesicke, P., Koukoulis, M., and Balis, D.: Merging total ozone data from different UV-VIS satellite sensors: GOME / SCIAMACHY / GOME-2. SPARC/IOC/WMO-IGACO workshop on Past Changes in the Vertical Distribution of Ozone, Geneva, Switzerland, 2011

Coldewey-Egbers, M., Loyola, D., Zimmer, W., van Roozendaal, M., Lerot, C., Dameris, M., Garny, H., Braesicke, P., Koukoulis, M., and Balis, D.: Spatial patterns of observed and modelled total ozone trends 1995-2009. Geophysical Research Abstracts, 13 (EGU2011-6117), European Geosciences Union General Assembly 2011, Vienna, Austria, 2011

Gimeno García, S., Schreier, F., Trautmann, T.: Three-dimensional radiative transfer: Effects of cloud variability on reflected radiances. Geophysical Research Abstracts, 13 (EGU2011-12827), European Geosciences Union General Assembly 2011, Vienna, Austria, 2011

Gottwald, M., Krieg, E., Lichtenberg, G., Slijkhuis, S., Noël, S., Bramstedt, K., Bovensmann, H., von Savigny, C., Snel, R., Krijger, M.: Nine Years of Atmospheric Remote Sensing with SCIAMACHY - Instrument Performance. Proceedings of the Geoscience and Remote Sensing Symposium (IGARSS 2011), 3538-3541, Vancouver, Canada, 2011

Hao, N., Valks, P., De Smedt, I., Rix, M., Loyola, D., Van Roozendaal, M., Zhou, B., Zimmer, W.: Satellite observations of changes in air quality at mega-events in China. Geophysical Research Abstracts, 13 (EGU2011-12827), European Geosciences Union General Assembly 2011, Vienna, Austria, 2011

Hao, N., Valks, P., Van Roozendaal, M., Zhou, B., Wang, S.S. and Loyola, D.: Observations of changes in air quality during the EXPO 2010 from satellite and MAXDOAS measurements. Sino-German Workshop, Hefei, China, 2011

Hao, N., Valks, P., Van Roozendaal, M., Wang, S.S., De Smedt, I., Zhou, B., Wang, Z.R. and Loyola, D.: Air quality measurements for the EXPO 2010 in Shanghai. 5th DOAS workshop, Mainz, Germany, 2011

Hao, N., Valks, P., Rix, M., De Smedt, I., Van Roozendaal, M., Zhou, B., Zimmer, W., Loyola, D.: Satellite observation of changes in air quality at mega-events in China. EUMETSAT Meteorological Satellite Conference, Oslo, Norway, 2011

Kahnert, M. and Rother, T.: A T-Matrix Approach For Particles With Small-Scale Surface Roughness, AAPP, 89/1, DOI: 10.1478/C1V89S1P045, Electromagnetic and Light Scattering XIII, Sicily 2011

Kiemle, S., Dietrich, D., Loyola, D., Heinen, T., Rotzoll, H.: Spatial Data Service Operations for MetOp/Gome-2 Atmospheric Composition Products. EUMETSAT Meteorological Satellite Conference, Oslo, Norway, ISBN 978-92-9110-093-4, 2011

Köhler, C.H., Trautmann, T., Lindermeir, E.: Radiative properties of mixed biomass-mineral dust aerosol in the thermal infrared during SAMUM-2. European Aerosol Conference, Manchester, United Kingdom, 2011

Lerot, C., Van Roozendaal, M., van Gent, J., Spurr, R., Loyola, D., Zimmer, W., Lambert, J.-C., Balis, D., Koukouli, M., Zehner, C.: The GODFIT/GDP v5 algorithm: basis of the total ozone essential climate variable. 5th International DOAS Workshop, Mainz, Germany, 2011

Lichtenberg, G., Gottwald, M., Doicu, A., Schreier, F., Hrechanyy, S., Kretschel, K., Meringer, M., Hess, M., Gimeno García, S., Bovensmann, H., Eichmann, K.-U., Noël, S., von Savigny, C., Richter, A., Buchwitz, M., Rozanov, A., Burrows, J.P., Snel, R., Lerot, C., Van Roozendaal, M., Tilstra, G., Fehr, T.: Nine Years of Atmospheric Remote Sensing with SCIAMACHY - Atmospheric Parameters and Data Products. Proceedings of the Geoscience and Remote Sensing Symposium (IGARSS 2011), 3680-3683, Vancouver, Canada, 2011

Loyola, D.: Wie steht es um die Ozonschicht? Klima-Chemie Modelle und Satellitendaten im Vergleich. DLR EOC Symposium, Oberpfaffenhofen, Germany, 2011

Loyola, D.: Ozon- und Spurengasmonitoring mit GOME-2. DLR EOC Symposium, Oberpfaffenhofen, Germany, 2011

Loyola, D., Coldewey-Egbers, M., Zimmer, W., Van Roozendaal, M., Lerot, C., Dameris, M., Braesicke, P., Koukouli, M., Balis, D., Lambert, J.-C.: Total column ozone ECV: Merging GOME-2, SCIAMACHY, GOME and perspectives for Sentinels -5p, -4 and -5. EUMETSAT Meteorological Satellite Conference, Oslo, Norway, 2011

Meringer, M.: Generation of Molecular Graphs and Applications in Chemistry. Navigating Chemical Compound Space for Materials and Bio Design, Workshop II: Optimization, Search and Graph-Theoretical Algorithms for Chemical Compound Space (CCSWS2), Los Angeles, CA, US, 2011

Meringer, M.: Molecular Structure Generation and its Potential for Environmental Analytics. Chemicals In the Environment - CITE Seminar Series, Leipzig, Germany, 2011

Passaro, A., Murray, N., Snel, R., Krieg, E.: Coupled CFD-DSMC Simulations for Contamination Evaluation on ENVISAT due to OCM Thruster Plumes. Proceedings of the 7th European Symposium on Aerothermodynamics, SP-692, ISBN 978-92-9092-256-8, 2011

Rix, M., Valks, P., Loyola, D., van Gent, J., Van Roozendaal, M., Spurr, R., Hao, N., Zimmer, W.: Monitoring of volcanic eruptions and estimation of SO₂ plume height from GOME-2 measurements. EUMETSAT Meteorological Satellite Conference, Oslo, Norway, 2011

Rix, M., Valks, P., van Gent, J., Hao, N., Loyola, D.: Observations of volcanic sulphur dioxide emissions with GOME-2 using standard and modified DOAS, 5th International DOAS Workshop, Mainz, Germany, 2011

Schreier, F., Gimeno García, S., Doicu, A., Lichtenberg, G., Trautmann, T.: Validation of Vertical Profiles & Column Densities Retrieved from Nadir IR Sounders, 3rd GOSAT RA PI Meeting Edinburgh, United Kingdom, 2011

Slijkhuis, S., Beirle, S., Kalakoski, N., Gleisner, H., Loyola, D., Mies, K., Wagner, T., Zimmer, W., Aberle, B.: Validation of the GOME-2 Total Column of Water Vapour product of the O3M-SAF. GEWEX/ESA DUE GlobVapour workshop on long term water vapour data sets and their quality assessment, Frascati, Italy, 2011

Valks, P., Hao, N., Loyola, D., De Smedt, I., Van Roozendaal, M., Theys, N., Rix, M., Lambert, J.-C., Pinardi, G., Slijkhuis, S., Wagner, T., Zimmer, W.: Operational O3M-SAF trace gas column products: GOME-2 NO₂, BrO, SO₂, CH₂O and H₂O. EUMETSAT Meteorological Satellite Conference, Oslo, Norway, 2011

Valks, P., Hao, N., De Smedt, I., Beirle, S., Pinardi, G., Lambert, J.-C., Loyola, D., Mie, K., Rix, M., Kalakoski, N.: Operational O3M-SAF trace gas column products: GOME-2 NO₂, BrO, SO₂, CH₂O, and H₂O . Geophysical Research Abstracts, 13 (EGU2011-12827), European Geosciences Union General Assembly 2011, Vienna, Austria, 2011

Vasquez, M., Kitzmann, D., Patzer, B., Rauer, H., Schreier, F., Trautmann, T.: Effect of Clouds on Earth-like Planetary Thermal Emission Spectra at High Resolution. EPSC-DPS Joint Meeting, Nantes, France, 2011

Vasquez, M., Kitzmann, D., Patzer, B., Rauer, H., Schreier, F., Trautmann, T.: Effect of Clouds on Earth-like Planetary Thermal Emission Spectra at High Resolution. EANA 11, European Workshop on Astrobiology, Cologne, Germany, 2011

Vasquez, M., Kitzmann, D., Patzer, B., Rauer, H., Schreier, F., Trautmann, T.: Effects of clouds on earth-like planetary thermal emission spectra at high resolution. International Symposium on Atmospheric Radiation and Dynamics (ISARD-2011), St. Petersburg, Russia, 2011

Vasquez, M., Kitzmann, D., Patzer, B., Rauer, H., Schreier, F., Trautmann, T.: Radiative impact of clouds in atmospheres of Earth-like extrasolar planets, Helmholtz Alliance *Planetary Evolution and Life*. Midterm Review Meeting, Berlin, Deutschland, 2011

Wagner, T., Beirle, S., Dörner, S., Mies, K., Loyola, D., Slijkhuis, S., Kalakoski, N.: Application of 15 years of global atmospheric water vapor column observations from GOME-1/2 and SCIAMACHY for climate studies. EUMETSAT Meteorological Satellite Conference, Oslo, Norway, 2011

Wagner, T., Beirle, S., Loyola, D., Mies, K., Slijkhuis, S.: Application of 15 years of global atmospheric water vapor column observations from GOME-1/2 and SCIAMACHY for climate studies. Geophysical Research Abstracts, 13 (EGU2011-12827), European Geosciences Union General Assembly 2011, Vienna, Austria, 2011

Wagner, T., Beirle, S., Loyola, D., Mies, K., Slijkhuis, S.: Application of 15 years of global atmospheric water vapor column observations from GOME-1/2 and SCIAMACHY for climate studies. GEWEX/ESA DUE GlobVapour workshop on long term water vapour data sets and their quality assessment, Frascati, Italy, 2011

Xu, J., Schreier, F., Doicu, A., Vogt, P., Trautmann, T.: First results of inversion for far infrared limb sounding. Geophysical Research Abstracts, 13 (EGU2011-12827), European Geosciences Union General Assembly 2011, Vienna, Austria, 2011

Xu, J., Schreier, F., Doicu, A., Vogt, P., Trautmann, T.: TELIS level 2 data processing: current status and first results. 6th Atmospheric Limb Conference, Kyoto, 2011

5.4 Attended Conferences and Professional Leaves

SPARC/IOC/WMO-IGACO workshop on Past Changes in the Vertical Distribution of Ozone, Geneva, Switzerland, January 25-27, 2011

Helmholtz Alliance *Planetary Evolution and Life* Midterm Review Meeting, Berlin, Germany, March 16/17, 2011

European Geosciences Union (EGU) General Assembly, Vienna, Austria, April 3-8, 2011

Navigating Chemical Compound Space for Materials and Bio Design, Workshop II: Optimization, Search and Graph-Theoretical Algorithms for Chemical Compound Space (CCSWS2), Los Angeles, CA, US, April 11-15, 2011

International Conference on Adaptive and Natural Computing Algorithms, Ljubljana, Slovenia, April 14-16, 2011

3rd GOSAT RA PI Meeting Edinburgh, United Kingdom, May 19/20, 2011

Sino-German Workshop, Hefei, China, May 31 – June 3, 2011

CITE Seminar Series, Leipzig, Germany, June 22, 2011

International Symposium on Atmospheric Radiation and Dynamics (ISARD-2011), St. Petersburg, Russia, June 21-24, 2011

European Workshop on Astrobiology, Cologne, Germany, July 11-14, 2011

5th DOAS Workshop, Mainz, Germany, July 13-15, 2011

IEEE 2011 International Geoscience and Remote Sensing Symposium (IGARSS), Vancouver, Canada, July 24-29, 2011

European Aerosol Conference, Manchester, United Kingdom, September 4-9, 2011

EUMETSAT Meteorological Satellite Conference, Oslo, Norway, September 5-9, 2011

Fall Meeting of Astronomische Gesellschaft, Heidelberg, Germany, September 19-23, 2011

EPSC-DPS Joint Meeting, Nantes, France, October 2-7, 2011

6th Atmospheric Limb Conference, Kyoto, Japan, November 29 – December 1, 2011

5.5 Diploma and Doctoral Theses

Alam, K.: Remote Sensing of aerosol characteristics and radiative forcing in Pakistan. Dissertation (Dr. rer. nat.), Faculty of Natural Sciences, Department of Geography and Geology, Centre for Geoinformatics, University of Salzburg, thesis defence December 2011, 147 p. (Supervisors: Prof. Dr. Thomas Blaschke, University of Salzburg and Prof. Dr. Thomas Trautmann)

Fagiolini, E.: The impact of atmospheric variability on the determination of the gravity field of the Earth. Dissertation, Faculty of Civil Engineering and Geodesy, Technical University of Munich. (Supervisors: Prof. Dr. Reiner Rummel, Technical University of Munich and Gottfried Schwarz)

Gimeno García, S.: Simulation of solar radiative transfer and comparison with spectro-radiometric measurements. Dissertation, Faculty of Physics and Earth Science, University of Leipzig. (Supervisor: Prof. Dr. Thomas Trautmann)

Köhler, C.H.: Observation and simulation of the longwave radiative effects for Saharan mineral dust plumes. Dissertation, Faculty of Physics and Earth Science, University of Leipzig. (Supervisors: Prof. Dr. Manfred Wendisch, University of Leipzig and Prof. Dr. Thomas Trautmann)

Otto, S.: Optische Eigenschaften nichtkugelförmiger Saharamineralstaubpartikel und deren Einfluss auf den Strahlungstransport in der Erdatmosphäre. Dissertation, Faculty of Physics and Earth Science, University of Leipzig, submitted October 2011. (Supervisors: Prof. Dr. Thomas Trautmann and Prof. Dr. Manfred Wendisch, University of Leipzig)

Rix, M.: Observation of volcanic SO₂ plumes based on the satellite-borne GOME-2 instrument. Dissertation, Faculty of Civil Engineering and Geodesy, Technical University of Munich, submitted July 2011. (Supervisors: Prof. Dr. Richard Bamler, Technical University of Munich and Dr. Pieter Valks)

Schüssler, O.: Combined Inversion Methods for UVVIS Nadir Sounding. Dissertation, Civil Engineering and Geodesy, Technical University of Munich. (Supervisors: Prof. Dr. Richard Bamler, Dr. Adrian Doicu and Diego Loyola)

Szopa, M.: Inversion methods for atmospheric nadir infrared sounding. Dissertation, Faculty for Mathematics and Science, University of Potsdam. (Supervisors: Dr. habil. Adrian Doicu and Prof. Dr. Thomas Trautmann)

Vasquez, M.: Simulation of the radiation field in planetary atmospheres. Dissertation, Centre of Astronomy and Astrophysics, Technical University of Berlin. (Supervisors: Prof. Dr. Heike Rauer, German Aerospace Center, Institute of Planetary Research and Dr. Franz Schreier)

Xu, J.: Inversion for Limb Infrared Atmospheric Sounding. Dissertation, Civil Engineering and Geodesy, Technical University of Munich. (Supervisors: Prof. Dr. Richard Bamler, Dr. Franz Schreier, and Prof. Dr. Thomas Trautmann)

Zlatkov, D.: Software Tool Development for Validation of Satellite Data. Master of Science Thesis, Earth Oriented Space Science and Technology ESPACE, Technical University of Munich, November 2011, 53 p. (Supervisors: Dr. habil. Adrian Doicu, Dr. Günter Lichtenberg, Dr. Serhiy Hrechanyy, and Prof. Dr. Thomas Trautmann)

5.6 Seminar Talks

Daniel Kitzmann (TUB-ZAA): Climatic effect of clouds in atmospheres of Earth-like extrasolar planets, January 25, 2011

Adrian Doicu: Direct and inverse problems in atmospheric remote sensing, February 1, 2011

Dmitry Efremenko: Implementation of radiative transfer equation solutions with small angle modification, February 22, 2011

Elisa Fagiolini: Atmospheric variability in connection with the gravity field of Earth system, February 22, 2011

Pascal Hedelt (LAB - Laboratoire d'Astrophysique de Bordeaux): Radiative transfer in the exosphere of Saturn's moon Titan, March 22, 2011

Jana Mendrok (Department of Space Science, Lulea University of Technology, Kiruna): SMILES Mission Overview and First Results, April 5, 2011

Peter Vogt (IMF-EV): Towards Verified Calibrated Radiance Spectra for TELIS, June 7, 2011

Van Snyder (JPL, NASA): Fortran Major Developments and CoArrays: Microwave Limb Sounder, July 4, 2011

Karsten Schmidt (and Michael Kahnert, Maxim Yurkin, and Tom Rother): Reciprocity in Light Scattering Computations, July 20, 2011

Meike Rix: Monitoring of volcanic sulfur dioxide emissions and estimation of the plume height using GOME-2 measurements, August 4, 2011

Silvia Nulli Smuraglia (Univ. Perugia): Monte Carlo method applied to radiative transfer, September 14, 2011

Dieter Kohlert (Hochschule Regensburg): Line-by-line computations with FPGA - Field Programmable Gate Arrays, September 27, 2011

Claas Köhler: Radiative Transfer Modelling of Saharan Dust within the Scope of SAMUM2, November 8, 2011

Jian Xu: TELIS Limb Sounding Retrievals, November 22, 2011

Michal Szopa: IASI Ozone Profile Retrievals with Runge-Kutta Regularization, December 6, 2011

Tom Rother: Verschränkte Zustände – nicht nur ein Phänomen in der Quantenmechanik!, December 15, 2011

Abbreviations and Acronyms

ADF	Auxiliary Data File
ADM	Atmospheric Dynamic Mission
AERI	Atmospheric Emitted Radiance Interferometer
AERONET	Aerosol Robotic Network
AIRS	Atmospheric Infrared Sounder
AOT	Aerosol Optical Thickness
API	Air Pollution Index
AP	Atmospheric Processors
ARF	Aerosol Radiative Forcing
ARM	Atmospheric Radiation Measurement
ASLI	Atmospheric Science Librarians International
AU	Astronomical Unit
AUTH	Aristotle University of Thessaloniki
BIRA	Belgisch Instituut voor Ruimte-Aëronomie
BIRRA	Beer InfraRed Retrieval Algorithm
CCD	Convective-Cloud-Differential
CF	Cloud Fraction
CGSTAB	Conjugate Gradient Stabilized
CGT	Cloud Geometrical Thickness
CKD	Correlated K-Distribution
CLO	Consolidated Level 0
COT	Cloud Optical Thickness
CTH	Cloud-Top Height
DDA	Discrete Dipole Approximation
DDSCAT	DDA Scattering
DE	Data Encryption
DFD	Deutsches Fernerkundungsdatenzentrum
DIMS	Data & Information Management System
DISORT	Discrete Ordinates Radiative Transfer
DLR	Deutsches Zentrum für Luft- und Raumfahrt
D-PAC	German Processing and Archiving Center
DSCS	Differential Scattering Cross Section
EASM	East Asian Summer Monsoons
ECM	Emission Control Measure
ECV	Essential Climate Variable
ENVISAT	Environmental Satellite
EO	Earth Observation
EOC	Earth Observation Center
ERS	European Remote Sensing Satellite
ESA	European Space Agency
ESOC	European Space Operation Center
ESRIN	European Space Research Institute
ESTEC	European Space Technology Center
EUMETSAT	European Organisation for the Exploitation of Meteorological Satellites
EV	Experimentelle Verfahren
GADS	Global Aerosol Data Set
GARLIC	Generic Atmospheric Radiation Line-by-Line Infrared Code
GCOS	Global Climate Observing Systems
GDP	GOME Data Processor
GEISA	Gestion et Etude des Informations Spectroscopiques Atmosphériques
GFZ	Geoforschungszentrum
GMES	Global Monitoring for Environment and Security
GOME	Global Ozone Monitoring Experiment
GOSAT	Greenhouse Gases Observing Satellite

HALOE	Halogen Occultation Experiment
HDD	Hard Disk Drive
HITRAN	High Resolution Transmission
HWHM	Half Width Half Maximum
IMF	Institut für Methodik der Fernerkundung
IPF	Institut für Planetenforschung
IUP-IFE	Institut für Umweltphysik / Institut für Fernerkundung
JPL	Jet Propulsion Laboratory
LAB	Laboratoire d'Astrophysique de Bordeaux
LbL	Line-by-Line
LIDAR	Light Detection and Ranging
MERLIN	Methane Remote Sensing Lidar Mission
MetOp	Meteorological Operational Polar Satellites of EUMETSAT
MIPAS	Michelson Interferometer for Passive Atmospheric Sounding
MIPAS-B	MIPAS for Balloons
MIRART	Modular Infrared Atmospheric Radiative Transfer
MLS	Microwave Limb Sounder
MODIS	Moderate Resolution Imaging Spectroradiometer
MOPITT	Measurements of Pollution in the Troposphere
MOZART	Model for Ozone and Related Chemical Tracers
MPIC	Max Planck Institute for Chemistry
NASA	National Aeronautics and Space Administration
NDACC	Network for the Detection of Atmospheric Composition Change
NLC	Noctilucent Cloud
O3M	Ozone Monitoring
OCR	Operation Change Request
OCRA	Optical Cloud recognition Algorithm
OPAC	Optical Properties of Aerosols and Clouds
OPC	Optical Particle Counter
PA	Physik der Atmosphäre
PILS	Profile Inversion for Limb Sounding
PIRATES	Programmer's Interface to Radiative Transfer Algorithms
PSC	Polar Stratospheric Cloud
ROCINN	Retrieval of Cloud Information using Neural Networks
RT	Radiative Transfer
RTS	RT Solutions
RTE	Radiative Transfer Equation
SAF	Satellite Application Facility
SAGE	Stratospheric Aerosol and Gas Experiment
SAMUM	Sahara Mineral Dust Experiment
SBDART	Santa Barbara DISORT Atmospheric Radiative Transfer
SCIAMACHY	Scanning Imaging Absorption Spectrometer for Atmospheric Chartography
SEMC	Shanghai Environmental Monitoring Center
SEU	Single Event Upset
SHDOM	Standard Harmonic Discrete Ordinate Method
SMHI	Swedish Meteorological and Hydrological Institute
SMILES	Superconducting-Submillimeter-Wave Limb-Emission Sounder
SMR	Sun Mean Reference
SOST	SCIAMACHY Operations Support Team
SQWG	SCIAMACHY Quality Working Group
SRON	Netherlands Institute for Space Research
TANSO	Thermal and Near Infrared Sensor for Carbon Observation
TELIS	TeraHertz Limb Sounder
TES	Tropospheric Emission Spectrometer
TOA	Top of Atmosphere
TOMS	Total Ozone Mapping Spectrometer

TTOC	Tropical Tropospheric Ozone Column
TUB	Technical University Berlin
TUM	Technical University Munich
UNEP	United Nations Environment Programme
UV	Ultraviolet
VCD	Vertical Column Density
WDC-RSAT	World Data Center for Remote Sensing of the Atmosphere
ZAA	Zentrum für Astronomie und Astrophysik

DLR at a Glance

DLR is Germany's national research center for aeronautics and space. Its extensive research and development work is integrated into national and international cooperative ventures. As Germany's space agency, the German federal government has given DLR responsibility for the forward planning and the implementation of the German space program as well as international representation of Germany's interests.

Approximately 7000 people are employed at sixteen locations in Germany: Köln (headquarters), Augsburg, Berlin, Bonn, Braunschweig, Bremen, Göttingen, Hamburg, Jülich, Lampoldshausen, Neustrelitz, Oberpfaffenhofen, Stade, Stuttgart, Trauen and Weilheim. DLR also operates offices in Brussels, Paris, Singapore and Washington, D.C.

Remote Sensing Technology Institute Institut für Methodik der Fernerkundung

DLR's Remote Sensing Technology Institute (IMF) is located in Oberpfaffenhofen, Berlin-Adlershof, and Neustrelitz.

IMF carries out research and development for retrieving geo-information from remote sensing data. It conducts basic research on physical principles of remote sensing and develops algorithms, techniques, and operational processing systems for synthetic aperture radar, optical remote sensing, and spectrometric sounding of the atmosphere. The processing systems are in operational use for national, European, and international Earth observation missions.

For preparation and in support of spaceborne missions IMF operates a suite of multi- and hyperspectral optical airborne sensors. The institute contributes its expertise to novel sensor and mission concepts.

The German Remote Sensing Data Center (DFD) and IMF form DLR's Earth Observation Center (EOC).



DLR

**Deutsches Zentrum
für Luft- und Raumfahrt e.V.**
in der Helmholtz-Gemeinschaft

Institut für Methodik der Fernerkundung
Oberpfaffenhofen
82234 Weßling

www.dlr.de/eoc